Advances in Manufacturing of the Tissue Engineered Muscle Repair (TEMR) Technology Platform

---

A Thesis

Presented to

the faculty of the School of Engineering and Applied Science

University of Virginia

---

in partial fulfillment
of the requirements for the degree

Master of Science

by

Joshua David Remer

August 2017

APPROVAL SHEET

This Thesis
is submitted in partial fulfillment of the requirements
for the degree of
Master of Science

Author Signature: J. David Remer

This Thesis has been read and approved by the examining committee:

Advisor: George Christ

Committee Member: Silvia Blemker

Committee Member: Gavin Garner

Committee Member: _____

Committee Member: _____

Committee Member: _____

Accepted for the School of Engineering and Applied Science:

Craig H. Benson, School of Engineering and Applied Science

August 2017

Advances in Manufacturing of the Tissue Engineered Muscle Repair (TEMR) Technology Platform

Introduction and Rationale

1. Incorporation of In Vitro Cell Conditioning for Enhanced Development of Tissue Engineered Skeletal Muscle Implants
   - 1.1. Introduction
   - 1.2. Applications of In Vitro Tissue-Engineered Skeletal Muscle
   - 1.3. In Vitro Bioreactor Treatments as a Guide for Enhanced Skeletal Muscle Tissue Engineering In Vitro
     - 1.3.1.Cyclic Mechanical Stimulation
     - 1.3.2. Dynamic Tissue Culture Bioreactors
   - 1.4. Neuro-Electrical Stimulation as a Guide for Enhanced Skeletal Muscle Tissue Engineering In Vitro
     - 1.4.1.Protocols for In Vitro Electrical Stimulation
     - 1.4.2.Protocols for In Vitro Neurotization of Skeletal Muscle
   - 1.5. Conclusions

2. Advances to the RTL Bioreactor
   - 2.1. Bioreactor Description
     - 2.1.1.Introduction
     - 2.1.2.Bioreactor Specs
     - 2.1.3.Bioreactor Protocol
     - 2.1.4.Bioreactor Notes
   - 2.2. Bioreactor Controller
     - 2.2.1.Introduction
     - 2.2.2.Previous Controller
     - 2.2.3.New Controller Development
     - 2.2.4.Device Specifications and Components
     - 2.2.5.PCB Realization
     - 2.2.6.Control Code
     - 2.2.7.User Interface
     - 2.2.8.ErrorTrack
     - 2.2.9.Malfunctions
     - 2.2.10. Future Directions
   - 2.3. Advances in Scaffold Mounting Capability
     - 2.3.1.Introduction
     - 2.3.2.Current Scaffold Mounting Method
     - 2.3.3.Improved Mounting Method
     - 2.3.4.Strain Heterogeneity Quantification
     - 2.3.5.Future Directions
   - 2.4. Advances in Bioreactor and Transport Design
     - 2.4.1.Introduction
     - 2.4.2.Bioreactor Updates
     - 2.4.3.Transport Chamber Design

Introduction and Rationale

The need for regenerative medicine is greater now than ever, as medical advancements allow survival of previously fatal conditions or injuries. However, with increased survival rates comes an escalation of tissue morbidity accompanied by permanent functional and aesthetic defects. Advances in tissue engineering have highlighted the potential of regenerative therapeutics to dramatically improve the treatment of these traumatic, genetic or acquired conditions. Even on a national scale, the massive potential impact of widespread regenerative medicine technology implementation has been recognized with the recent founding of the Advanced Regenerative Manufacturing Institute (ARMI); a ManufacturingUSA initiative funded by the Department of Defense, to provide a centralized consortium for development of breakthrough approaches to overcome the current hurdles preventing more efficient clinical translation of tissue engineering/regenerative medicine technologies.

Specifically in the realm of skeletal muscle tissue engineering, our lab has developed a tissue-engineered muscle repair (TEMR) system which has shown great promise in preclinical studies, and is rapidly approaching submission of an IND application to support implementation in a “first in man” pilot study with our first generation TEMR technology. However, more widespread clinical application of the TEMR product will require further optimization of the production process, characterization of the various components of the TEMR technology, as well as refinement of the functional evaluation of the final product. To this end, this thesis has focused on improvements to the following:

- Bioreactor design, control and transportation of the engineered product
- Materials Characterization
- In situ assessment of functional recovery following implantation in a biologically relevant skeletal muscle traumatic injury model.

We consider the rationale for each of these briefly below, and discuss them in much more detail in the body of the thesis.

The first hurdle to overcome lies in the optimization of the in vitro development portion of the TEMR technology. Efforts within this segment are largely focused on increasing reliability and consistency of our tissue bioreactor system. Specifically, we will examine the development of a new bioreactor controller system with increased precision and reliability, as well as upgrades to the bioreactor protocol and physical design. In addition, we have developed a transportation system capable of sustaining viable TEMR constructs from the manufacturing site to the hospital for surgical implantation.

Second, our tissue repair method is based on a porcine-derived bladder acellular matrix (BAM). This material was selected as the basis for our tissue repair due to its biocompatibility for cell attachment and bioreactor preconditioning in vitro, as well as its suture-retention capability and favorable degradation profile following implantation in vivo. Essentially the BAM serves simply as a cell delivery vehicle via its advantageous biomechanical properties. However, to fully optimize our material repair strategy, it is essential to possess more detailed understanding of the physical and mechanical characteristics of the BAM. These are highly relevant considerations with respect to the interaction of cells with the BAM, the interaction of BAM with native tissue, and the reproducibility of the material for production scale up and implementation. This thesis will approach materials characterization of the BAM via several methods of thickness measurements, stress-strain characterization, and examination of physical structure via several microscopic imaging modalities.

Finally, in vivo/in situ data would provide more detailed physiological assessment of the functional relevance of our tissue engineered muscle repair technology. To this end, we have adapated and further refined an in situ method of active force measurement in the rat latissimus dorsi (LD), and compared it to the existing in vitro methods of evaluating force recovery.

Incorporation of In Vitro Cell Conditioning for Enhanced Development of Tissue Engineered Skeletal Muscle Implants

David Remer[1], Juliana Passipieri[1], George Christ[1,2]

[1]Department of Biomedical Engineering, University of Virginia, Charlottesville, VA 22908

[2] Department of Orthopaedic Surgery, University of Virginia, Charlottesville, VA, 22908

Corresponding Author:

George J. Christ, Ph.D.

Professor of Biomedical Engineering and Orthopaedic Surgery

Mary Muilenburg Stamp Professor of Orthopaedic Research

Director of Basic and Translational Research in Orthopaedic Surgery

Head, Laboratory of Regenerative Therapeutics

University of Virginia

Phone: (434) 924-5794

Email: gjc8w@eservices.virginia.edu

Fax: (434) 982-3870

1.1 Introduction

Skeletal muscle anatomy and physiology

Skeletal muscle is a fascinating and complex tissue responsible for voluntary body movements. Accounting for nearly 40% of the human body mass, skeletal muscle is composed of several hierarchical units, beginning with microscopic sarcomeres comprised of actin and myosin filaments in register. The sarcomeres are serially organized in large parallel groups to form myofibrils. Numerous myofibrils, in turn, are packed in a parallel fashion to form a myofiber. The myofiber represents the basic functional unit of skeletal muscle, consisting of the physiological and structural mechanisms required for muscle stimulation and contraction (i.e., excitation-contraction coupling; EC coupling). Myofibers, in turn, are surrounded by a network of extracellular matrix (ECM) proteins composed almost entirely of collagen and hydrated proteoglycans, referred to as the endomysium. A large group of myofibers bound together forms a fascicle. The fascicle is surrounded by a similar but thicker ECM known as the perimysium. Finally, groups of fascicles form the actual muscle body, the epimysium, which is covered by an ECM. The net result of such organization is a rigid yet deformable structure, which can support much of the passive load placed on muscle (MacIntosh, Gardiner, and McComas 2006), (Lieber 2002).

Upon muscle activation, each sarcomere contracts a microscopic distance. Owing to the sarcomeres' series organization, the contractions sum to provide the total myofibril, and thus, myofiber shortening distance, while the parallel myofiber organization multiplies the force of the contraction. Longitudinal force transmission comprises the classical view of muscular contraction and occurs parallel to the muscle fiber direction, employing the sarcomeric

contraction to act upon the muscle's attachment tendons, However, during muscle contractions, force is transmitted not only longitudinally, but also laterally. Lateral muscle force transmission occurs through the muscle's extracellular matrix – perpendicular to the direction of the muscle fiber – and serves to evenly distribute contractile force across the myofibers (Ramaswamy et al. 2011) (Maas and Sandercock 2010)(Huxley, Andrew, Sir 1980) (Street 1983). Like most complex tissues/organs, the integration of the vascular and neural components in the extracellular matrix among the muscle fibers creates an intricate and sophisticated signaling muscle architecture and excitation-contraction (EC) signaling network. This complexity ensures that in vitro tissue engineering of physiologically-relevant, contractile skeletal muscle remains a major challenge. Despite considerable recent advances, skeletal muscle tissue engineering is still at a relatively early stage of development.

Skeletal muscle wound healing

In the normal wound healing process, native skeletal muscle employs the existing ECM as a "template" to aid the regeneration of damaged myofibers. This strategy works extremely well for relatively small gaps in the muscle continuity following injury/trauma – such as damage incurred during exercise or minor lacerations. However, in instances when significant amounts of all components of muscle tissue are simultaneously damaged or missing (e.g., muscle, vessel, nerve, ECM), a condition referred to as volumetric muscle loss (VML) results. VML injuries are defined by a degree of muscle tissue loss that exceeds the endogenous regenerative capacity of skeletal muscle resulting in permanent functional and cosmetic deficits (Grogan, Hsu, and Skeletal Trauma Research Consortium 2011). VML and VML-like injuries can occur from trauma (battlefield injuries and accidents), as well as a range of other congenital and acquired

conditions (Thiele et al. 2014) (Baugh et al. 2013) (Holcomb et al. 2006). In general, loss of ≈10% muscle mass in a given location is sufficient to result in VML (Passipieri and Christ 2016), where structural and functional recovery is incomplete. The unmet medical need for improved treatment of VML and VML-like injuries is a major driving force for development of improved methods for in vitro creation of implantable therapeutics for restoration of skeletal muscle tissue form and function in vivo. The purpose of this report is to review current investigative efforts to optimize in vitro conditioning with this lofty goal in mind.

The establishment of relevant metrics for evaluation of engineered tissues is critical to judging the fidelity of their physiological significance. Of note, the easily recognizable functional and structural hallmarks of native skeletal muscle function outlined above and covered in many published reports (Gilbert 2000) (Shadrin, Khodabukus, and Bursac 2016) (Jolesz, F and Streter, F A 1981), provide objective indices by which to measure the progress and success of tissue engineered skeletal muscle development (implantable or otherwise). The most critical intrinsic factors for assessment include the creation of functional contractile machinery (see above), as well as fiber alignment, vasculature, and neural coupling/excitation. Various groups have created engineered muscle constructs in vitro that possess one or several of these characteristics to some degree; however, none have successfully recapitulated all of the characteristic features of mature adult-phenotype skeletal muscle in vivo.

1.2 Applications of In Vitro Tissue Engineered Skeletal Muscle.

There exist at least 4 major applications of skeletal muscle tissue engineering, all of which would benefit from optimization of in vitro conditioning protocols. They are: 1) in vitro studies of muscle tissue damage and repair (Cook et al. 2016), 2) in vitro models for drug and toxicity testing

(including personalized medicine) (Madden et al. 2015), 3) creation of mature muscle tissue for soft robotics or bulk muscle replacement in vivo (Duffy and Feinberg 2014) (Bian and Bursac 2009), and 4) creation of implantable regenerative templates for muscle replacement and repair in vivo (Corona et al. 2014). For our purposes, we will focus on the end goal of developing implantable therapeutics for treatment of, for example, VML or VML-like injuries. This approach could one of take several forms:

Implantable therapeutics for growth in a host site, then transfer to another site for functional restoration.

In this case, an engineered muscle tissue scaffold could be implanted subcutaneously for a growth period, during which the in vivo environment provides the necessary support to flourish (i.e., the body is the bioreactor). After this maturation, the scaffold could be removed and employed as needed as an autologous muscle graft (Juhas, Ye, and Bursac 2016).

Implantation of a mature muscle construct.

This would essentially be the ultimate development and aggregation of diverse and currently nascent tissue engineering technologies. To achieve a native-like phenotype of mature, contractile muscle, the in vitro myogenic microenvironment must be optimized to include functional vasculature, neural innervation, chemical signaling, and mechanical connection. Understandably, no one has yet been able to approach a realistic implementation of this concept.

Implantation of a phenotypically immature construct developed in vitro that generates new tissue using the body as a second bioreactor after implantation in vivo.

As one might imagine, in order to more closely approximate the complexity of the in vivo environment, investigators have evaluated many combinations and permutations of in vitro

conditions. While we recognize the unequivocal importance of endogenous chemical signaling and morphogenic factors, as well as the impact of biomaterial integration to more fully recapitulate the conditions required for native myogenesis, those considerations and their influence on development of in vitro muscle tissue engineering have recently been discussed elsewhere ((Passipieri and Christ 2016) (Syverud, VanDusen, and Larkin 2016) (Rangarajan, Madden, and Bursac 2014)) and will not be further considered herein. Thus, we will confine our review to evaluation of two other modalities that are critical for development of tissue engineered skeletal muscle (Figure 1). These two modalities/factors are listed below and will be discussed in order.

1.3 In Vitro Bioreactor Treatments
1.4 Neuro-Electric Stimulation

1.3 In Vitro Bioreactor Treatments as a guide for enhanced skeletal muscle tissue engineering in vitro.

1.3.1 Cyclic Mechanical Stimulation.

The importance of mechanical action/stimulation to skeletal muscle formation, homeostasis and growth is well documented (Pollard, McGonnell, and Pitsillides 2014) (Hall 2010) (Schiaffino et al. 2013). During fetal myogenesis, for example, both passive and active skeletal muscle motion are required for proper development. Passive skeletal muscle stretch induced by skeletal bone growth partially fulfills the requirement for physical movement by causing release of the protein kinase mTOR, which in turn leads to muscle hypertrophy (Goodman, Hornberger, and Robling 2015). On the other hand, voluntary auto-activation of the fetus' skeletal muscle causes release of insulin-like growth factor-1 (Tidball 2005) (Perrone,

Fenwick-Smith, and Vandenburgh 1995) and establishes a resident population of satellite stem cells (Saha et al. 2006). Taken together, these motions stretch immature, fused primary and secondary myotubes and encourage the highly up regulated fetal satellite stem cell population to utilize those existing myotubes as templates in forming more mature myotubes and then functionally mature, contractile myofibers. In developmental myogenesis, muscle contraction induced by neural stimulation is also a requirement for full maturation; the applicability of this latter concept to in vitro tissue engineering of skeletal muscle will be discussed in a later section of this chapter.

Toward this end, as outlined in Table 1, there are an increasing number of investigators exploring the utility of cyclic stretch bioreactor methods to improve tissue engineered skeletal muscle formation and function, both in vitro and in vivo (Brown 2000) (I. Martin, Wendt, and Heberer 2004), (An and Li 2014) (Table 1). While active force production is the ultimate gold standard by which to evaluate the success of tissue engineered skeletal muscle development, the number of research groups measuring active force production of engineered muscle tissue is still surprisingly small. In short, although recent results are encouraging, there is still significant work in the optimization and application of in vitro stretch protocols for development of more biomimetic engineered skeletal muscle.

As noted above, a major driver for development of improved skeletal muscle tissue engineering is creation of therapeutic solutions for functional and cosmetic restoration of VML or VML-like injuries. Since VML can result from a variety of congenital (i.e., congenital malformations) and acquired (genetic or infection) conditions, the clinical presentation varies across a spectrum of cosmetic and functional deficits. Nonetheless, surgical removal of 10-30%

of muscle mass reproducibly results in permanent functional deficits in biologically relevant animal models (Passipieri and Christ 2016). In such a situation, lacking capacity for functional recovery, muscle will either attempt to “repair” itself with non-contractile ECM and/or leave a void. One method to mitigate the aesthetic and functional deficits associated with VML is providing the native muscle with cues for regeneration that are otherwise lacking in adult mammals. Tissue engineering (TE) and regenerative medicine (RM) strategies, or TE/RM, are at the forefront of development for treatment of VML injuries.

The benefits of in vitro stretch preconditioning for TE/RM applications has been recently reported with the development of a tissue-engineered muscle repair (TEMR) technology platform (Moon et al. 2008) (Machingal et al. 2011) (Corona et al. 2012) (Corona et al. 2014) (Figure 2). The TEMR technology consists of using a sheet-like decellularized extracellular matrix derived from the lamina propria of a porcine bladder as a delivery system for the implantation of muscle progenitor cells. This collagen-based material is rich in elastic fibers (Andersson and McCloskey 2014), with an abundance of collagen I, III & IV and to a lesser extent collagen II, as well as laminin and elastin (REDDY et al. 2000) (Chun et al. 2007). These features permit attachment of myogenic progenitor cells, and allow organization of a nominal monolayer of cells. In addition, it is sufficiently durable to withstand bioreactor preconditioning (i.e., stretch) and surgical implantation ((Machingal et al. 2011) (Corona et al. 2012) (Corona et al. 2014)) and has been shown to promote cell growth and differentiation (De Filippo, Yoo, and Atala 2002) (Yoo et al. 1998).

Following seeding with myogenic progenitor cells (MPCs), the entire construct is subjected to cyclic mechanical preconditioning in a custom cyclic stretch bioreactor prior to

implantation, thus encouraging the seeded muscle progenitor cells (MPCs) to align and/or fuse into multinucleated myotubes. In fact, the in vitro preconditioning prior to TEMR construct implantation promoted enhanced in vivo regeneration in two distinct rodent VML injury models. The first model was created in mice and entailed the removal of 50% (~25mg) of the latissimus dorsi (LD). In this instance, not only was 72% of native LD contractile force recovered by the implantation of the TEMR constructs, but desmin-positive myofibers, blood vessels, and neurovascular bundles were all detected in the implanted region (Machingal et al. 2011). The second, larger VML injury model was based on the surgical resection of 20% of the tibialis anterior (TA) in rats (63.1 – 70.8 mg), in which TEMR implantation restored 61% of function over non-repaired muscle within 3 months of implantation (Corona et al. 2014).

Initial investigations have also demonstrated that repeat MPC seeding during bioreactor preconditioning increases the number of multinucleated myotubes present on the TEMR construct. Furthermore, following implantation in the mouse LD VML injury model, retrieved muscles with myotube-enhanced TEMR constructs displayed 120% greater and 110% greater force generation than the unrepaired LD muscles with VML injuries at 1 and 2 months post-implantation, respectively (Corona et al. 2012). In addition, Western blotting was performed to quantify the expression of proteins involved in force production and transmission (desmin, JP1, and myosin), and EC-coupling (RyR1). Pax7 levels were also analyzed and found to be significantly elevated in all TEMR treated animals at 2 months post-implantation, indicating an ongoing process of tissue regeneration. The utility of repeated MPC seeding during bioreactor preconditioning is under further investigation in our group.

In addition, other research groups have also found some benefits to employing cyclic mechanical stretch for tissue engineering of skeletal muscle. For example, Flexcell™ (Flexcell International Corporation, Burlington, NC) is one of a few commercially-available mechanical strain bioreactor systems. The method of applying stretch consists of seeding cells onto a flexible membrane that, when distorted by vacuum pressure on the lower side of the membrane, stretches the seeded cells uniaxially or biaxially, depending on the setup. Two strain gauges are used to monitor strain across the 6 culture plates. Although the system has been used for many cell types (Jiang, Wang, and Tang 2016) (Chua et al. 2016), for skeletal muscle it has produced mixed results with respect to maturation of myotubes (Dugan, Cartmell, and Gough 2014). This could be due in part to an imperfect choice of scaffolding material onto which the cells were seeded, as well as excessive stretch amplitude, or excessive stretch frequency. The other primary commercially available bioreactor is called the STREX (STREX, San Diego); it operates very similarly to the Flexcell, however the uniaxial and biaxial stretch devices are separate units. In addition, the company offers a stretch bioreactor that includes electrical stimulation of the construct. Such stretch protocols have been known to increase tissue organization and force generation in engineered skeletal muscle for quite some time (Edman, Elzinga, and Noble 1978). While the stretch provided by these and similar devices seems to have improved various phenotypic aspects of engineered skeletal muscle (Powell et al. 2002) (Vandenburgh et al. 1991) (Vandenburgh et al. 1989), thus far, the impact on recovered force generation following implantation in vivo has not been determined.

A group from Johns Hopkins has created the most advanced stretch bioreactor to date (Cook et al. 2016). Although it has not yet been used on engineered skeletal muscle, the device

is capable of providing cyclic stretch, electrical stimulation, active force measurement, and digital image correlation simultaneously for four tissue samples held within its culture chamber. The technology provided by such a device could likely be extremely useful in further elucidating in vitro conditions required for more optimized in vitro engineered skeletal muscle tissue products.

It is worth noting that static strain is only rarely utilized as a mechanical loading protocol for developing engineered skeletal muscle (Vandenburgh 1987). Such is the case in Heher et al (Heher et al. 2015) where they developed a novel, static-strain bioreactor that stretched myoblasts embedded in fibrin over 6 days. They observed increases in sarcomeric patterning, myotube diameter and length, and an up regulation of myogenic markers.

1.3.2 Dynamic Tissue Culture Bioreactors

Stretch is not the only target of bioreactors being utilized for in vitro treatments of tissue-engineered muscle. A critical issue facing viable engineered skeletal muscle solutions is nutrient transport to cells (I. Martin, Wendt, and Heberer 2004). For constructs of a clinically or commercially-relevant size, inadequate nutrient transport can result in a necrotic tissue core surrounded by viable cells (N. Bursac et al. 1999) (Hinds et al. 2011). In this regard, dynamic tissue culture bioreactors (Figure 1) are designed to mitigate this issue, and some general categories for these devices would include: 1) Stirring Flask bioreactor, 2) Rotating Wall bioreactor, and 3) Perfusion-based bioreactors. Here we will only briefly cover each, as several reviews have thoroughly discussed them in detail (An and Li 2014) (Grayson et al. 2009) (Abousleiman and Sikavitsas 2006). In addition, a summary of the experimental implementation of these bioreactors in tissue engineered skeletal muscle applications can be found in Table 1 (see (Rangarajan, Madden, and Bursac 2014)).

Stirring Flask Bioreactors

The stirring flask is a very basic mechanical action bioreactor. Generally, the tissue construct is suspended by a string or piece of hardware from the top of the vessel allowing it to hang fully immersed in the media filling the vessel. A magnetic stirrer bar at the bottom of the flask provides the rotational force. This stirring action enhances oxygen diffusion into the media and ensures greater tissue contact with nutrients and morphogenic factors than can be achieved by normal diffusion in static media. Stirring flask bioreactors have been used with success in engineering of cardiac (N. Bursac et al. 1999) (Carrier et al. 1999) and cartilage (Vunjak-Novakovic et al. 1996) tissue, but less so with skeletal muscle (Bardouille et al. 2001). One potential drawback is that he turbulent flow caused by a stirring flask bioreactor has been known to cause damage to shear-sensitive cells and thus reduce cell viability (Carrier et al. 1999) (Papadaki et al. 2001). Interestingly, the stirring flask bioreactor can also be used in a cell seeding capacity. In this scenario, the construct (substrate/biomaterial only) is suspended in a cell-seeding solution. The rotational motion of the construct in a cell suspension uniformly transports cells to the construct surface via convection (Vunjak-Novakovic et al. 1996).

Rotating Wall Bioreactors

The rotating wall bioreactor (RWB) vessel is an improvement over the spinner flask, as the laminar flow produced within the media induces far less shear stress on the tissue construct. The RWB was first introduced by NASA as a cellular microgravity simulator (Rangarajan, Madden, and Bursac 2014). The device consists of two concentric cylinders; between the two of them is sufficient space for a tissue construct to float freely. The inner cylinder rotates and the laminar media flow produced by the Coanda effect suspends the tissue construct between the two

cylinders in a state of simulated microgravity. When cardiac (Nenad Bursac et al. 2003) (Papadaki et al. 2001) and skeletal muscle (Slentz, Truskey, and Kraus 2001) (Molnar et al. 1997) engineered tissues were cultured in RWBs the results was a more mature muscle construct. RWBs have also been used for culture of other cell types (Nishi et al. 2013) (Radtke and Herbst-Kralovetz 2012) (Skardal et al. 2010) (bone marrow mesenchymal stem cells, human vaginal epithelial cells, and human intestinal epithelial cells, respectively), but no recent application(s) for skeletal muscle was discovered.

Perfusion Bioreactors

Perfusion bioreactors display significant variations in design. The main requirement is that some type of pumping mechanism continuously cycles media through tissue constructs. Such a design ensures that nutrient transport to the interior portion of the construct is enhanced (Abousleiman and Sikavitsas 2006). The breadth of design variation in perfusion bioreactors is consistent with the numerous potential applications. For example, perfusion bioreactors have been employed for skeletal muscle tissue culture experiments on the Space Shuttle (Chromiak et al. 1998). The continuous media cycling increased morphogen and nutrient diffusion from the media to the constructs relative to that observed for batch-changed (24-hr intervals) media culture methods. In general, use of perfusion bioreactors for skeletal muscle tissue engineering results in increased maturity and functionality (Cerino et al. 2016) (Cimetta et al. 2007).

Table 1. Summary of the effect of cyclic stretch bioreactors in skeletal muscle tissue engineering (seleted).

Reference	Substrate	Model	Description	Stretch Protocol	Active Force	Quantitation	Results
(Powell, 2002)	Collagen/Matrigel	Human Muscle	Culture in MATRIGEL/collagen	5-15% strain, 8 days	NA	Histology	-Myofiber area increased. 40%, -Thickness increased 12%
(Moon, 2008)	BAM	Human MPC	LD Implant 1-4 wks	5 days	1% tetanus, 10% twitch, of Native force	Histology	Increased alignment
						SEM	Increased cell alignment and organization
(Machingal, 2011)	BAM	Rat LD, 50% injury	LD Implant 2 mo	10% stretch, 15x/h, 7 days	72% of Native Force	Histology	Desmin-positive myofibers, blood vessels, neurovascular bundles
(Govoni, 2014)	Hyaluronan mesh	Rat MSC	Novel cyclic-stretch bioreactor development	1.67Hz 1wk	NA	Histology	Thicker MSCs and multilayer development
						SEM	Significantly thicker MSCs
(Corona, 2012)	BAM	Rat LD, 50% injury	LD Implant 2 mo Double Seeding	10% stretch, 15x/h, 5-7 days	1mo, Po 120% > than NR. 2mo, Po 110% greater than NR.	Histology	Vascular and Neural Presence at interface. Pax7 elevated in all TEMRs
						Western Blot	Increased desmin, myosin, ryanodine receptor, and JP1 expression.
(Corona, 2014)	BAM	Rat TA, 20% injury	TA Implant 3 mo Double Seeding	10% stretch, 15x/h, 7 days	TEMR treated was 61% greater than NR	Histology	Increased macrophage presence
(Dugan, 2014)	Collagen 1	C2C12 and hAD-MSC mono and co-culture	Stretch reduced striation	1Hz 12% Amp Sine wave, 7 day	NA	qRT-PCR	Reduced Titin expression after cyclic stretch

LD: latissimus dorsi; hAD: human adipose-derived; h: hour; JP1: junctophilin; TA: Tibialis anterior; MSC: mesenchymal stem cell; mo: months; Po: max isometric force; wks: weeks;

1.4 Neuro-Electrical Stimulation as a Guide for Enhanced Skeletal Muscle Tissue Engineering In Vitro

In addition to mechanical stimulation, neural excitation is well established as a necessary component of skeletal muscle development, being considered one of the most important developmental cues (Ross, Duxson, and Harris 1987). In fact, in-utero stimulation of developing skeletal muscle by motor neurons is essential to proper tissue development, as denervation results in primary myotubes that are incapable of maturing into secondary myotubes and subsequently attaining the adult myofiber phenotype (Wilson and Harris 1993). Furthermore, it is well documented that a lack of skeletal muscle innervation will cause muscle atrophy (Pellegrino and Franzini 1963) (Bodine et al. 2001) (Järvinen et al. 2007). Even in mature muscles in vivo, with intact innervation, electrical field stimulation of skeletal muscle alone cannot elicit as much force as a direct neural activation (Walters, Garg, and Corona 2015). The latter observation is not surprising given the differences in the complexity of the signaling cascades involved in electrical stimulation (i.e., muscle depolarization) versus neural activation of muscle contraction at the neuromuscular junction (NMJ). More specifically, a normal, neurally-mediated muscle activation results when motor neuron action potentials result in release of acetylcholine into the synaptic cleft at the NMJ (Figure 1). Acetylcholine then binds to and activates postsynaptic nicotinic membrane receptors in the motor end plate, resulting in opening of these channels, causing a massive influx of sodium into the postsynaptic muscle fibers (Hall, John E 2010) (MacIntosh, Gardiner, and McComas 2006) (Lieber 2002). The resultant membrane depolarization spreads across the sarcolemma into the t-tubule invaginations, and induces Ca^{2+} release from the sarcoplasmic reticulum thus initiating a muscle contraction. While the

complexities of the excitation-contraction coupling mechanism in skeletal muscle are beyond the focused aims of this review, more details can be found in various review articles (Bannister 2016) (Rebbeck et al. 2014) (Gundersen 2011). Suffice it to say that in light of the critical importance of the NMJ to skeletal muscle development, maturation, homeostasis and function in vivo, investigators have tried to recapitulate the key aspects of that process by using a variety of methods/protocols to electrically excite skeletal muscle in vitro, in the absence of bona fide neuromuscular transmission. The overall goal is to provide a biomimetic cue in vitro for synaptic neuromuscular transmission in vivo. Herein, we will review two such approaches; in vitro electrical stimulation and then in vitro neurotization, respectively. Neurotization here refers to the implantation or provision of neural input to an otherwise un-innervated muscle/engineered muscle tissue.

1.4.1 Protocols for In Vitro Electrical Stimulation

In this regard, in vitro electrical stimulation has been noted to promote cell alignment, enhance myotube fusion and regulate fiber type in tissue engineered skeletal muscle (Figure 1) (Langelaan et al. 2011), (Serena et al. 2008), (Salmons and Vrbová 1967) (Juhas, Ye, and Bursac 2016). While such results are clearly encouraging, there are obvious physiological distinctions between neurotransmission (i.e., chemically mediated)-induced depolarization of skeletal muscle in vivo versus voltage/current-induced depolarization of skeletal muscle in vitro. In the realm of tissue engineering, most attempts to model muscle development in vitro have necessarily employed exogenous electrically-mediated depolarization in the absence of a neural component. However, a few groups have also attempted neurotization in vitro for tissue

engineering. We will first review studies of electrical stimulation and then alternative strategies to supply more physiologically-relevant neural components.

While the absence of in vivo neural activation results in muscle malformation, relatively little is understood regarding how to successfully simulate the impact of neural impulses in the absence of neural innervation via electrical stimulation of engineered skeletal muscle in vitro (Dennis et al. 2009). In this context, the effect of electrical stimulation on in vitro myogenesis has been studied (Donnelly et al. 2010) (Dow et al. 2004), and the results were not always positive (Stern-Straeter et al. 2005). However, as much of tissue engineering methodology is a study in biomimicry (Grayson et al. 2009), progress in the broader understanding of myogenic physiology has allowed advances in electrical stimulation methodology, as seen, for example, in the successful reports of tissue engineered cardiac muscle studies (Feng et al. 2005). In these studies, 1-2Hz stimulation (20 ms 5-20V pulses) was applied to a cardiomyocyte-laden gel in combination with mechanical stretching. This combination resulted in an enhancement of contractility. Some progress has also been made in applying electrical stimulation to in vitro skeletal myogenesis, where increases in myotube density, differentiation, thickness, alignment, spontaneous contractility and expression of cell-specific biomarkers indicating myotube fusion (Flaibani et al. 2009) (70mV, 3ms pulse, 0.03Hz, 4 h stimulus) have been observed.

Khodabukus and Baar (Khodabukus and Baar 2011) evaluated the effect of continuous electrode stimulation for 24 hours on C2C12 myoblasts. Constructs were stimulated in 0.4s duration 10Hz trains at 0.5-4 V/mm followed by 3.6s of rest. The pulse width ranged from 0.25-16ms and varied with the voltage to maintain constant pulse energy. Interestingly, electrochemical damage was observed to be dependent on excessive stimulus voltages; at or

above 6x rheobase (the minimum current resulting in a cellular action potential) and not on increasing pulse width (Khodabukus and Baar 2011). After 24 hours of electrical stimulation at field strengths varying from 0.707-1.414V/mm and corresponding pulse widths to maintain constant energy (0.5-2ms), active force production of the muscle constructs consistently increased approximately 2.5 fold to 0.67kN/m^2 or approximately 0.56% of native skeletal muscle force.

Several commercially-available options exist for applying electrical stimulation to tissue engineered skeletal muscle. These include the now out-of-production Grass stimulator (Grass Medical Instruments; Quincy, MA) (Tchao et al. 2013), the STG1000 series stimulator (Multi Channel Systems; Reutlingen, Germany) (Stern-Straeter et al. 2005) and the Ionoptix C-Pace; (Ionoptix; Westwood, MA). In 2010, Fujita et al employed the C-Pace device in an experiment to evaluate the impact of electrical stimulation on murine C2C12 myoblasts during myogenesis. The cells were initially unresponsive to electrical stimulus, however within 2 hours of stimulation at a frequency of 1 Hz with 10ms duration (1V/mm pulses), significant contractile responses – approximately 10x the unstimulated value – were observed concurrent with rapid sarcomere development. A week-long stimulus at these settings resulted in significantly increased force generation capabilities of C2C12 myoblasts in culture; approximately 0.88uN per myotube was measured, which was roughly ten times higher than the non-stimulated sample (Fujita, Shimizu, and Nagamori 2010). Interestingly, a sustained stimulation of 10Hz caused no contractility and prevented sarcomere development (Fujita, Nedachi, and Kanzaki 2007). The C-Pace has also been used in other skeletal muscle (Langelaan et al. 2011) and cardiomyocyte electrostimulation trials (Chan et al. 2013).

Donnelly et al (Donnelly et al. 2010) developed a novel, low cost, electrical stimulus bioreactor that permits independent control of the voltage, frequency, pulse width, and work-to-rest ratio (i.e., duty cycle). Interestingly, they found that 2-dimensional muscle constructs responded to high frequency, short duty cycle (100Hz, 0.3ms) stimulation with a 10% increase in protein synthesis, indicating maturation of the construct. In addition, they stimulated 3-dimensional engineered muscle constructs at 100Hz for 7 days at various voltages from 1.25V/mm – 5V/mm; these responded most positively to the 2.5V/mm, 0.1ms pulse width stimulation with roughly a doubling of force production – to ~40uN while the 5V/mm stimulus negatively impacted active force production.

Interestingly, electrical field stimulations of greater than 0.25ms pulse width have been shown to essentially bypass the t-tubule structure, instead causing uniform calcium release from the sarcoplasmic reticulum (Cairns, Chin, and Renaud 2007). Greater pulse widths do not appear to damage the muscle, (Khodabukus and Baar 2011), but the physiological depolarization mechanism responsible for normal sarcomeric calcium release is still bypassed. A more detailed description of the excitation-contraction coupling mechanism can be found elsewhere (Bannister 2016) (Rebbeck et al. 2014) (Gundersen 2011), but clearly, a more faithful recapitulation of excitation-contraction coupling in vitro appears to be required to guide further advances in in vitro skeletal muscle tissue engineering.

In summary, while such in vitro electrical stimulation can undeniably modulate the myogenic phenotype in vitro, it is equally clear that such stimulations do not yet capture the physiological impact of key aspects of neural innervation in vivo. Thus, despite progress and promise, there remains room for improvement regarding optimization of electrical stimulation

protocols in vitro as a surrogate for neural activation in vivo. As such, neurotization is another strategy being considered for this purpose.

1.4.2 Protocols for In Vitro Neurotization of Skeletal Muscle

In vivo neurotization of implanted tissue-engineered skeletal muscle constructs has been shown to significantly increase force production and maturity of the constructs (Dhawan et al. 2007) (Juhas et al. (Juhas et al. 2014). Williams et al. (Williams et al. 2013) also performed in vivo implantation of an engineered muscle construct along the femur in a rat hindlimb, and the sural nerve was sutured to the construct. One week after implantation, the active force produced by the construct increased 245% from 192 μN to 549 μN. Additionally, implanted constructs developed a capillary system and displayed the beginning of alpha bungarotoxin clustering, consistent with early stage development of NMJs. Van Dusen et al. (VanDusen et al. 2014) went even a step further, with respect to multi-tissue integration, and created a tissue-engineered skeletal muscle unit, or "SMU". This implantable construct consisted of engineered skeletal muscle with engineered myotendinous junctions attached. Twenty eight (28) days after implantation at the site of a surgically created VML injury in the rat tibialis anterior muscle (with a motor nerve sutured to the construct), the constructs displayed increased muscle fiber alignment as well as numerous nerve fibers extending from the grafted nerve into the construct; the nerves terminated at acetylcholine receptor clusters, thus providing evidence for the in vivo development of neuromuscular junctions. These studies clearly highlight the salutary effects of neurotization of implantable tissue engineered skeletal muscle, and below, we describe the impact of in vitro neurotization.

One promising method of achieving such neurotization in vitro is via neuron-myogenic co-culture. For this strategy, there is no control over the number of NMJs that may form as the co-cultured MPCs and nerve cells mature. In normal, in vivo developmental muscle physiology, individual neonatal muscle fibers are polyneurotized, but the fibers transition within several weeks to single-point (fiber) innervation via a not entirely clear mechanism (Colman, Nabekura, and Lichtman 1997) of neural pruning (Walsh and Lichtman 2003) (Balice-Gordon and Lichtman 1994) (Jansen and Fladby 1990). As the vast majority of native skeletal muscle fibers only possess one NMJ (Hall, John E 2010), excess NMJs formed in the neural co-culture scenario may also be pruned upon maturation, although to our knowledge, this in vitro scenario has not been rigorously examined.

The first well-known co-culture between muscle and neural cells was reported by Askanas et al (Askanas et al. 1987), when human muscle fibers were cultured with fetal rat spinal cord, leading to formation of neuromuscular junctions after 7-10 days, and postsynaptic nicotinic acetylcholine receptors were readily detectable after 2-7 weeks of culture. Similarly, another study of co-culture of mouse myotubes and rat spinal cord triggered significant fusion of myotubes into myofibers – some reaching 1 cm long, and formed well-developed sarcomeres and mature NMJ metabolic enzymes (Wagner et al. 2003). Umbach et al (Umbach et al. 2012) cultured C2C12 myoblasts and embryonic stem cell-derived motor neurons. Dual patch-clamp measurements confirmed the presence of spontaneous and stimulated neurotransmitter release from newly-formed NMJs as well as the presence of robust synapses. Morimoto et al (Morimoto et al. 2013) performed murine neural/myogenic co-culture on a micropatterned surface and observed formation functional NMJs and contractile fibers. Finally, Martin et al (N. R. W. Martin

et al. 2015) attempted a more physiologically-relevant murine 3d neural co-culture and observed formation of striated myotubes and a 1.5 fold increase (4.16mN from 1.71mN) in tetanic active force production over monoculture myocytes when electrically stimulated.

The recent work of Scott et al. (Scott et al. 2017) provides interesting contrast to co-culture of neural and myogenic cells. These investigators used agrin-coated microspheres embedded into fibrin biomaterial constructs to evaluate the possibility of exerting high spatial control over development of skeletal muscle acetylcholine receptor (AChRs) clusters. The constructs were then seeded with C2C12 myoblasts or rat muscle derived cells (MDCs) and placed in a cyclic stretch bioreactor. Interestingly, the combination of embedded agrin-coated microspheres and bioreactor-preconditioning displayed a strong synergistic relationship with respect to dramatically enhanced formation of AChRs, relative to the presence of agrin-coated microspheres in static MDC seeded fibrin-based constructs. As this was a preliminary study, results are very encouraging but much work remains on the path to in vitro functional innervation of engineered skeletal muscle tissue using this strategy.

In summary, neural stimulation is a critical modulator of skeletal myogenesis both in vivo and in vitro. Applying what is known about this process in vivo to improved design of tissue engineered skeletal muscle in vitro remains a major challenge. Current approaches are diverse, and it may be that a combination of electrical stimulation coupled to identification of strategies that more faithfully recapitulate neurochemical synaptic transmission will ultimately be required to ensure creation of a more physiologically-relevant adult muscle phenotype in vitro.

Table 2. **Summary of Effect of Electrical or Neural Stimulation on In Vitro Skeletal Muscle Tissue Engineering (Selected)**

Reference	Substrate	Model	Description	Stimulus Protocol	Active Force	Quantitation	Results
(Askanas, 1987)	NA	Human Myofibers	Innervate myofibers w/ fetal rat spinal cord	NA	NA	Cytochemistry	Presence of new nACh receptors
(Wagner, 2003)	NA	Mouse Myotube	Co-cultured mouse muscle and fetal rat spinal cord	NA	NA	Electrophysiology	Ach receptors displayed mature phenotype
(Stern-Straeter, 2005)	Fibrin	Rat Myoblast	Electrical stimulation effect examined on 3d myoblasts	6.8mA, 4ms pulse for 250ms, every 4s, 8 days	NA	qRT-PCR	MyoD, myogenin and AChR-ε Decrease
(Fujita, 2007)	Coverslips, Culture Plates	C2C12	Control Ca^{2+} transients with electrical pulse stimulation	10 Hz Continuous , 2h	NA	Calcium Imaging, Immunoblotting	Lack of contractility or sarcomere assembly
(Flaibani, 2009)	Micro-Patterned poly-L-lactic Acid	Rat Satellite Cells	Effect on alignment and differentiation of micropatterned substrate and electrical stimulation	70mV, 3ms pulse, 0.03Hz, 4 h	NA	Immunostaining, RT-PCR, Galvanotaxic Analysis	Increased differentiation, density, thickness, alignment, fusion, contractility
(Fujita, 2010)	Collagen	C2C12	Use UV-crosslinked film to measure active myotube contractility	1 Hz, 1V/mm, 10ms pulse, 1wk	~10x increase	Western Blot, Fluorescence Microscopy Active Force Production	Thicker stimulated cell layer, Up regulation of Bcl-2, Incr. Protein Content
(Donnelly, 2010)	Sylgard PDMS	C2C12	Novel electrical-stimulus bioreactor development	4x 0.1ms pulses in .4s train, rest 3.6s, 1.25-5 V/mm, 7 days	~2x increase	Active Force Production	Stimulation at 2.5V/mm had best results for 3d constructs
(Khodabukus and Baar, 2011)	Fibrin	C2C12	Inversely vary pulse width and voltage to maintain constant energy	10Hz, 0.4s train, rest 3.6s, 0.5-4V/mm, pulse width 0.25-16ms	~2.5x increase	Active Force Production	Voltages greater than 0.5 and less than 3V/mm increased force. Damage caused by excess voltage (>3 V/mm)
(Umbach, 2012)		C2C12	Development of low-density neural co-culture method	NA	NA	Microscopy and electrophysiology	Presence of functionally mature NMJs after 1-2 d
(Morimoto, 2013)	PDMS	C2C12	Neural co-culture on patterned substrate	NA	NA	Immunocytochemistry, RT-PCR	Functional NMJs and contractile muscle fibers
(Martin, 2015)	3d Fibrin Construct	Rat Myoblast	3d Neural coculture	NA	~1.5x increase 4.16uN vs 1.71uN	Immunohistochemistry, Active Force Production	Increased force production, formation of striated myotubes
(Scott, 2017)	Fibrin	C2C12 and rat MDC	Localized agrin placement	Cyclic stretch bioreactor	NA	Histofluorescence	Increased concentration of AChRs commensurate with cyclic stretch

AchR: acetylcholine receptor, MDC: muscle derived cells; NMJ: neuromuscular junctions, PDMS: polydimethylsiloxane

1.5 Conclusions

In vitro development of implantable tissue engineered skeletal muscle for treatment of VML and VML-like conditions is a rapidly developing field with revolutionary potential for therapeutic improvement of functional outcomes. The sheer complexity of myogenesis and myogenic physiology means that this will ultimately be a daunting task. Recent trials – built upon years of accumulated knowledge – have shown that a focus on in vitro methods such as cyclic stretch and neuro-electric stimulus can indeed improve the functional capacity of engineered skeletal muscle implants. By no means, however, are improvements to this technology limited to these factors. In fact, improved functional outcomes and more wide spread clinical applications of implantable tissue engineered skeletal muscle technologies for VML repair, will likely require increasing levels of technological sophistication/complexity to ensure a more faithful recapitulation of the native muscle phenotype and function.

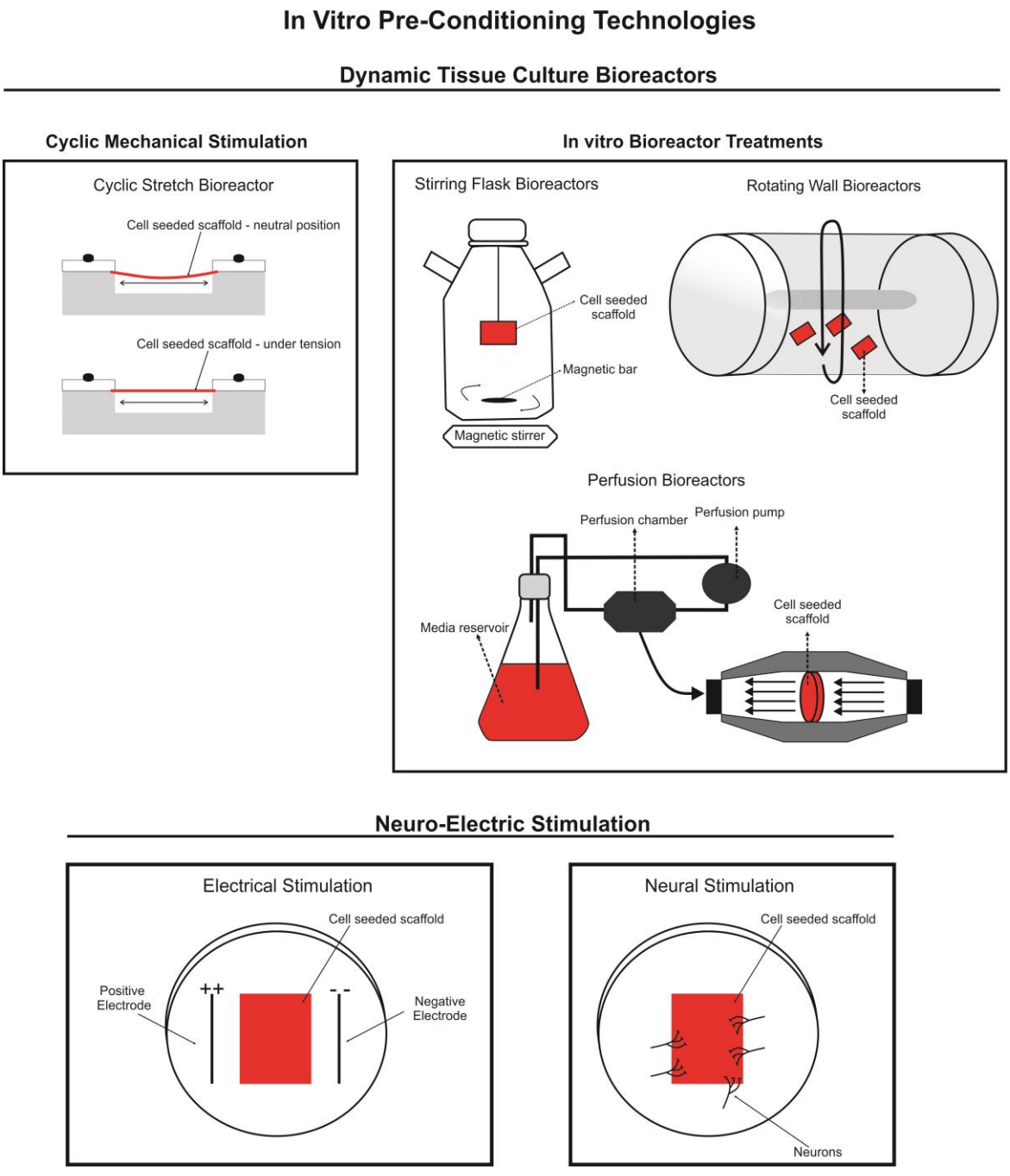

Figure Legends

Figure 1: In vitro pre-conditioning technologies. Technologies can be divided in 2 categories: dynamic tissue culture bioreactors and neuro-electric stimulation. Dynamic tissue culture bioreactors can be further divided into cyclic mechanical stimulation (i.e. cyclic stretch bioreactor) and in vitro bioreactor treatments (i.e. stirring flask bioreactors, rotating wall bioreactors and perfusion bioreactors). Neuro-electric stimulations can be done via electrical stimulation or neural stimulation.

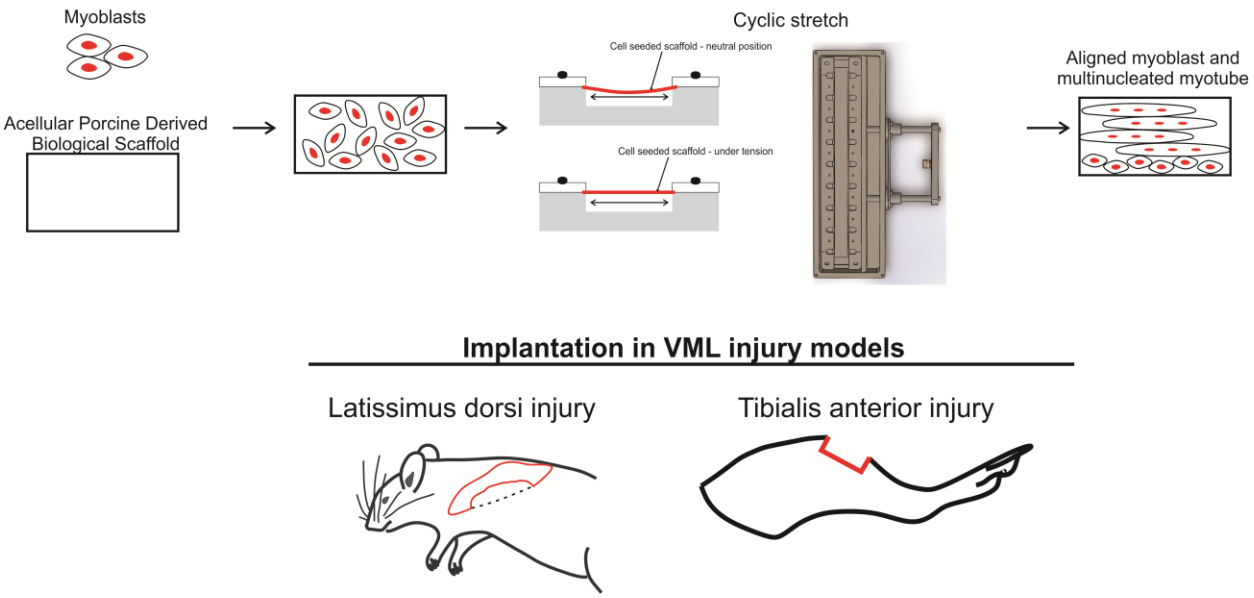

Figure 2: Schematic representation for the application of TEMR (Tissue Engineered Muscle Repair) constructs in TE/RM. Myblasts are seeded in a acellular scaffold derived from the lamina propria of a porcine bladder. In vitro cyclic stretch preconditioning lead to cell alignment and myoblast fusion into myotubes. Construct is implanted in different VML injury models, including the resection of 50% of a mouse latissimus dorsi muscle and the resection of 20% of a rat Tibialis anterior muscle (Machingal et al. 2011) (Corona et al. 2012) (Corona et al. 2014).

2. Advances to the Regenerative Therapeutics Bioreactor

2.1 Bioreactor Description

2.1.1 Introduction

As briefly discussed in the previous section, the Regenerative Therapeutics Lab (RTL) employs a custom-designed bioreactor for maturation of implantable muscle cell-seeded constructs. The inspiration for this bioreactor was also described in the previous section, however, the actual implementation, construction, and protocol are all custom-developed. This brief section will describe bioreactor specifications, and the bioreactor portion of TEMR production.

2.1.2 Specifications

The RTL bioreactor is a device designed to apply cyclic stretch to extracellular matrix (ECM) scaffolds. Before installation in the bioreactor, these scaffolds are seeded with muscle progenitor cells (MPCs) which attach to the scaffold and form an implantable construct known as a Tissue-Engineered Muscle Repair, or TEMR. Two main manifestations of the bioreactor exist; the older one is designed such that the scaffolds are fixed in the bioreactor when mounted, the newer design allows the scaffolds to be fixed onto a removable "frame" which is placed into the bioreactor (Figure 2.1.1). The implications of this design are thoroughly discussed in Section 3. For the purposes of this thesis, we will focus on the newer generation of removable-frame bioreactors.

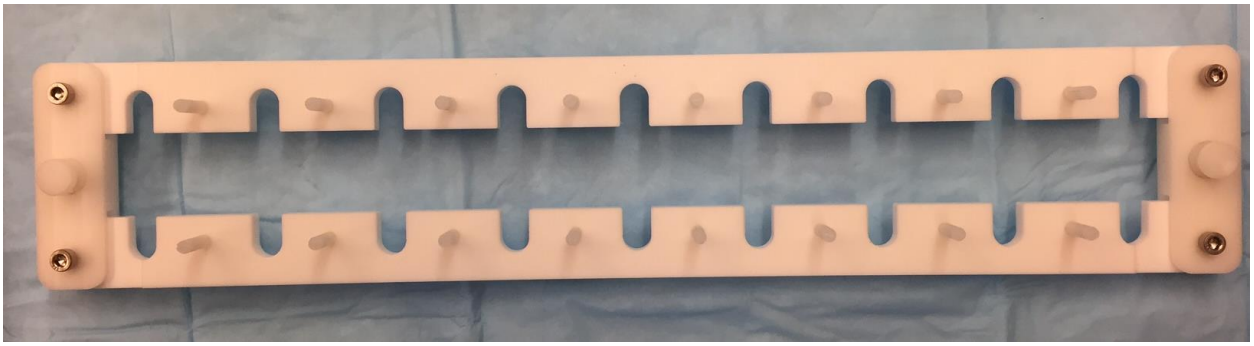

Figure 2.1.1, Bioreactor Removable "Frame"

In its most-used iteration, the bioreactor holds 8 scaffolds concurrently, each with an installed length (space between frame bars) of 3.0cm (Figure 2.1.2). The TEMR scaffolds are secured into place within the bioreactor by means of Teflon (PTFE) clamps mounted on nylon upright threaded posts; the clamps are compressed on the post by nylon thumbnuts. The bioreactor is fabricated from Teflon, stainless steel, acrylic, and nylon. The body of the bioreactor as seen in Figure 2.1.3 is milled from a single block of Teflon, thus ensuring structural and liquid integrity.

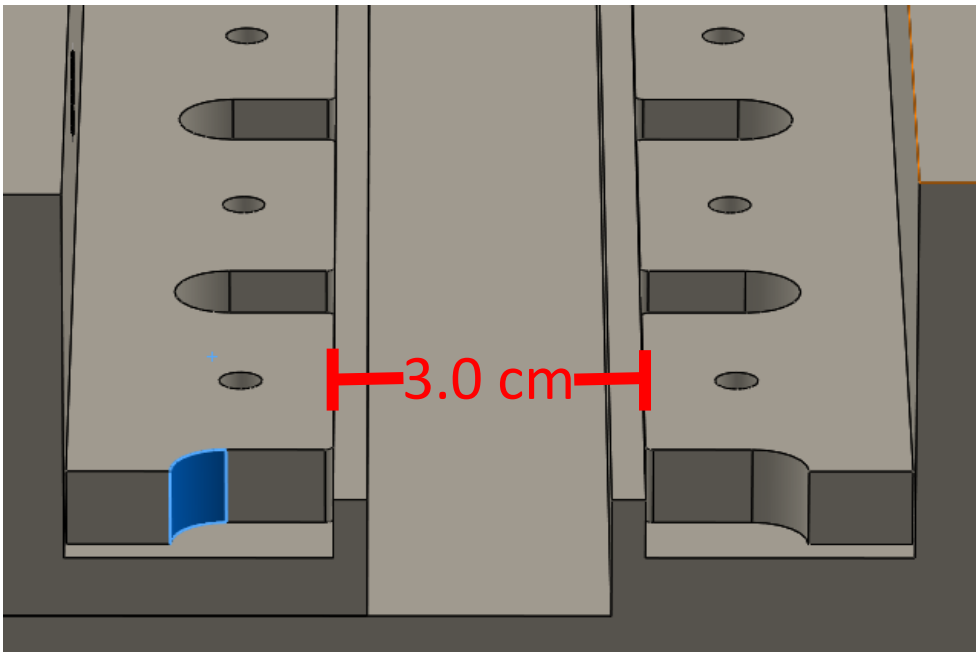

Figure 2.1.2, 3.0cm scaffold mounting distance

As previously mentioned, the scaffolds are mounted onto a removable frame assembly. They are secured into place via Teflon clamps positioned over upright threaded nylon studs. When fitted with

Figure 2.1.3, Bioreactor Body, Translating Arm, and Motor

nylon nuts, the studs allow compression of the clamp, thus holding the scaffold in place. The frame is held into place within the bioreactor via a friction fit. One side of the frame is held stationary within the body, while the other sits in a laterally translating Teflon “arm”. The translating arm is connected by a series of stainless steel components to a custom Haydon Kerk/Ametek (Waterbury, CT) linear stepper motor situated horizontally at the front of the bioreactor body. These are all also visible in Figure 2.1.3. In default operation (see Chapter 3), the motor stretches the installed scaffolds by a preset distance of 3mm, or 10% strain.

While much of the bioreactor consists of custom-designed components, all hardware is off-the-shelf. Due to the softness of Teflon, HeliCoils (Stanley Engineered Fastening, USA) are used in the design. They are installed in the motor plate mounting holes as well as in all the body holes used to secure the lid.

2.1.3 Bioreactor Protocol

Based on previous work (Corona, Ward, Baker, Walters, & Christ, 2014), we have developed and maintained a protocol for the bioreactor stretch sequence. Immediately upon starting the protocol, the secured TEMR scaffolds are cyclically stretched 10% of their 3cm starting length; 3mm. Each 10% stretch occurs over the course of 10 seconds, and the retraction is over the same time period. This cycle is repeated three times a minute for the first five minutes of the hour. Thus, the stretch-retraction cycle occurs continuously for 15 repetitions over five minutes. The device then waits for 55 minutes and repeats the cycle. New trials within the lab are investigating the possibility of increasing the stretch magnitude or perhaps increasing the number of stretches per hour.

2.1.4 Bioreactor Notes

The bioreactor in its current iteration is a robust piece of equipment. All components within the device are capable of ethylene oxide sterilization at 37C. In fact, some bioreactors within the lab have completed this cycle more than 100 times, with no ill effects. It is, however, important to note that the

manufacturer of the motor – Haydon Kerk – does not guarantee the motors' performance after exposure to these conditions due to the increased risk of corrosion.

The only outstanding weakness in the current design are the screw interfaces with the Teflon body. To strengthen these joints, HeliCoils are installed in all structural support holes on the body. HeliCoils act like wall anchors and expand when a screw is inserted, thus increasing the gripping force of the screw in the soft Teflon. However, care must still be taken when assembling or disassembling the bioreactor. Force when tightening should not exceed ¼ turn past hand tightness.

2.2. Bioreactor Controller

2.2.1 Introduction

Figure 2.2.1, Regenerative Therapeutics Bioreactor

As discussed in previous sections, employing a bioreactor to apply cyclic stretch to developing tissue-engineered muscle repair (TEMR) scaffolds yields significant improvement over non-stretched scaffolds. However, a mechanism is required to provide precise, simple, and cost-effective control to the bioreactor. As previously described in the Specifications section of Chapter 2, the bioreactor consists of a large Teflon body equipped with a linear stepper motor. The motor is attached via stainless steel hardware to a slide mechanism capable of concurrently stretching 8 scaffolds. The scaffolds are normally stretched 10% (3mm) beyond their starting length of 3.0cm. To provide sufficient accuracy, a precise stepper motor is necessary. A semi-custom model (E43H4P-05-A01) from Haydon Kerk is employed which allows control resolution as fine as 0.25µm linear travel. Control of this assembly is currently achieved via a microcontroller-based device with an extremely simple user interface. A printed circuit board (PCB) implementation which shortens and simplifies assembly of the controllers is in its third generation. Although stepper motors are extremely precise in their movement, a software and hardware device upgrade is in development which tracks any motor movement error via a digital encoder and alerts the user if error is detected. The entire assembly is currently U.S. Patent Pending.

2.2.2 Previous Controller

Before the microcontroller-based device was created, the bioreactor controller employed in the Regenerative Therapeutics Laboratory consisted of a custom PC-based program communicating via USB with a Phidget 1067 bipolar stepper motor driver module. While this assembly successfully controlled the bioreactor stepper motors, it had several distinct disadvantages. First, the user interface (UI) was

not intuitive. It was a "building block" style program where the user designed a step for the program to follow; once the step design was completed it was placed into a column of rows through which the program continuously cycled. Second, the program suffered from temporal inaccuracy. Due to lack of internal clock referencing, the timing would drift as much as an hour over the course of the week-long experimental protocol. This caused some difficulty in accurately timing experiments as well as simply being unacceptably imprecise for a piece of research equipment. However, the most significant limitation of the previous controller was the fact that each PC was only able to control one bioreactor. This fact drove up both financial and physical space costs; a PC and Phidget assembly costs anywhere from $400-1000 as well as requiring significant laboratory space.

A previous UVA BME capstone team from 2015 had attempted to solve this issue via a new MATLAB-driven user interface, however, their solution was never fully functional nor complete, and still required one PC per bioreactor. Clearly, a better, cheaper solution was necessary.

2.2.3 New Controller Development

In developing a new controller system, we had several criteria that needed to be met:

1) Precise stepper motor motion control with resolution of 5μm or less.

2) Simple user interface

3) Maintain temporal accuracy to within 1 second/wk

4) Cost less than the existing system

With easy-to-use microcontrollers at historically low prices, a microcontroller-driven control system was an attractive option for our lab. We consulted Dr. Gavin Garner from the Mechanical and Aerospace Engineering Department, and based on his extensive experience with Parallax microcontroller systems, developed a controller system architecture based on the Parallax Propeller microcontroller (Parallax Inc, Rocklin, CA). This system utilized entirely off-the-shelf components, significantly driving down the unit cost.

2.2.4 Device Specifications and Components

This new generation of bioreactor controller meets or exceeds all the aforementioned criteria, with the almost exclusive use of readily-available off-the-shelf components. This section will detail each component of the controller, as seen in Table 2.2.1, then describe the operating characteristics of the device. In addition, a reference table of system resolutions is visible in Table 2.2.2.

Active Components	Description	Source
Propeller Chip	Microcontroller	Parallax
A4988 Stepper	Linear Motor Driver	Pololu
DS3234 RTC	High-Accuracy Clock	Sparkfun
ADM1602K Screen	LCD Screen	Sparkfun
S LCD Backpack	Serial Driver for Screen	Sparkfun

Table 2.2.1, Bioreactor Controller Active Components

System Name	Resolution
CPU Speed	6.25MHz
Stepper Motor Drive	0.25µm
RT Clock	± 2 sec/year
Encoder	400 counts/rev

Table 2.2.2, Bioreactor Controller Component Resolutions

Propeller Mini

The “brain” of the controller system is the Parallax Propeller microcontroller. We utilized this 8-core, 32-bit processor in a space-saving, $24.99 breakout board configuration called the Mini. In the stock configuration, the device is equipped with a 5MHz crystal. However, replacing the crystal with a 6.25MHz unit allowed it to be overclocked to 100Mhz and ensured the ability to write timed code with far less calculation required (10ns per clock). For ease of use, the unit is programmed with Parallax’s proprietary programming language called Spin. In this application, it is powered by a 12VDC source. The board’s onboard 5V regulator is used to power some of the other components which require a 5VDC power source. The Mini’s programming interface is via a USB cord equipped with Parallax’s USB-to-serial conversion tool called the Prop Plug. The Propeller “brain” of the system is utilized for several functions in this application; accepting user input in the setup phase, receiving data from the real-time clock, sending control signals to the stepper motor driver, and outputting relevant data to the LCD screen.

A4988 Stepper Motor Controller

While the Propeller is capable of producing the signal necessary for controlling the bioreactor’s linear stepper motor, realization is simplified by employing a microstepper driver chip. This allows the Propeller to simply send a single pulse every time the motor is required to perform a microstep. The microstepper controller translates this signal into a pulse-width-modulation (PWM) power signal, which is how the bipolar stepper motor in the bioreactor assembly is energized to move. The coil current output from the A4988 is manually set to output a maximum of 0.7A via a small potentiometer on the A4988’s breakout board. In addition, the A4988 has selectable microstep values; full, ½, ¼, 1/8, and 1/16. For this application, 1/16 steps are selected to increase position resolution ($1/16^{th}$ of 1.8° per step or 0.1125°/microstep). Based on this microstepping and the thread size of the leadscrew (0.00396875mm of linear translation per microstep), a resolution of 0.25µm is achieved. This is 20x better than our maximum acceptable resolution of 5µm.

DS3234 Real Time Clock

Keeping time is a critical function of the bioreactor controller, as our specific protocol is timed to occur on the first 5 minutes of each hour for 5 days. As previously mentioned, our former PC-based control system tended to drift up to an hour during the course of the protocol. To combat this issue, we employ a DS3234 real-time clock chip which is accurate to ±2 sec/yr. We employ the low-cost ($19.95) breakout board realization from Sparkfun. The device communicates with the Propeller Mini via serial peripheral interface (SPI) and reports seconds, minutes, hours, day, date, month, and year. In addition, this specific board incorporates a replaceable 12mm 1.5V CR1225 lithium button cell battery which maintains clock data when system power is off. To set the clock, Dr. Garner wrote a script in Spin which can be uploaded to the Mini and sets user-determined values in the clock. Once the normal bioreactor controller protocol is uploaded and running on the Mini, one of the Mini's 8 processors is used to

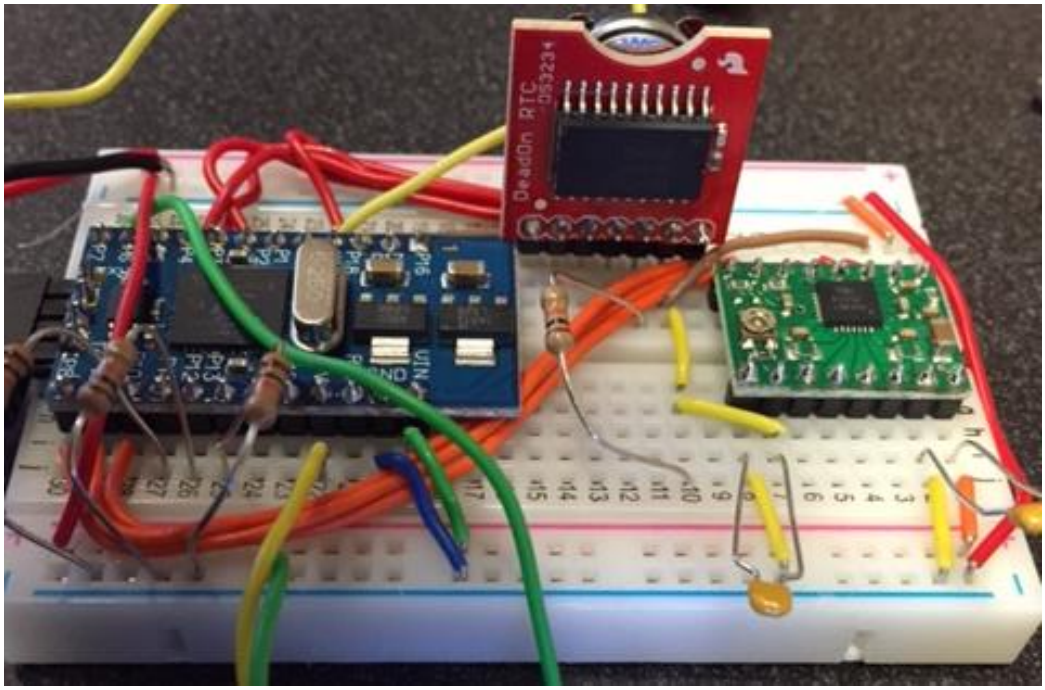

Figure 2.2.2,
Prototype Next-Generation Bioreactor Controller

constantly receive timing information from the clock. This data is used in two main ways. First, when a user starts the bioreactor controller protocol via the button-based user interface, the system waits until the next minute to begin the protocol. This simplifies record keeping by assuring that all program actions occur on a minute value. In addition, the protocol has variable settings which, due to computational error, change the duration of the motor running by a minute amount. The system references back to the clock for timing after each of these motions, which keeps the protocol precisely timed.

ADM1602K LCD Screen and S LCD Backpack

This basic 16x2 white on black LCD screen serves to display options for the user interface and pertinent protocol information. On its own, the LCD screen uses HD44780 commands, which requires 11 GPIO pins; this is a significant pin burden for almost any microprocessor. To counter this, we employ the SparkFun Serial Enabled LCD Backpack. This converter solders directly into the screen's 11 input pins and accepts single-wire serial (default 9600 bits per second baud rate) ASCII outputs from the Mini and converts them into HD44780 commands usable by the screen. In addition, 5V power output from the Mini's voltage regulator is input to the serial backpack and provides power to the screen.

2.2.5 PCB Realization

The configuration of the first prototype of this next generation bioreactor controller (BrC) can be seen in Figure 2.2.2. Although this prototype provided the desired performance characteristics, such an implementation was too fragile for the heavy use required of a BrC. In addition, some of our partner labs across the country require BrCs to be shipped to them, and a breadboard-based arrangement is unsuitable for such shipment, as breadboard wires are simply held in place by friction and can come loose. Thus, a logical option to "clean up" the design as well as fortify it for transport was to create a PCB implementation.

To create such a device, multiple software packages were evaluated to determine which would be most suitable. Autodesk EAGLE was selected, which is a freely-available, widely-used PCB-design

package. While the software has a somewhat steep learning curve, once comfortable, a user is able to take advantage of an assortment of built-in features including lead autorouting and interference testing. Within the program, product design occurs in two phases. First, individual components for placement on the PCB are either designed or pulled from the relatively extensive object library. While passive elements such as resistors and capacitors were contained in the library, all other components had to be custom designed. The components are then (non-geometrically) laid out as a schematic in the project workspace and connections are drawn. An image from this design stage is visible in Figure 2.2.3. Next, the layout is transferred to a spatially-relevant rendering of the PCB design which includes all PCB features such as through-holes, component locations, and connection routing. Figure 2.2.4 represents this step. Finally, when all design is finished, EAGLE allows the export of industry-standard PCB design files called Gerber files. These can be sent directly to a PCB manufacturer. The PCB for the bioreactor controller was designed for simplicity, space saving, and low cost. To meet these criteria, several design specifications had to be ensured. For simplicity, the design is such that all components can simply be dropped into the appropriate place on the PCB and soldered with no additional wiring. To ensure conservation of physical space, board components are physically located as close to each other as possible while still providing room for relatively low-trained personnel to perform the component soldering. Low cost was achieved via contracting a Hong Kong-based company called Seeed that specializes in low-cost, low-volume PCB manufacturing. With quantities of 10 PCBs per order, the unit price was only $4.90, although lead time was approximately 3-4 weeks. The majority of controllers currently are 2nd-generation PCB-based, although the 3rd generation has been received and assembly is beginning. An assembled 2nd generation BrC PCB is shown in Figure 2.2.5.

In its finished state, the PCB contains header pin holes for all passive and control components, system power (12VDC), three user-interface buttons, four motor output leads, power and transmission to the screen, and inputs for the encoder error-control mechanism.

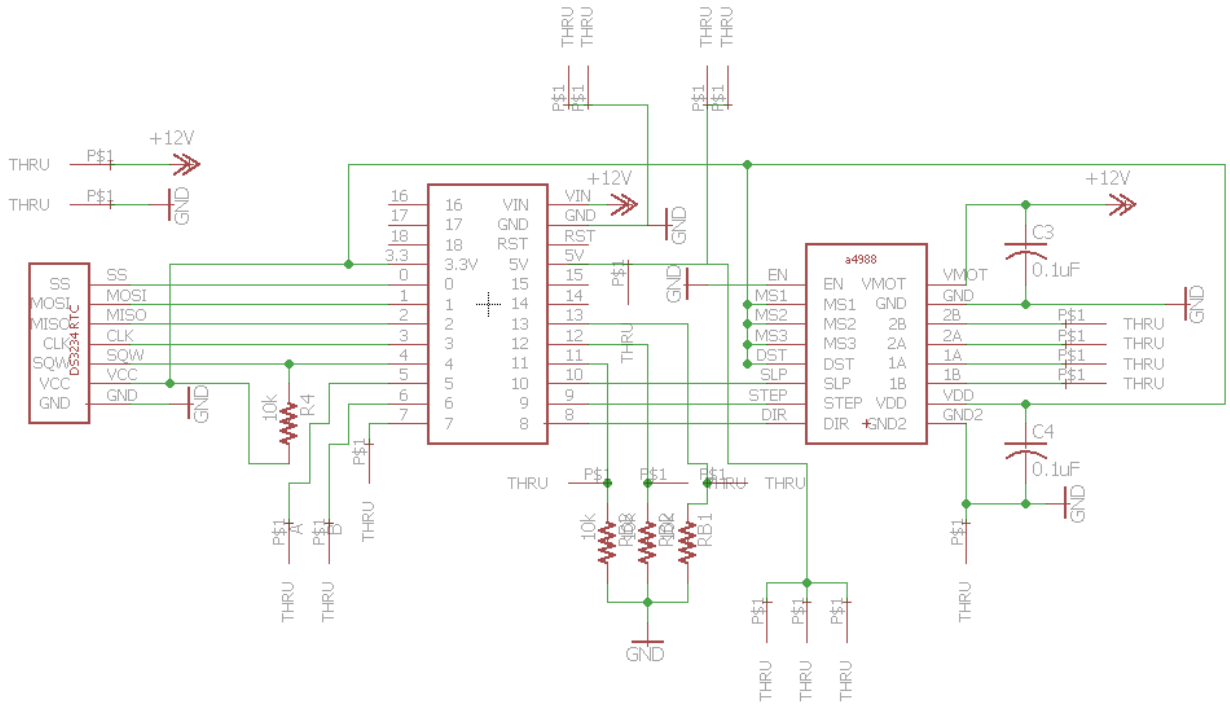

Figure 2.2.3, BrC PCB
Eagle Schematic

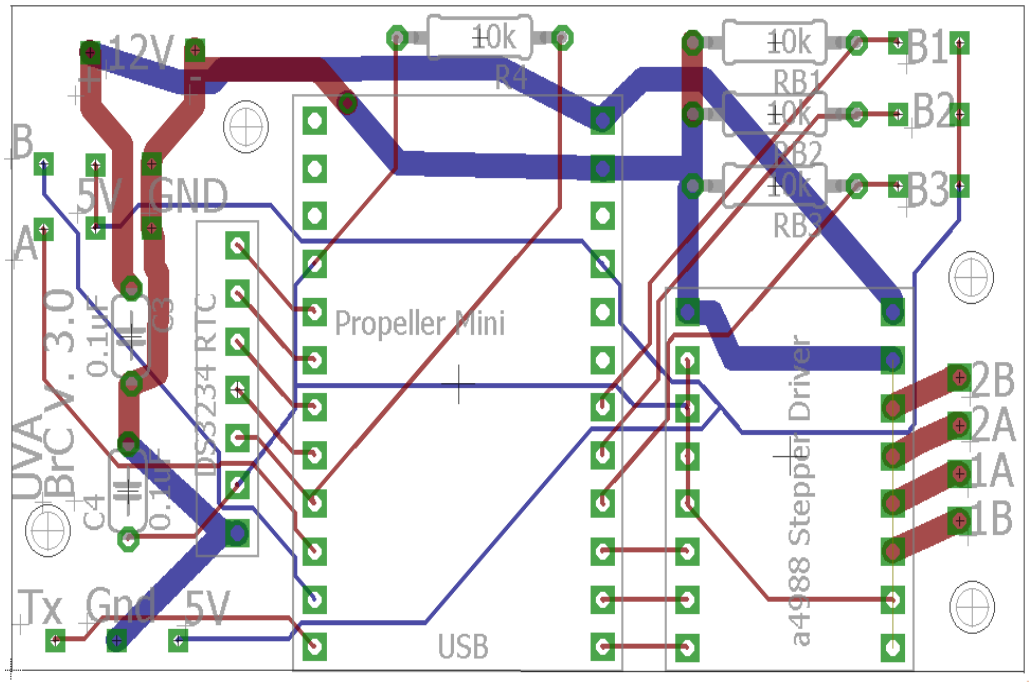

Figure 2.2.4, BrC PCB Eagle
Board Layout

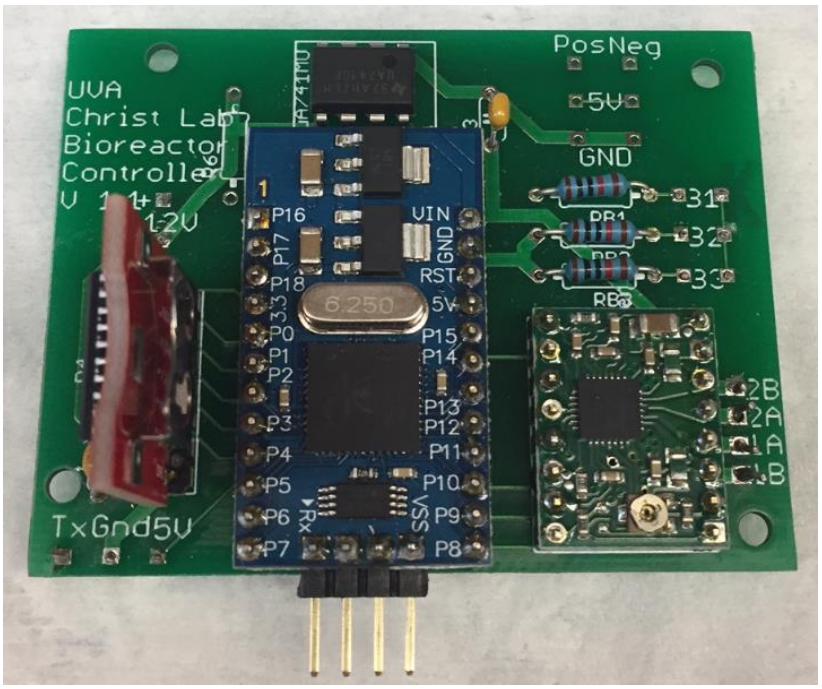

Figure 2.2.5, 2nd Generation Assembled BrC PCB

Figure 2.2.6, BrC GUI

2.2.6 Control Code

With the prototype implementation of the bioreactor controller designed by Dr. Gavin Garner, no user interface (UI) was necessary, as the device continuously ran after it was powered on. Bioreactors could be attached and detached from the control signal as needed. Indeed, to allow multiple bioreactors to run concurrently, the control signal from the Propeller Mini was "daisy-chained" to multiple, individually-powered stepper motor driver chips. In this way, multiple bioreactors could be run while ensuring that excess current was not required from a single stepper controller. Although multiple bioreactors were able to run, the experimenter was still required to record the start time and manually disconnect the bioreactor when the appropriate cyclic stretch period (5 days) had elapsed.

Additionally, the control code written by Dr. Garner applied to an idealized bioreactor where no backlash existed within the system. However, due to some flexibility in the physical design of the bioreactor and motor interface, some finite rotation of the motor is able to occur without horizontal translation of the scaffold holder assemblies. Thus, physical manipulation of the motor was undertaken to determine the amount of such backlash in the assembly. After multiple measurements, an average value of about 2000 was determined which is added to the number of steps the motor should travel in each stretching and retracting motion to account for approximately 500μm of backlash in the leadscrew.

2.2.7 User Interface

To mitigate this manual intervention required in the stretch process and to increase the flexibility available to the experimenter, a graphical user interface (GUI) was developed. This interface is based on a three-button input, and output from a 16x2 LCD screen. The GUI is written in the main control loop of the Propeller Mini. Upon powering the system up, the user lands on the main menu, which displays "Bioreactor Controller v. 1.2" on the top line, and the options "Go," "Setup", and "Info" on the bottom line. Figure 2.2.6 shows the main menu and GUI flow. Upon selecting "Info", the user is

taken briefly to a menu showing the developers, date, and information regarding the device, then returned to the main menu.

If “Setup” is selected, the first menu option is “Stretch”. The default value here is 3000µm, and the user is able to adjust this value up or down by increments of 10µm. Upon selecting the correct value, “Next” is selected. The next screen allows the user to select the duration of the experiment; default is 5 days or 120 hours. After this, the user can select the specific type of motor installed on the bioreactor. The preset is for our custom Haydon Kerk model, but two others are available. Each motor type required specific tuning within the code based on the varying linear travel per step of each stepper motor. On the next screen, the question “Delay Start?” appears. If “Yes” is selected, an adjustable preset value of 24 hours is programmed to pass before the device will begin the protocol. When setup is complete, the user is returned to the main menu.

If “Go” is selected, the system waits until the top of the next minute before starting. Again, this simplifies internal record-keeping for the device. While running, the device will display the number of repetitions – defined as the number of complete hour-long run cycles – and the start time. After the protocol has been completed, the screen shows “Protocol Success.”

2.2.8 ErrorTrack

Due to this device’s future involvement with an FDA-sanctioned clinical trial, I preemptively developed a system capable of ensuring the rotational travel of the bioreactor stepper motor matches the software commands. This system utilizes a US Digital E5 400 count/rev digital quadrature encoder mounted on a customized stepper motor from Haydon Kerk. The encoder is of the optical variety; it employs a slotted disk attached to the stepper motor’s shaft which alternately blocks and passes light based on the shaft position. Passed light is recorded as a digital 5V signal, while blocked light is 0V. As it is a quadrature encoder, two signals are collected; one 90 degrees out of phase with the other. The sequence of changes in this 2-bit Gray code signal allows the determination of the direction of rotation

and total distance traveled. The ErrorTrack system is written into the code for the Propeller Mini and requires two GPIO pins; one for each signal coming out of the encoder. Based on the number of motor revolutions necessary for the bioreactor to achieve 3mm (or otherwise selected) linear travel, a theoretical count of encoder signals for a full stretch cycle can be calculated. At the beginning of the stretch cycle, ErrorTrack starts with a count of zero. It then observes the direction of rotation and increments upon stretching or decrements upon retraction. When the bioreactor has completed a full extension, the number of count signals received from the encoder should match (within a very small, roughly 0.1% error tolerance) the theoretical count calculated within the code. Once the bioreactor returns to the retracted position, ErrorTrack's count should have decremented back to zero. If these conditions fail to be met, ErrorTrack will alert the experimenter.

2.2.9 Malfunctions

In the period since the new generation of microcontroller-based BrCs has been developed, several device malfunctions have occurred. First, one of the LCD screens suffered an internal error and ceased functioning. Second, one of the Propeller Mini units also ceased function after some unknown event, although it is suspected to have been due to an electrical short after inadequate training of undergraduate assistants aiding in device assembly. The device uses Category 8 (CAT8) Ethernet cable to connect the controller to the bioreactor and 4-pin XLR connectors at the bioreactor end of the cable. A trend has been observed of accidentally severing the wires within the cable when cutting through insulation to solder connections to the controller and XLR connector. Extra caution is thus required, and several existing BrC units have required re-soldering of the cable leads.

2.2.10 Future Directions

Although significant progress has been made in the bioreactor controller, further advances await. The simplest is the standardization of all motors across bioreactors. This will eliminate the motor selection section of the setup menu, as well as lessen the risk of a user incorrectly selecting a motor in

the BrC setup phase. Next, a touchscreen interface would be a relatively easy upgrade to make to the design; however the value added would be almost solely aesthetic, as function is projected to remain almost identical to the current three-button interface. Finally and most involved, real-time tracking of the forces and strain of TEMR constructs being stretched would allow the BrC to dynamically alter the stretch protocol. Instead of applying a constant 10% strain, for example, the system could utilize load cells to apply a given stress value which the system would maintain over time. Currently, this is not feasible as scaffold remodeling occurs over the course of the stretching protocol and thus the stress-strain relationship is not fully constant over time. A group from Johns Hopkins has created a bioreactor system containing the necessary hardware to perform this protocol, although their control system is computer-based and not cost or space optimized (Cook et al., 2016). However, the next chapter will discuss my co-mentorship of a UVA BME capstone team that worked this year on developing a method to reduce errors in strain while allowing continued use of our existing bioreactor and bioreactor control equipment.

2.3. Advances in Scaffold Mounting Capability

2.3.1 Introduction

As previously discussed, in the UVA Regenerative Therapeutics Lab, we employ a cyclic stretch bioreactor to provide mechanical stimuli to maturing muscle progenitor cells seeded onto extracellular matrix scaffolds. Cyclic stretch has repeatedly been shown to encourage the maturation and function of these cells (Pollard, McGonnell, and Pitsillides 2014) (Hall 2010) (Schiaffino et al. 2013); a necessary factor for development of implantable constructs. Our proprietary bioreactor has the capacity to stretch eight mounted scaffolds using one stepper motor and the controller described in the previous section. The scaffolds are individually, manually mounted in the bioreactor and tensioned by eye. The bioreactor stretch protocol is then begun, and scaffolds are removed at the end of the cycle.

Although positive results have been observed from use of the bioreactor in producing these implantable constructs, several issues exist with the design of the system as it currently stands. First, there is very little control over the mounting method, leading to possible variances in static strain across the individual scaffolds. Second, there is currently no way to observe this strain experienced across all and between each scaffold in the bioreactor. Finally, our system possesses no method to quantify the passive forces experienced by the scaffolds during the stretch protocol.

The BME capstone team which I co-mentored this year took on the challenge of designing solutions to some of these issues. The team's final developments addressed the mounting methodology and strain quantitation issues. Their work can easily stand as the basis for another team's capstone project.

2.3.2 Current Scaffold Mounting Method

The current method for mounting TEMR scaffolds into the bioreactor assembly consists of several steps; mounting mechanisms and a mounted scaffold can be observed in Figure 2.3.1. First, the two sides of the bioreactor stretching mechanism are spaced properly – to 3cm – and filled with cell proliferation media. Next, the entire width of the shorter dimension side of the TEMR is placed onto one edge of the stretching assembly. This end is secured by a Teflon clamp and secured with a single nylon thumbscrew. Then, the opposite side of the TEMR is draped across the media-filled space to reach the opposing ledge of the stretching assembly. It is tensioned by eye to the proper value, and set on the ledge while the clamp is lowered and tightened. Unfortunately, as the scaffold must be released for the clamp to be lowered, there is no way to maintain the desired tension while the clamp is being tightened. This results is notable variance across scaffold mounting tensions. While this method produces TEMR mountings that appear similar to the eye, it is important to recall that the TEMR is a large-scale amalgamation of many micro-scale cellular units. Consequently, values such as TEMR pretension that exhibit a notable variance in the current method could be experienced as a much larger effect on the several-orders-of-magnitude-smaller muscle progenitor cells.

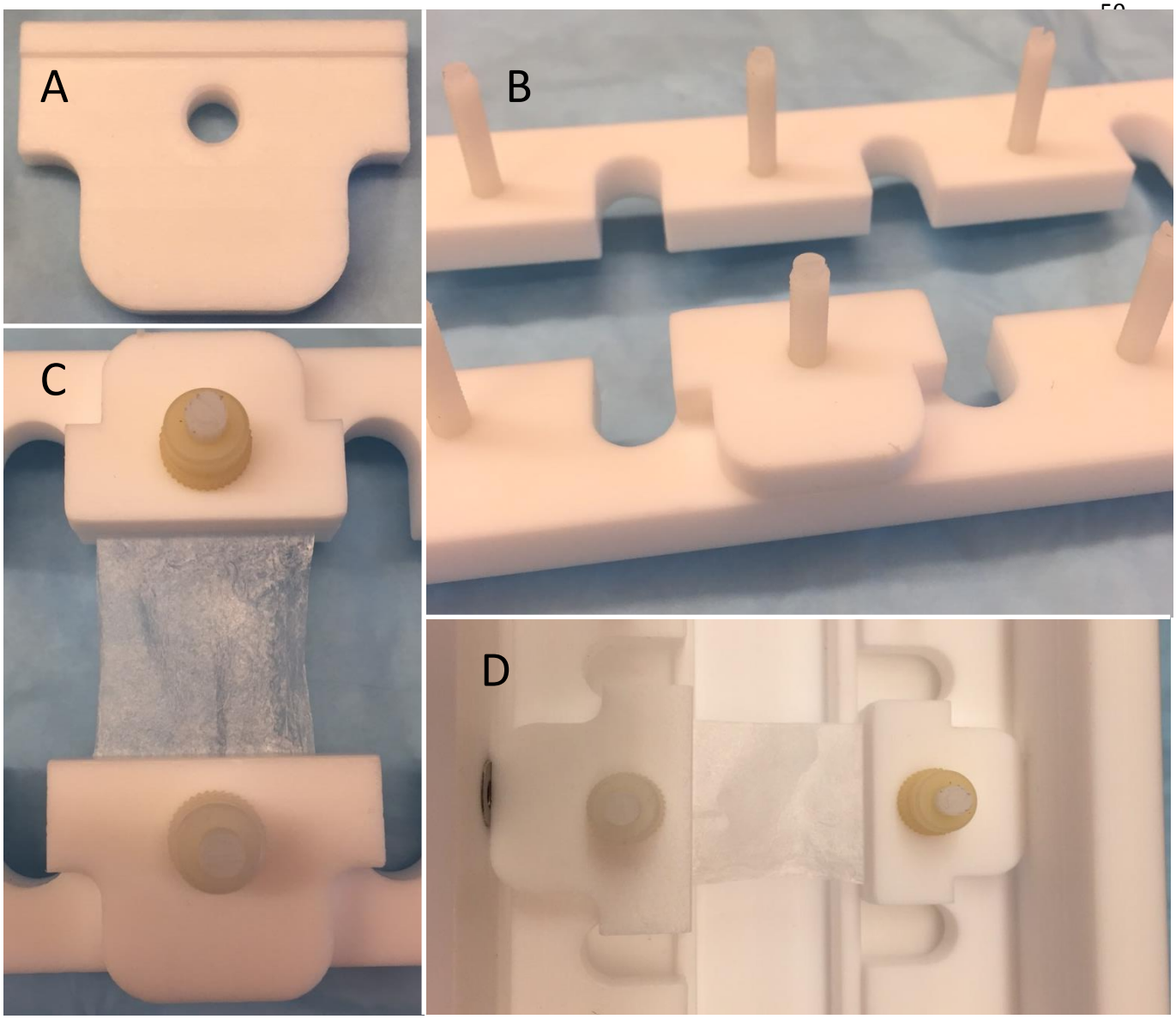

Figure 2.3.1, BAM Mounting Assemblies

A. Teflon Clamp
B. Crossbar Assembly with Teflon clamp and upright nylon threaded posts
C. Example Mounted BAM; note nylon thumbnuts for clamp compression
D. Mounted BAM in bioreactor (simulated, so no media present)

2.3.3 Improved Mounting Method

Thus, there exists a strong impetus for standardizing the bioreactor mounting method for TEMRs. The capstone team and I worked over the past year to develop ideas for such a system. The chosen design employs a new device – a novel "mounting chamber" – designed for precise and repeatable mounting of individual TEMR scaffolds which can be transferred in mounted configuration to a ready bioreactor. Figure 2.3.2 shows a rendering of this device. The chamber currently exists as a 3d-printed prototype, but a future version would be machined from Teflon, as the bioreactors are. The device primarily consists of the electronics housing, a polymer frame where the clamps rest, a load cell, and a precision clamping/tensioning system. Together, these contribute to creation of a more repeatable method for mounting TEMR scaffolds in our bioreactor system. The chamber is designed to be placed in a large cell culture dish to contain media. Both ends of the device have the clamping system designed for mounted transfer to the bioreactor, but one end contains the precision tensioning mechanism while the other interfaces with a load cell to help calibrate the tensioning.

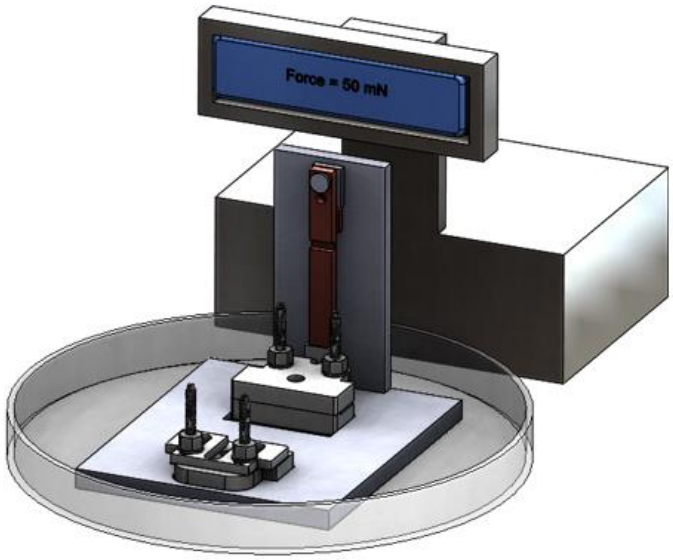

Figure 2.3.2, Prototype Mounting Chamber

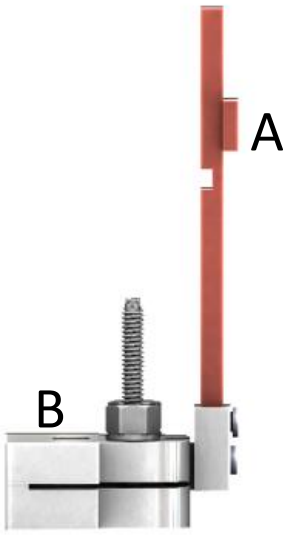

Figure 2.3.3, Load Cell
A) Point of attachment to device wall
B) Clamping mechanism

Load Cell

In this application, the load cell is employed to ensure precisely applied preload values across and among scaffolds. To our knowledge, no study has yet examined the effect of preload upon engineered tissue scaffolds. If no preload is desired, then the load cell is still essential to ensure even, resting-length strain across the scaffold being mounted.

The cell is employed as shown in Figure 2.3.3 where it is mounted vertically on the wall of the mounting chamber, and one end is inserted into an end of the scaffold clamping mechanism. This configuration allows the cell to record the bending moment caused by the pretensioning occurring at the other end of the TEMR. The load cell output is converted to a user-friendly format through a series of steps which will shortly be discussed.

The cell is a LQB630-50G model from Cooper Instruments (Warrenton, VA). It uses a Wheatstone-Bridge-like arrangement of sputtered thin-film strain gauges to produce highly linear signals (0.1% deviation) with a 10VDC excitation. As load cells produce a very low output voltage, the output signal is run through a universal strain gauge amplifier. We chose a model from Industrologic (SGAU, Industrologic, MO) which provides the excitation voltages to the load cell and reads the differential input signal. Depending on the input voltage to the amplifier, various output voltages from the amplifier can be achieved. The amplifier was set to output the range of 0-3.3V corresponding with the range of 0-50g. Two potentiometers on the amplifier allow precise tuning and drift calibration to ensure the exact voltage output. From the amplifier, the signal is input into a 16-bit analog-to-digital converter (Sparkfun, CO). This signal directly outputs to the digital inputs of a Raspberry Pi 3 microprocessor. The lack of analog inputs on the Pi necessitated the employment of the ADC. As the Pi is a powerful device with a user-friendly interface, the output from the load cell can be displayed on a monitor directly connected to the Pi. Real-time force output from the load cell will be utilized in the improved mounting protocol.

Tensioning Mechanism

The tensioning mechanism must operate such that repeatable, precise values can be achieved when mounting scaffolds, yet interface with the existing bioreactors with no modification. The design is such that the scaffold is clamped into place on the load cell side and lightly draped across the center support "bridge" to the opposite clamp assembly, spaced exactly 3cm from the fronts of each clamp. The bottom clamp rests nearly flush with the bridge level, so the scaffold can simply be draped onto it. Emanating from the bottom clamp are two upright posts near the left and right edges, as seen in Figure 4.4A. After the scaffold is draped, a thin center clamp with small, tooth-like protrusions on the bottom is placed over the bottom clamp and upright posts. The center clamp can translate forward and back on the posts by means of highly elliptical guide grooves. This portion is seen in Figure 2.3.4B. The center clamp is lightly tightened by means of thumb screws on the upright posts, and the proper tension is achieved by translating the clamp forward and back while monitoring the load cell digital output. The center clamp is then tightened securely, and the scaffold is ready for mounting in the bioreactor. This process simply involves transferring the mounted scaffold and clamp assembly out of the mounting chamber and onto the mounting posts of the 3cm-spaced bioreactor. As the bioreactor is designed to provide 10% strain to the constructs, the tensioning mechanism must also ensure this requirement is

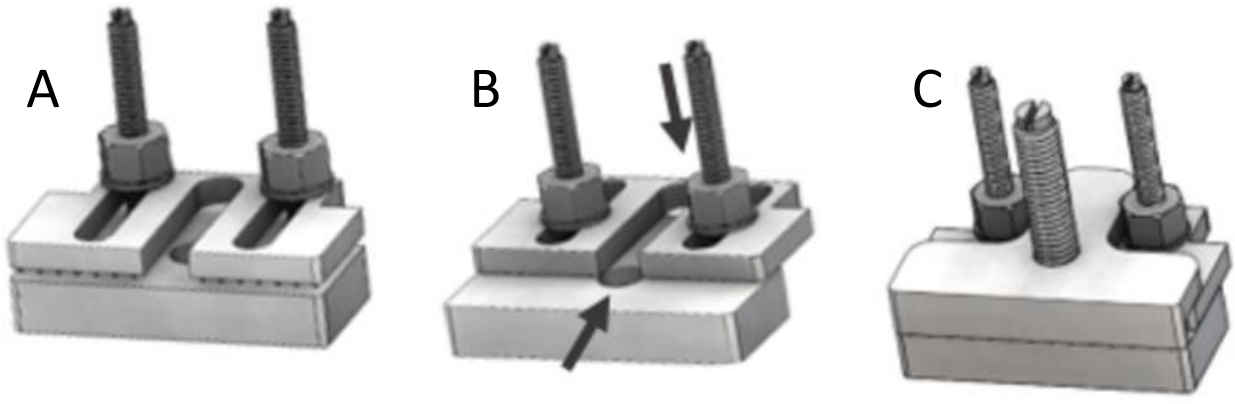

Figure 2.3.4, New Tensioning Mechanism
A) Bottom and Center Clamp
B) Translated/Tensioned Center Clamp
C) Mechanism mounted in bioreactor, with top clamp

fulfilled. Due to the design of the center clamp, the scaffold could effectively be "clamped" at a distance slightly greater than 3cm. To counter this, once the scaffold is placed into the bioreactor, a narrow top clamp which fits between the two upright posts and extends to exactly the front edge of the bottom clamp is placed over the bioreactor mounting post and secured with a thumbscrew (Figure 2.3.4C). This tensioning method is designed to simplify scaffold mounting and ensure consistency across manufactured scaffolds by standardizing pretension values and guaranteeing that the effective distance of stretch is exactly 3cm.

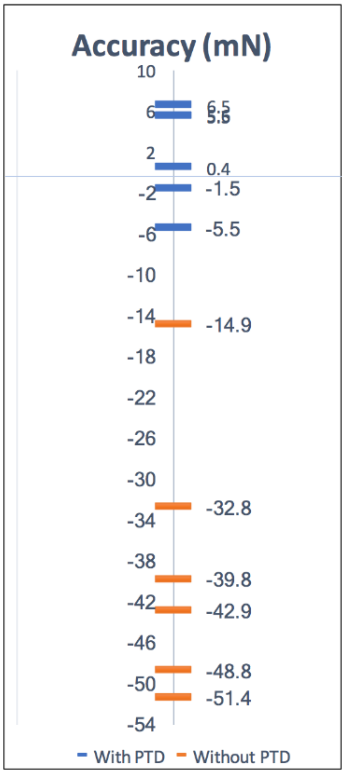

Figure 2.3.5, Tension Trial Results

Prototype Tensioner Testing

To determine the functionality of the prototype tensioning device over the manual mounting method, the team performed several mounting trials, shown in Figure 2.3.5. The blue bars indicate mounting trials using the new device, while orange points are of the manual mounting method. All values are expressed as mN deviation from the desired BAM tension. It is readily apparent that the mounting device provides a much decreased level of variability and is notably more accurate than the manual method.

2.3.4 Strain Heterogeneity Quantification

Although mechanical and methodological design improvements can theoretically ensure consistency in scaffold production, a need still exists for verification of this enhancement. A method to achieve this verification is via digital image correlation, or DIC. In this method, a digital camera is used to video record in real time the area of interest – in this case a bioreactor-mounted scaffold. Contrast is added to the area to enhance the ability to identify individual points of interest within the area. A program performs a frame-by-frame analysis of the video and tracks each of the contrast points within the area of interest. The program references the location of each point to its original position (in the first

frame) and outputs two heat-map style gradient displays for each frame; one in the x direction of stretch and one in the y direction A potential result for such a process can be seen in supplemental figure S3.3.

These heat maps provide valuable information as to the uniformity of loading and strain across bioreactor-mounted scaffolds. However, one more step must be taken before useful information can be extrapolated from the DIC. If the camera is stationed directly above the scaffold, then the stretch is only occurring at one side of the image frame (standardized as the right side). In an analysis of a perfect stretch cycle at the fully extended position, this would result in a strain gradient ranging from 3mm on the far right side of the scaffold to 0mm at the far left side. However, we are interested in seeing the change in strain relative to the center of the scaffold; thankfully a solution to this issue is relatively simple. In the current analysis, image frames are taken at 1 second intervals. Given that the total strain of 3mm occurs over 10 seconds, we know that each second of stretch results in a strain of 300μm. We assume that the scaffold is a linear, homogenous structure, so the far right side experiences 300μm of strain, the far left experiences 0μm, and the center experiences 150μm. Since we are interested in referencing our measurements to the center of the scaffold, exactly half of the recorded displacement of the far right side can be subtracted from the entirety of the displacement gradient map. While essential to perform in the x-axis gradient analysis, this post processing is also very important to perform in the y-axis analysis as points at the top and bottom of the scaffold will tend to be pulled to the center of the scaffold as strain increases. Preliminary testing of carefully-mounted scaffolds in the bioreactor have exhibited quite uniform strains across the scaffolds, but much testing remains to be done in developing this important verification method.

2.3.5 Future Directions

While the progress in methodology and device development made by the capstone team is important and novel, much work still remains to be accomplished. One future development of this work

could include development of a next-generation “smart” bioreactor. Similar to the idea of Cook et al (2016), such a system would be equipped with load cells (or comparable force measurement devices) for each scaffold within the bioreactor. The new “smart” bioreactor could have built in digital image correlation analysis for each scaffold. A user interface, driven by the Raspberry Pi embedded computer, would display data from the load cells and the DIC in a user-friendly format which would be used to verify consistent production quality across scaffolds in the bioreactor at multiple time points within the normal stretch protocol. This development, perhaps along with a more ergonomically-designed bioreactor, could even eliminate the need for a mounting chamber, and precise, repeatable mounting of scaffolds could be achieved directly in the bioreactor. In addition, force and image correlation data from trials across many scaffolds could perhaps lead to insights into the optimization of tensioning and stretch protocols for BAM scaffold production.

2.4. Advances in Bioreactor and Transport Chamber Design

2.4.1 Introduction

As previously discussed at length, the bioreactor employed in our lab is a custom device, engineered over several generations into its current design. These include changes in material composition and physical configuration into a form which functions as a consistent piece of laboratory equipment. However, as the TEMR technology approaches the first phase of human clinical trials, attention must be devoted to ensuring extreme levels of quality control in all levels of TEMR production. Given that the bioreactor is an essential component of TEMR manufacture, the same precision and quality control must be extended to this device as well. To this end, I have worked to refine the design and production of the bioreactor.

In addition, for clinical human trials, the TEMR scaffold must be transported from the GMP production facility to the site of surgical implant. The challenges associated with shipping a highly delicate live tissue scaffold are obviously large. The constructs could easily be damaged by impulse forces during shipping, and also require continuously elevated CO2 and temperature levels. With the exclusion of elevated temperatures, we have attempted to design a Transport Chamber system capable of enduring shipment while maintaining cell viability.

2.4.2 Bioreactor Updates

The original version of the bioreactor was manufactured by Cross Technologies (W-S) based on research and design drawings provided by Dr. Christ and colleagues at Wake Forest. Two generations of the 8-scaffold capacity Cross bioreactor are commonly used within the lab. The former entails a rigid mounting structure. This design is simplified by the low parts count, however, the design also makes it impossible to remove scaffolds from the bioreactor without dismounting them from their attachment points; a necessary step for scaffold shipment. The newer Cross model is designed with a removable "frame" assembly that was originally intentioned for use with a bi-directional seeding chamber used in

TEMR production. However, the removable frame is actually an excellent starting point for a highly-compatible TEMR transport system; this development will be addressed in the next section. Both generations of bioreactors are constantly in use within the Regenerative Therapeutics Lab, but as the newer “removable-frame” generation holds more potential for future development, all of the updates have been focused on this generation. We currently possess two next-generation bioreactors, with the design based on group input, the CAD work by myself and machining by the UVA Physics Machine Shop.

The first noted deficiency within the Cross bioreactor was the fit between the frame assembly and the bioreactor itself. In the Cross design, a spacing gap of over 2mm on each side of the frame was present. Due to the bioreactor’s normal range of motion of only 3mm, this gap meant that in normal operation, the frame holding the scaffolds could potentially not be stretched at all. If mounting occurred properly and the frame was butted up against the inside edge of the bioreactor mounting areas, then theoretically the tensioning of the scaffolds would ensure a normal stretch protocol occurred by keeping the mounting assembly butted against the edge of the frame. However, this ideal condition may or may not be regularly accomplished, so the CAD file was modified by reducing the gap to 0.25mm on each side. In the next-generation bioreactor’s physical manifestation, this has ensured a very smooth, yet snug fit of the frame into the bioreactor.

The second issue to ameliorate involves the nylon mounting posts in the long frame crossbars. Interviews of regular bioreactor operators led me to discover this issue. To mount a scaffold, the sample is set into place, a Teflon clamp is placed over it, and the assembly is tightened onto the crossbar by means of a nylon thumbnut seated into a through-hole drilled into the crossbar. The ramification of this design is that often, the nylon post turns with the thumbnut. Thus the post can either completely come out the top of the bar or, more commonly, extend through the bottom of the bar. This voids the system

of symmetry and creates an unstable frame assembly. To remedy this issue, first the thickness of the frame crossbars was slightly increased to give the posts more material to grasp. Next, the post mounting holes were changed to a blind cut with roughly 0.5mm of material left at the bottom of the hole, as seen in Figure 2.4.1. While not preventing the nylon post from being unscrewed, this design change does ensure that the post can no longer protrude through the bottom of the frame.

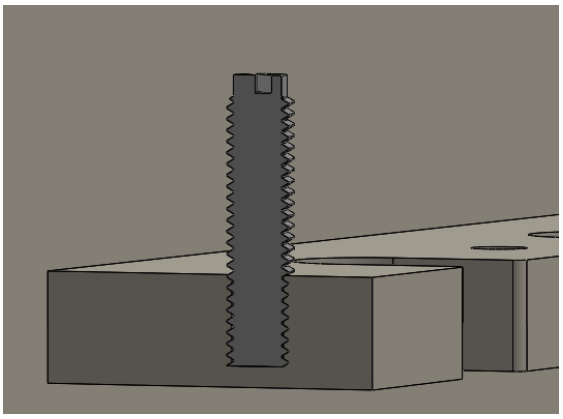

Figure 2.4.1, Modified Crossbar

Two other design changes were accomplished relatively easily. First, the Cross-design bioreactor had spaces in the lid for 4 barbed ½" male hose ports and three 0.22µm filter papers for air exchange. The filter papers are kept in place by means of either a Teflon or stainless steel ring compressing the paper against the wall of the hole in the lid. However, the barbed hose ports were always kept capped, and the exact original intention for them is unknown. Thus, these hose ports were eliminated from the next generation design. Next, the lid of the Cross bioreactor is manufactured from Teflon, with a small acrylic viewing window screwed into place near the center of the lid. To save weight, increase simplicity, and lower the risk of contamination, the lid design was changed to a solid sheet of ¼" thick acrylic. To ensure a good seal with the bioreactor with only one screw in each corner of the bioreactor, the natural concavity of the acrylic sheet was designed to face up, such that it presses down in the middle of the bioreactor when secured by the corners.

Finally, an important design change occurred as a result of discussing the design with one of our collaborator teams at Wake Forest University RMCC. This team is a major part of the effort to gain FDA approval for a TEMR human trial. They are also ultimately handling the implementation of TEMR transport from the site of manufacture to the site of implantation. To ensure the capability of shipping

in a very limited selection of heated external containers, the team has requested several different bioreactor capacities. The implications of this are even more pertinent to the development of the transport chamber and will thus be discussed in the next section. However, to meet the requests of our collaborators, two new bioreactor designs to fit 3 and 4 scaffolds, respectively, were created. All updates applied to the next-generation 8-scaffold bioreactors were incorporated in these designs. While neither of the designs has yet been manufactured, the models are complete in case the need arises. The

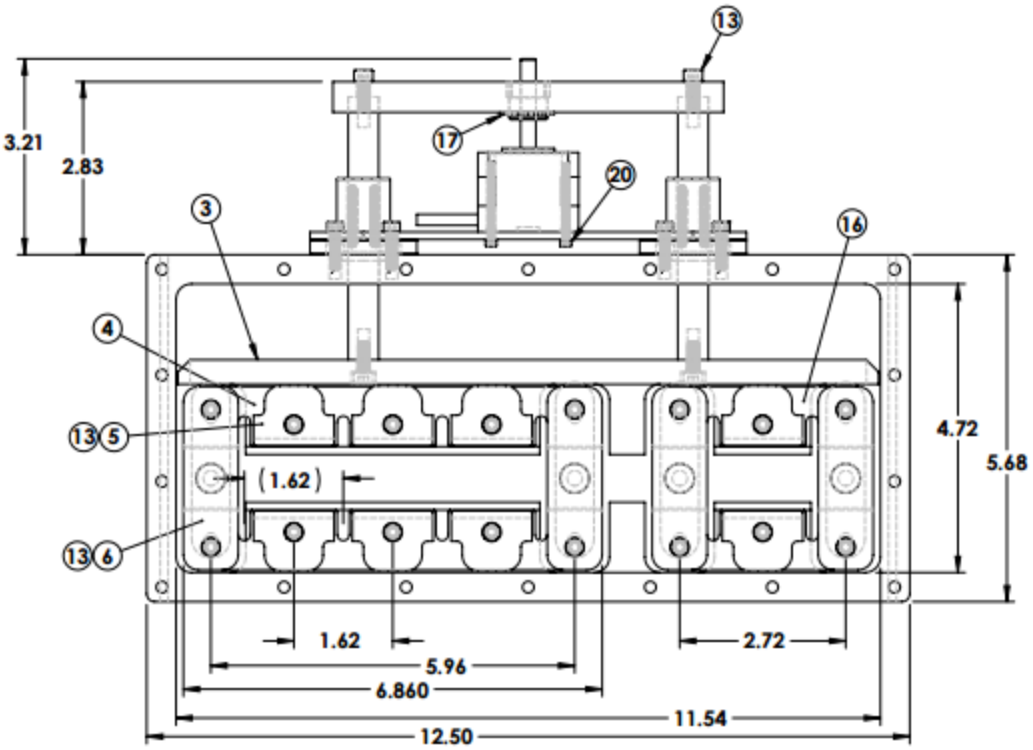

Figure 2.4.2, 2+1 Bioreactor Drawing (Piper)

collaborating team later decided that they preferred to ship two scaffolds and keep one for quality control testing in this initial submission for an IND. To further reduce shipping container size, the new design modified from the original by Piper Plastics consists of a single-scaffold frame situated next to a two-scaffold frame. A drawing of this design can be seen in Figure 2.4.2.

2.4.3 Transport Chamber Design

In addition to the updates made to the bioreactor system, a method needed to be developed to transfer the TEMR scaffolds from the production facility to the implant site in the proposed upcoming human trials. These constructs are not only highly sensitive to impulse forces, they also require an

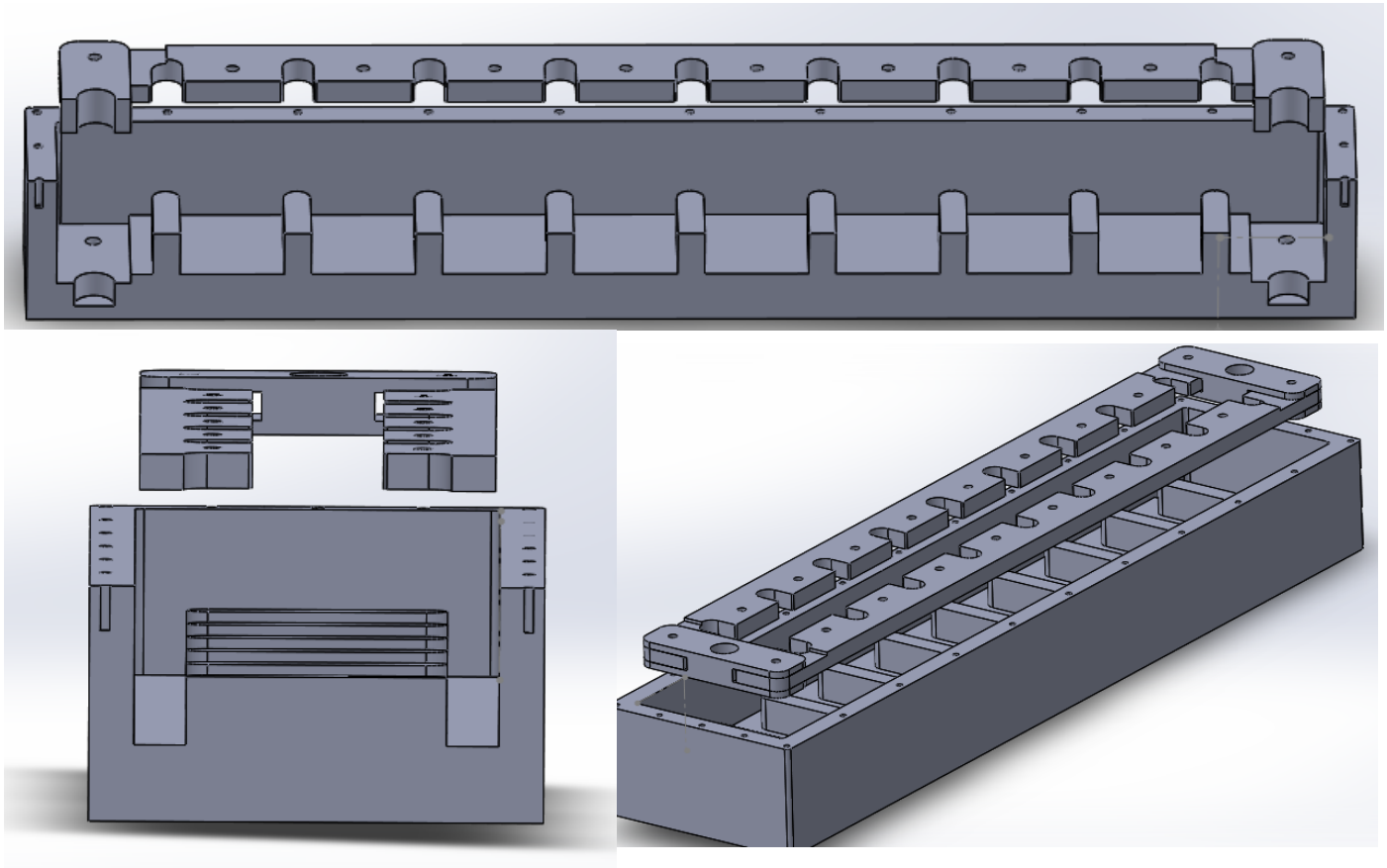

Figure 2.4.3, Prototype Transport Chamber

elevated CO2 environment, submersion in cell media, and a constant 37C temperature. These conditions must be maintained for up to 36 hours; the maximum estimated time for domestic shipping to occur from the GMP facility (Wake Forest University) to the implant facility in a worst-case scenario. Thus, design of such a system was initiated. From the beginning, the design of the transport chamber was such that the frame assembly from the bioreactor could be removed and directly placed into the chamber (Figure 2.4.3). The chamber was designed such that upon lowering the frame into place, the length of each frame-mounted scaffold was held at exactly 3.0cm; the same scaffold initial length as in the

bioreactor. Minimal clearance was provided for the frame to smoothly slide into the transport chamber body. In addition, upright bars between each of the scaffold mounts prevented lateral frame movement and served as baffles for impulse forces transmitted through the media in the horizontal direction.

Our collaborators at Wake Forest took it upon themselves to ensure the elevated temperature requirement during shipping was met. To do this, they have located a company which produces electrically-powered, heated shipment vessels. The transport chamber can simply be placed inside, padded, and shipped.

The requirement for an elevated CO2 atmosphere was slightly more difficult to meet; it was complicated by the fact that pressurized CO2 containers – which could be used to maintain the TEMRs' environment – are not permitted on commercial flights. However, after consulting individuals involved in shipment of live cells, we realized that the CO2 produced by the cells as a byproduct of cellular respiration would be sufficient to maintain the elevated CO2 environment. Thus, the solution was to design the chamber with a hermetic seal. To develop this seal, an o-ring was determined as the best solution. Parker-Hannifin (Lexington, KY) was chosen as the supplier due to their large variety of custom-sized o-rings. A ring with dimensions near that required by the transport chamber was located from their product offering. Because the o-ring was slightly larger than optimal for the transport chamber, the chamber walls had to be slightly thickened to accommodate. A gland was then cut in the chamber-to-lid sealing surface of the chamber in accordance with engineering specifications provided by Parker Hannifin.

In addition, the possibility of impulse forces transmitting from the chamber walls, through the cell media, then to the TEMR scaffolds during shipment was of significant concern. These forces, while not quantified, could be capable of ripping the cells off of the constructs. In developing a solution to this issue, aerospace engineering principles were employed. To prevent fuel sloshing within airplane fuel tanks and a subsequent large shift in center of mass, foam blocks are often inserted into the tanks. This

same method was applied to the initial design of the transport chamber. First, an FDA-approved reticulated polyurethane foam which was initially designed for skin contact in negative pressure wound therapy (INOAC A45M) was located. Extra head space was added into the transport chamber such that the foam could sit directly on top of the baffle crossbars and the upper frame protrusions and then be lightly compressed by the action of the lid sealing.

Thus, the protocol of transport chamber use would involve first removing the scaffold frame from the bioreactor and placing it into the chamber. Next, cell media would be poured into the chamber to submerge the scaffolds. The foam baffling would be placed on top, and more media poured onto it until saturated. The lid would be lightly screwed into place, but not yet sealed. The entire assembly would be placed in the incubator to ensure adequate CO2 concentration in any remaining air in the chamber. Still inside the incubator, the lid would then be completely sealed.

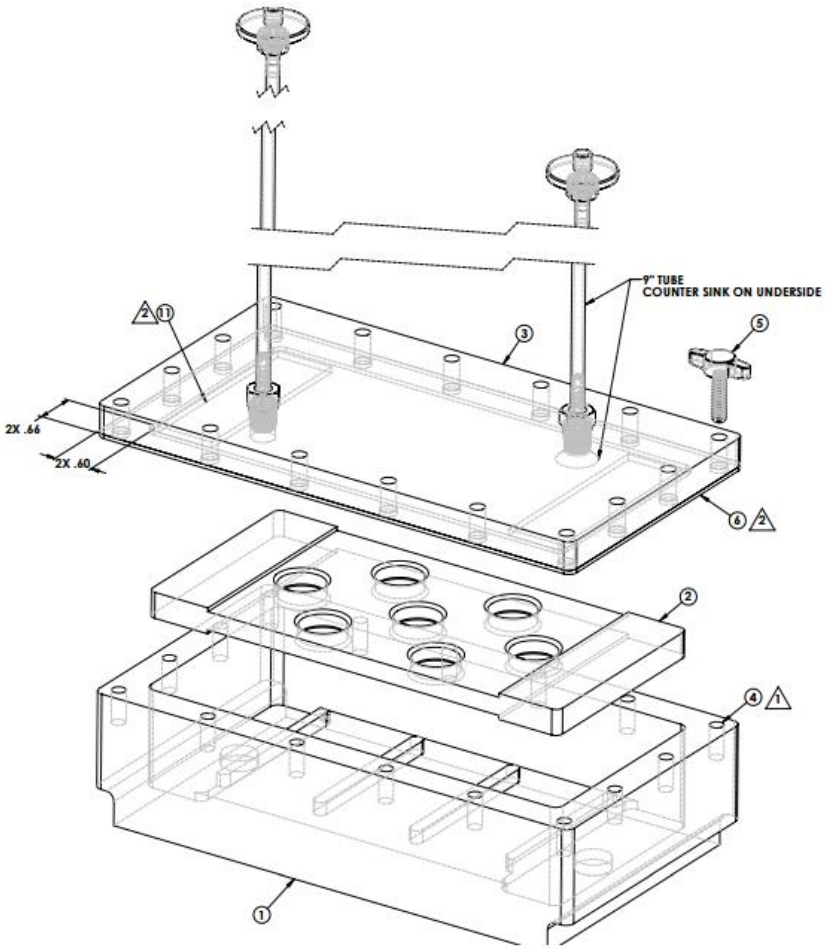

Figure 2.4.4, 1st Generation Transport Chamber (Piper)

Current Transport Chamber Design

While all of these concepts made it into the initial transport chamber prototype, several changes have been made in the current 1st generation design (Figure 2.4.4). Design work beyond the prototype was turned over to Piper Plastics. The major change

is the reduction in size to a capacity of only 2 scaffolds. The foam baffling system is currently eliminated, as there was concern that the polyurethane could release particulate into the media. While this raises the risk of forces during shipping damaging the scaffolds, testing on the foam would have to be carried out to ensure no particulate leaching from the foam occurs. In addition, sealable hose barbs were added to the lid to allow CO2 evacuation of the chamber's atmosphere.

2.4.4 Future Directions

While only in the very early stages of the methodology for transporting TEMR scaffolds from the manufacturing site to the implant site, the current system meets all of the requirements for a successful transport – at least on paper. A future design may be combined with the bioreactor into one unit; such a device would not only decrease the capital investment into equipment, it would also reduce the amount of handling and time scaffolds spend outside of media. I personally believe that an impulse-reduction baffle system similar to the foam design will be necessary, but upcoming transportation trials with the chamber will be necessary to determine. Finally, future development of a device capable of maintaining its own elevated temperature would also reduce cost by eliminating the need to place the transport chamber into another, temperature-controlled shipment vessel supplied by another company.

3. BAM Scaffold Characterization

3.1 Introduction

The bioreactor-conditioned TEMR is based on a naturally-derived porcine bladder ECM. This isotropic material, composed almost entirely of collagen (Sicari et al., 2014), is prepared entirely manually and is thus subject to significant variances in physical characteristics. Up to this point, only a small amount of effort has been placed into the characterization of this material (Badylak, Freytes, and Gilbert 2009) (Rosario et al. 2008). However, as the possibility of human treatments based on the TEMR technology approaches, both regulatory power and scientific rigor dictate that characterization of porcine bladder acellular matrix must be pursued. Here we will discuss BAM preparation, mechanical characterization via strain testing and two imaging modalities, and the effect of the bioreactor preconditioning on the BAM constitution. As well as fulfilling the simple need for materials characterization, the values from these tests are needed for a finite element computer model of our rat LD injury model.

3.1.1 BAM Preparation

While quantitation of strain across scaffolds is essential to ensure consistent output of tissue-engineered scaffold production, another highly important factor which has largely been uncontrolled is the thickness of the scaffold itself. BAM scaffold is derived from the lamina propria of porcine bladder (Sicari et al., 2014). Upon receipt of raw bladders, the bladders are trimmed of excess external tissue, separated from the ureter, cleaned of any remaining internal contents, and sliced down one side to create a roughly flat surface. Next, the sliced bladders are placed into a decellularizing solution for several days. The solution is washed off over the course of several more days, and the lamina propria is separated from the remaining bladder tissue. This extremely delicate operation is performed manually, and the thickness is gauged by eye and feel, while also requiring a skilled operator to ensure minimization of rips and tears to the lamina propria during removal. The separated lamina propria is

further washed, remaining excess tissue is removed, and the lamina propria is cut to appropriate scaffold dimensions and draped onto silicone molds for lyophlization and sterilization. At this point, scaffolds which survived the lyophilization and sterilization processes are approved for use in experimental rat implant surgery within the lab.

3.2 Mechanical Characterization

We have performed two modalities of mechanical strain testing on BAMs, with the current one being far superior to the former. Initially, the only equipment available to us for such testing was an Instron universal testing rig with a 100N load cell. To effectively use this system, a "dogbone" die was custom ordered (Figure 3.1) to give the test sample the necessary shape. Due to the samples' thinness, shaped samples were then mounted in a sandpaper "frame" which ensured that the sample would not slip during the test sequence. Finally, the frame was vertically mounted into the Instron's sample grips and these were tightened. Unfortunately, due to the samples' relatively low ultimate tensile strength (on the order of single Newtons), the resolution provided by the 100N load cell was quite poor. Along

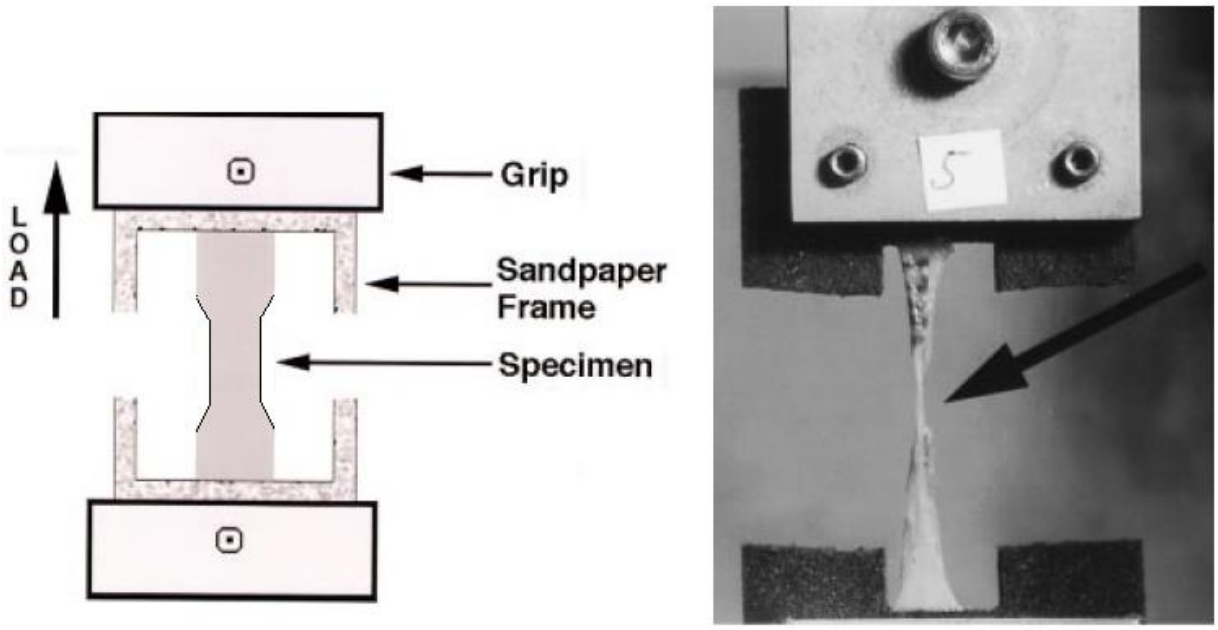

Figure 3.1, Sample Instron Mounting
A) Showing dogbone die sample profile, B) Showing sample after reaching yield point

with the poor resolution, the sample mounting process proved difficult and introduced notable variance into the result. A better method arose with the availability of a new piece of equipment.

3.2.1 Biaxial Testing Protocol

The CellScale BioTester (Waterloo, ON) biaxial strain tester is purpose-built for mechanical testing of soft biological materials. Equipped with 2.5N load cells, resolution is also significantly (40x) better than with the Instron. In addition, to use this device, a specialized sample shape is not required, thus simplifying operation. As it is a biaxial tester, the device is capable of gripping the rectangular sample from all four sides or just opposing sides. The grip is by means of a set of varied-width rake-like hooks called BioRake (Figure 3.2). Five hooks puncture and grip each side; these are spaced from 0.7mm to 2.2mm depending on the selection. The sample is placed horizontally in a liquid bath – Krebs Ringer if the sample involves muscle cells – and the hooks are secured into the sample. Hunter Wallace, a BME graduate student in the UVA M3 Lab, has taken the primary role of performing mechanical strain testing on the BAM scaffolds. In a normal protocol, a sample roughly 1.1x1.5cm is cut from the scaffold with a scalpel. After mounting on the BioRake system, the sample is lowered into a Krebs Ringer bath. Trials with various strains on the BAM have shown that 10% causes no noticeable damage. Thus, the samples are stretched from 0-10% over a period of 30 sec/stretch 10 consecutive times. Finally, the samples are stretched past their ultimate yield point. The recorded data is normalized to the area of the sample.

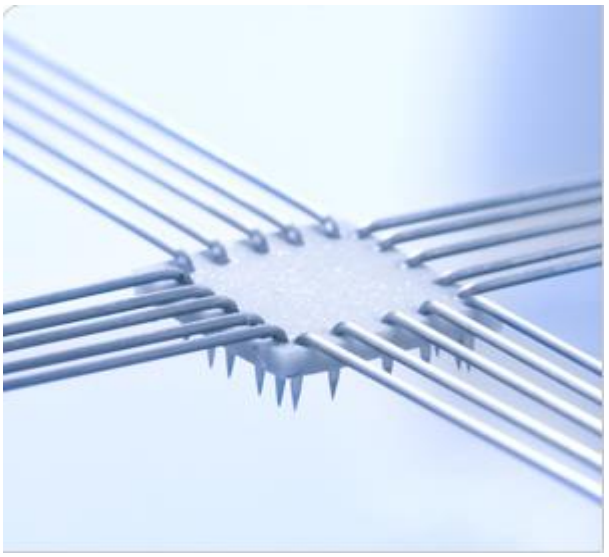

Figure 3.2, CellScale BioRake Product Image

3.2.2 Scaffold Thickness Measurement Protocols

Within the BAM preparation method, there exists possibility for significant variation of scaffold thicknesses. While ones that appear excessively thick by eye are rejected, the range of acceptable

scaffolds is currently unknown. In addition, full mechanical characterization of the scaffolds via stress-strain mechanical testing requires thickness measurements. Thus, a significant impetus exists for a standardized thickness-measurement method to be developed. This became an aim of the BME Capstone team's project. Three major methods for this measurement were proposed and have been explored.

The first method involved basic histology techniques. Hydrated BAM scaffolds were suspended vertically in a melted paraffin wax block such that a BAM cross-section was visible when sectioned with a microtome. After sectioning, the samples were microscopically imaged (Figure 3.3) and compared to the image scale bar. ImageJ (NIH) was then employed to measure the scaffold thickness. However, this method proved difficult, as the embedding process and microtome sectioning often caused rips within the sample, causing a large variance within collected thickness data.

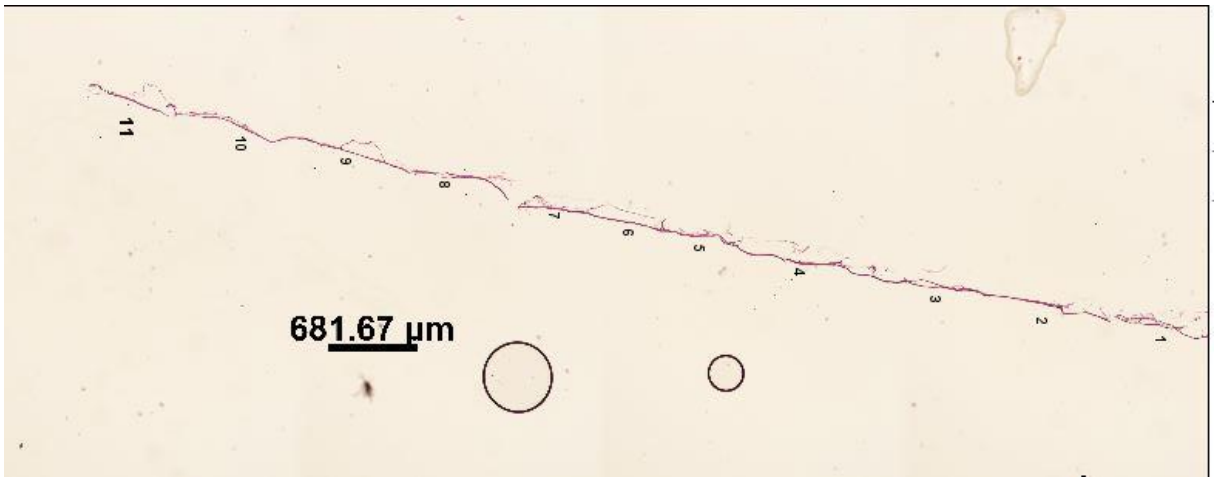

Figure 3.3, Representative Cross-Section Histology of BAM scaffold

The next method employed for measuring scaffold thickness is based upon confocal microscopy. First, the BAM scaffolds were stained with DAPI to increase fluorescence. The samples were then placed into the microscope and several segments on each scaffold randomly chosen for analysis. The z-stack feature was used to determine the scaffold thickness; first the z-plane was lowered until no signal was visible. The height was gradually increased until the signal increased sufficiently to determine that the bottom plane of the scaffold had been reached. The z height was further increased until the same criteria was met for the top of the scaffold. The difference in z-height was then recorded as the scaffold

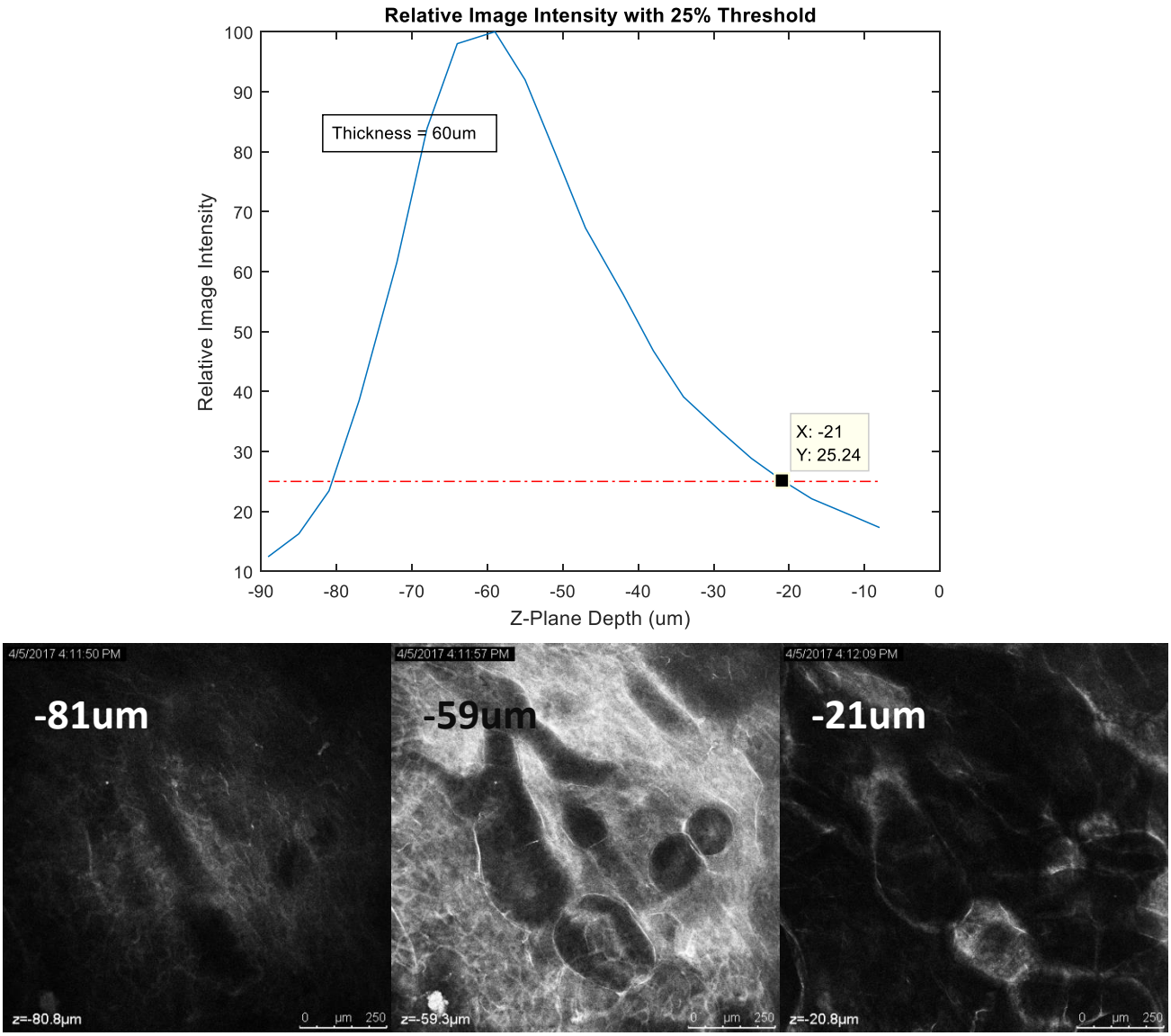

Figure 3.4, Confocal
Analysis of BAM Thickness

thickness. To reduce manual selection error in this process, we created a MATLAB program which measures the signal intensity from each of the z-stack images, resulting in a graphical output of the signal intensity of each frame as seen in Figure 3.4. When the top or bottom surface of the scaffold is reached, the graph shows an inflection point; these are automatically selected as the top and bottom surfaces by the program. This method is rather time-intensive but serves as a good validator for the third thickness measurement method.

The third and final method we have developed for determining thickness of BAM scaffolds involves mechanical contact. The system is based off of a Mitutoyo Absolute Digimatic Indicator (Mitutoyo USA) with 0.001mm resolution. This indicator is equipped with a lift lever and mounted onto a ring stand assembly. Due to the extreme thinness of the scaffold material, it is important that the downward force of measurement be distributed over a large area. Thus, we have replaced the standard domed presser foot with a 1cm diameter foot. The foot contacts a flat-milled aluminum block as shown in Figure 3.5. To ensure accurate and repeatable measurements, the contact between the foot and block is calibrated before each use by shimming the aluminum block. This contact is assured by means of feeler gauges down to 0.02mm thickness. A team of 3rd-year undergraduates co-mentored by Jon Taylor-Fishwick and myself took on the project of developing this method to examine intra and inter scaffold thicknesses. The relatively simple process of measurement begins with the foot-to-surface calibration. A precise parallel contact is ensured by pressing a 0.02mm feeler gauge around the contact area. Next, the Digimatic's presser foot is raised by means of a lift lever which allows the BAM to be slid underneath the foot. The team took 3 repeated thickness measurements are taken at each of 6 locations on the scaffold. In common

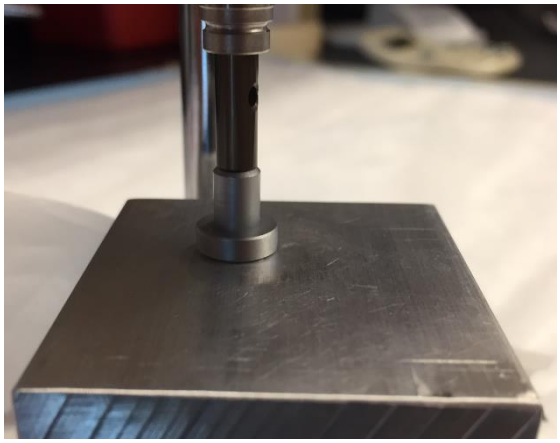

Figure 3.5, Digimatic Presser Foot on Aluminum Block

application of this thickness measurement modality, the number of collected sample will be cut down to either 6 total or 3 total, depending on the findings of normal variability within the scaffolds.

3.2.3 BAM Molecular Imaging

To acquire further characterization of the BAM scaffolds, we performed atomic force microscopy (AFM) on several BAM samples. To our knowledge, we are the first to perform AFM on porcine lamina propria. While providing incredible resolution, the downside is that the area being imaged is incredibly small. Thus, compositional variabilities existing over a scale larger than several microns are not apparent.

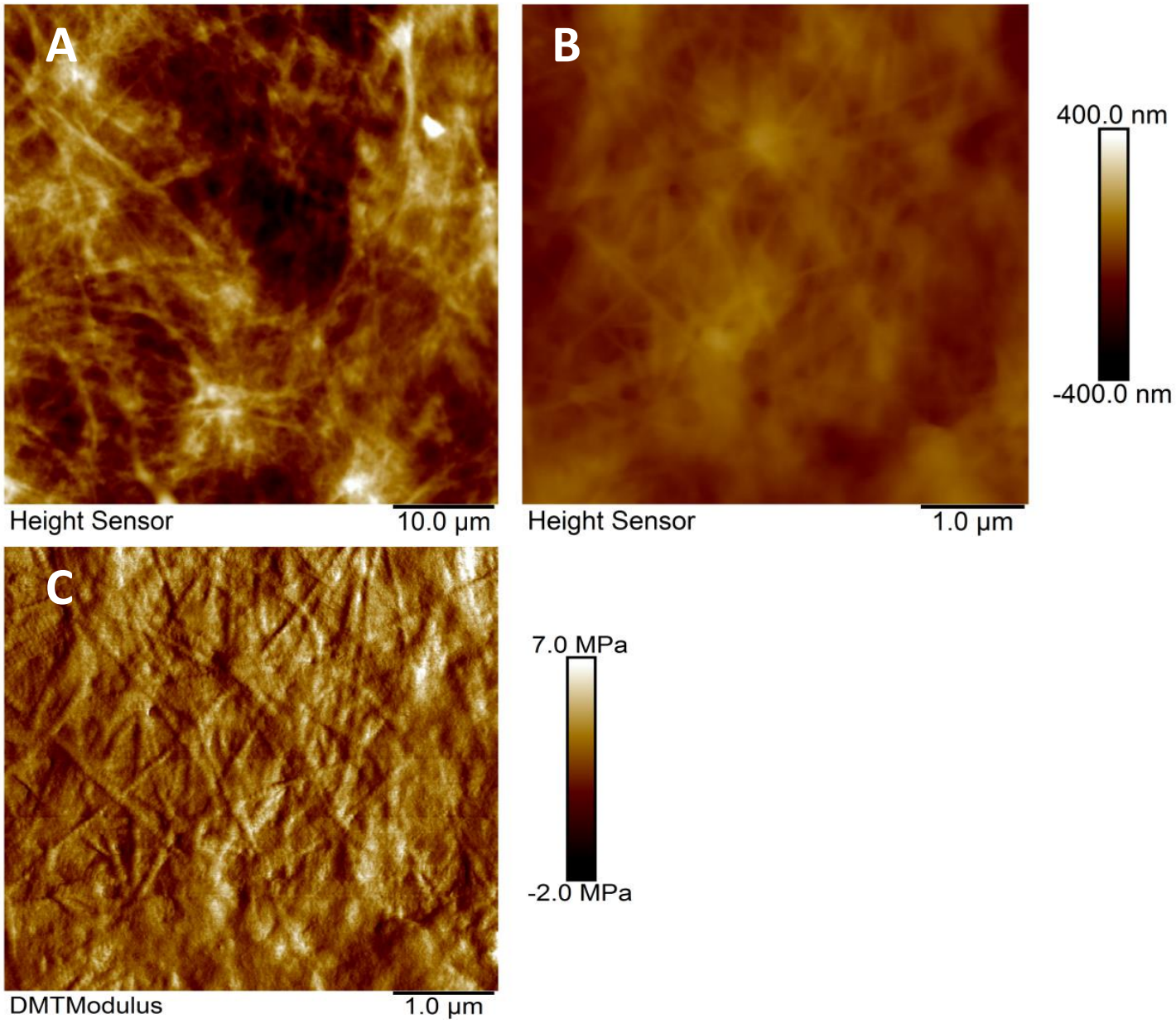

Figure 3.6, AFM Imaging of BAM
A) Collagen fibers visible B) Isotropic collagen fibrils visible C) D-period segmenting visible

Figure 3.6 A and B show the AFM imaging at two magnifications. In the 10µm scale bar image (A), collagen fibers can be observed as the bright, ~15µm-wide strands. As the magnification increases to a scale bar of 1.0µm (B), individual ~50nm-wide collagen fibrils become visible. These fibrils become even more visible when the modulus of the surface is examined (C). In addition, the 67nm staggered spacing of collagen molecules is visible as an apparent segmenting of the fibrils (Riso, Kaasik, & Seene, 2016). Clearly, the fibrils exhibit complete isotropy.

3.3 Characterization Experimental Results

3.3.1 BAM Thickness

A series of Digimatic thickness measurements were run on 35 BAM scaffolds. The purpose of this trial was to further characterize the variability in raw BAM scaffolds. For each one, three measurements

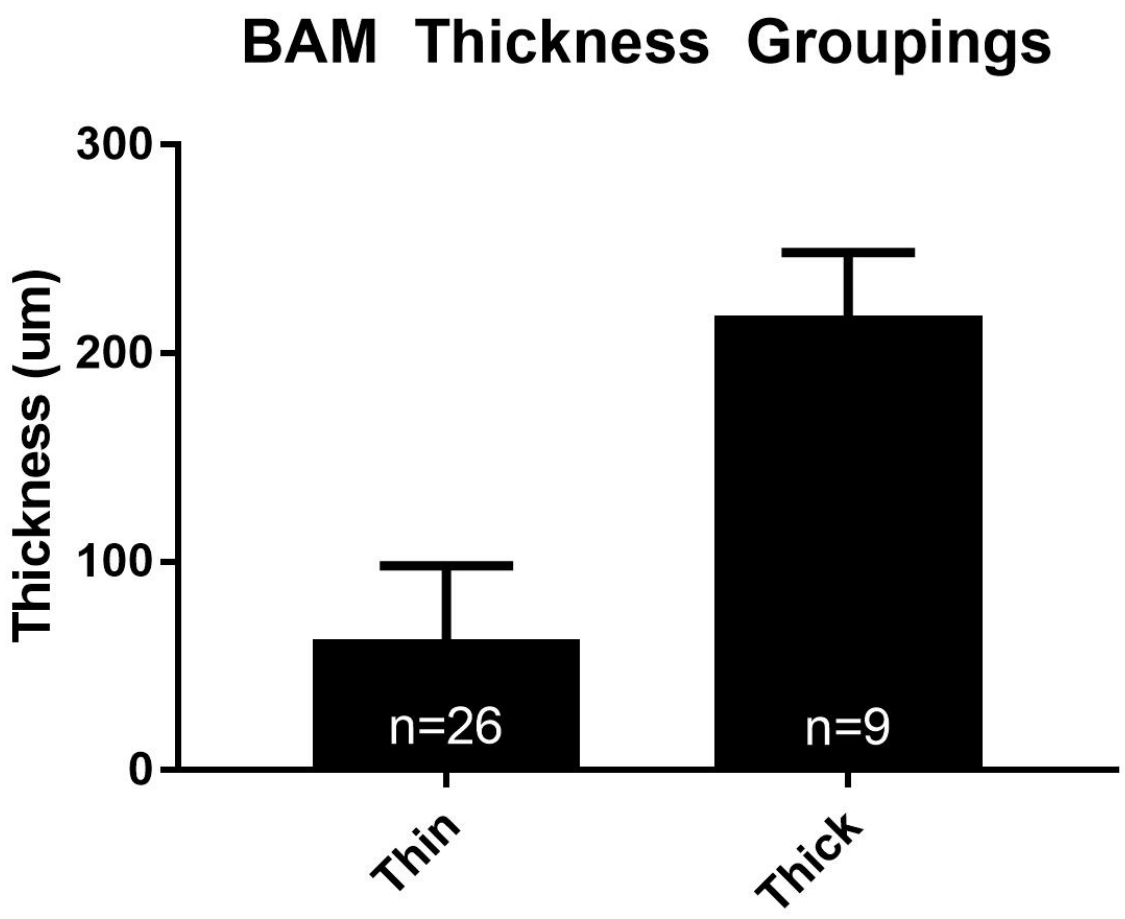

Figure 3.7, BAM Thickness Groupings

were taken: top left, center right, bottom left. These positions were judged to adequately capture the variance within the scaffold. The BAMs tended to fall into either a “thin” or “thick” grouping, with the majority (n=25) falling into the “thin” group. This grouping had an average thickness of 62.99µm with a standard deviation of 6.894. The less-populated “thick” group (n=9) had an average thickness of 217.9µm with a standard deviation of 10.13. A graphical comparison of the two groups can be seen in Figure 3.7. In addition, representative examples of “thin” and “thick” samples are shown in Figure 3.8. It is apparent that significant variance exists within the scaffolds, but the implications of this on TEMR consistency will not be known until a trial of TEMR production and implantation on known-thickness scaffolds is completed and the degree of regeneration is evaluated. At this point, discriminatory qualifications for acceptable scaffolds can be selected with confidence.

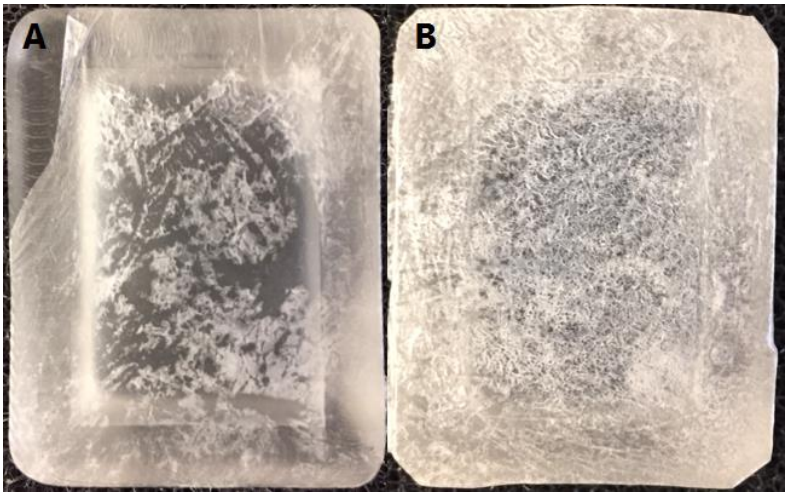

Figure 3.8, Representative BAM Thickness Samples A) Thin Scaffold, B) Thick Scaffold

3.3.2 Biomechanical Properties

Scaffold mechanical properties were measured by the CellScale biaxial tester in several different scenarios. First, a variety of components involved in TEMR production were tested to acquire a baseline understanding of the stress-strain properties of each. These included BAM scaffolds, BAM scaffolds seeded with MPCs, native LD muscle from the area of injury, explanted muscle treated with BAM, explanted muscle treated with TEMR, and non-repaired muscle. This data was collected before scaffold thickness had begun to be measured, however. This data can be found in supplemental Figure S3.1. Very recently, 10 BAM scaffolds were measured for thickness and then stress-strain tested (Figure 3.9). However, 2 of these samples were extremely thin (~20µm, shown in purple). This extreme thinness

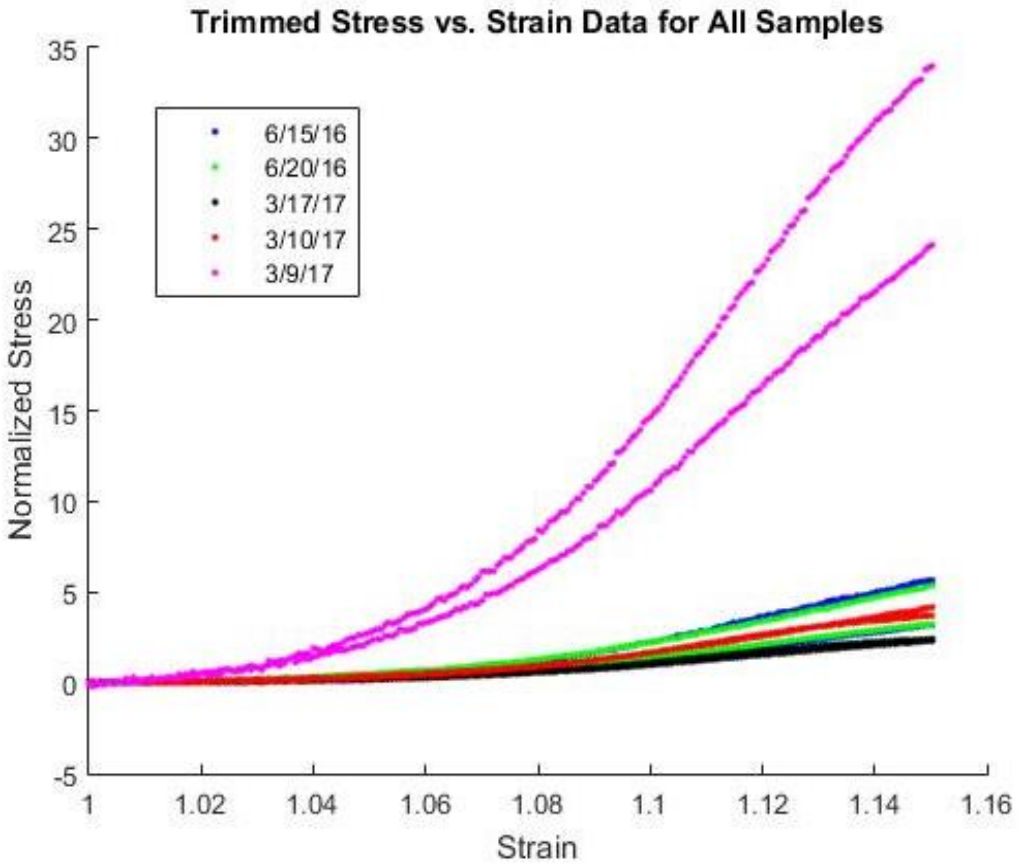

Figure 3.9, Stress-Strain Testing Data for All BAM Samples

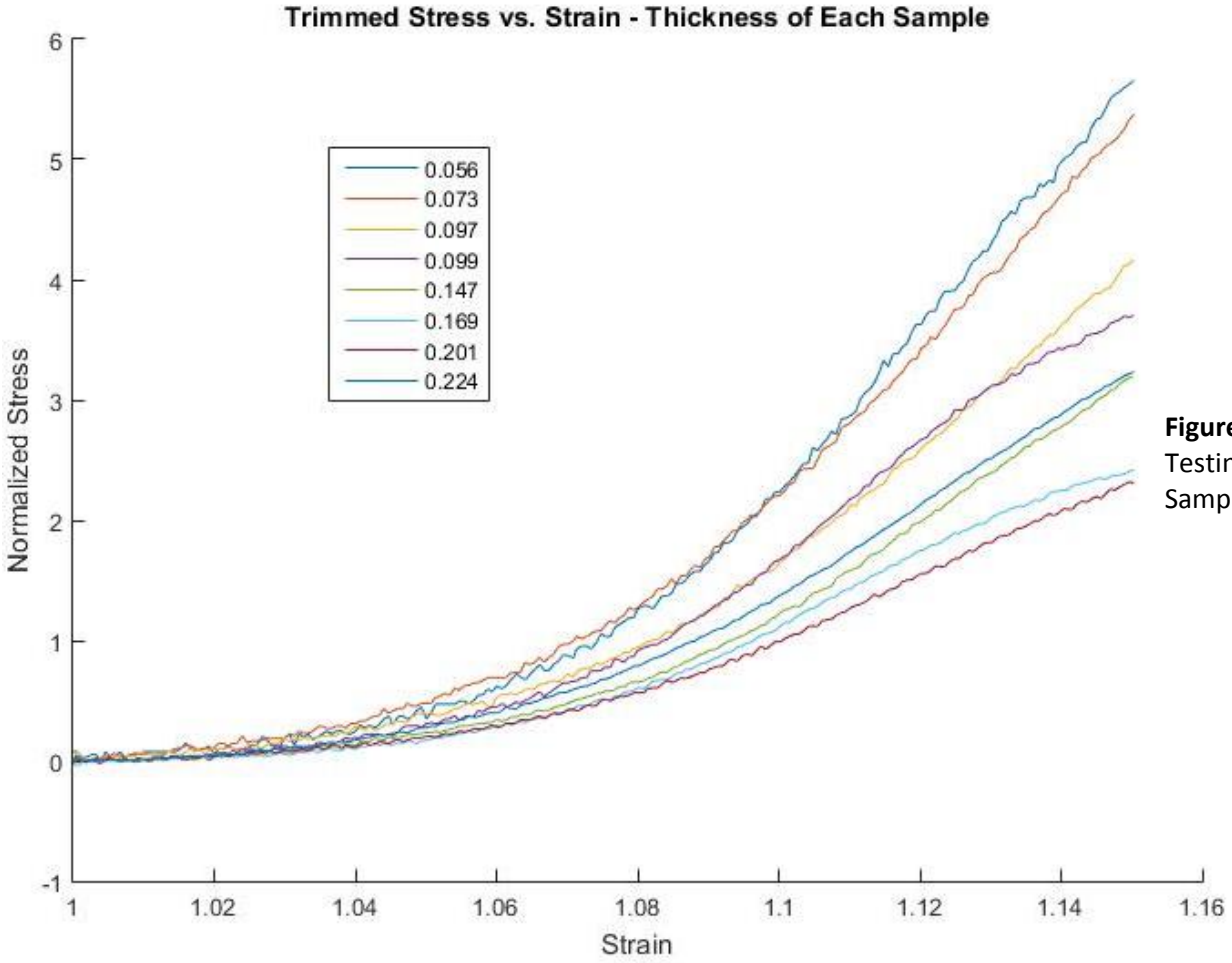

Figure 3.10, Stress-Strain Testing Data for Selected BAM Samples, with Thicknesses

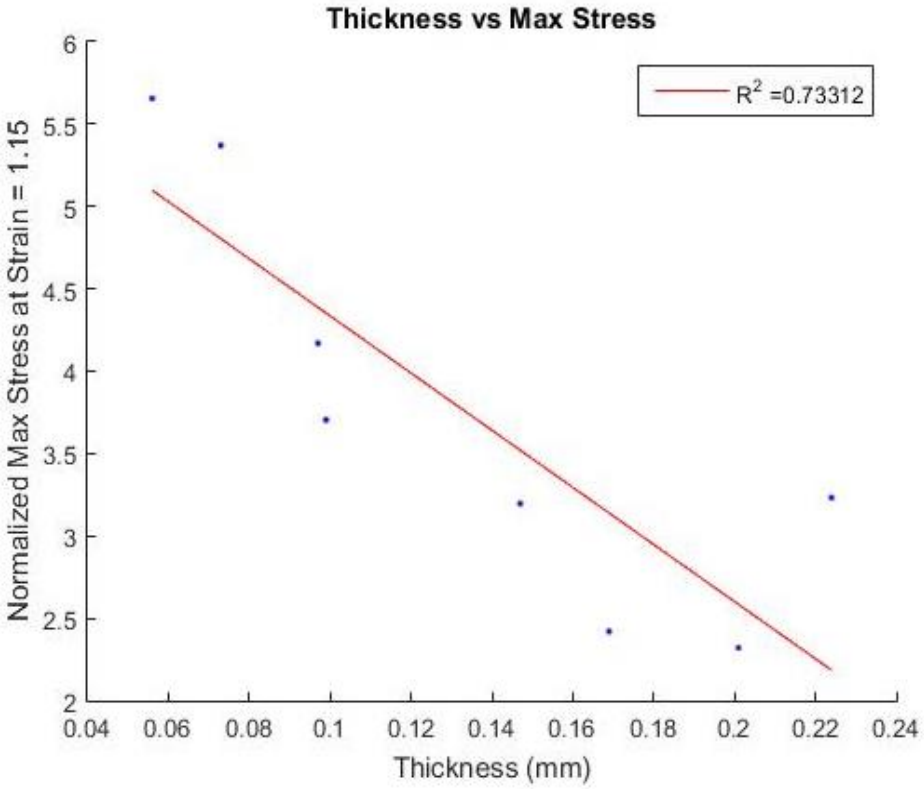

Figure 3.11, Thickness to Max Stress Relationship, with Linear Fit

precluded clear analysis of the rest of the samples so the points were excluded from the data analysis. However, these points may be significant and will be thus addressed shortly. The trimmed data is shown in Figure 3.10; it is apparent that BAM scaffolds can exhibit a range of stiffness properties. The thickness (mm) of each sample is indicated in the legend. Visually, from Figure 3.10, it appears that scaffold thickness does have some effect on stiffness, but not perfectly linearly. This trend is further elucidated in Figure 3.11, which applies a linear fit to the thickness/stress relationship of each tested BAM.

The two “outlier” points from the previous paragraph were extremely smooth, visually-homogeneous samples. Thus is in contrast to some of the thicker samples which contain multiple layers – sometimes not uniform – of extra ECM material. I believe that the “effective” thickness of BAMs in the calculation of stress to strain ratio may be far less than the thick samples’ measurement would indicate. If this is the case, it means that the majority of stress is being born in each BAM by a relatively thin layer of highly-uniform ECM proteins. In thicker BAMs, two possibilities exist to account for the visually

apparent relationship between thickness and stress. First, the uniform stress-bearing layer could be thicker. Second, the remaining thickness is comprised of non-uniform-thickness collagen/ECM layers; these could bear some of the stress via lateral force transmission. I believe this composition most closely represents the reality of BAM composition, which introduces the idea of BAM thickness heterogeneity.

3.3.3 Effect of BAM Thickness Heterogeneity on Stress-Strain Relationship

As is evident in the last section, the measured thickness of the BAMs has an effect on the stress-strain relationship, but it is far from linear. This apparent paradox becomes less confusing when the method of thickness measurement is taken into account. The digimatic gauge employs a 1cm diameter presser foot; this mechanical method means that roughly the highest thickness in that 1cm diameter area is the value that will be recorded. From visual analysis (Figure 3.8) and previous experience, we know that

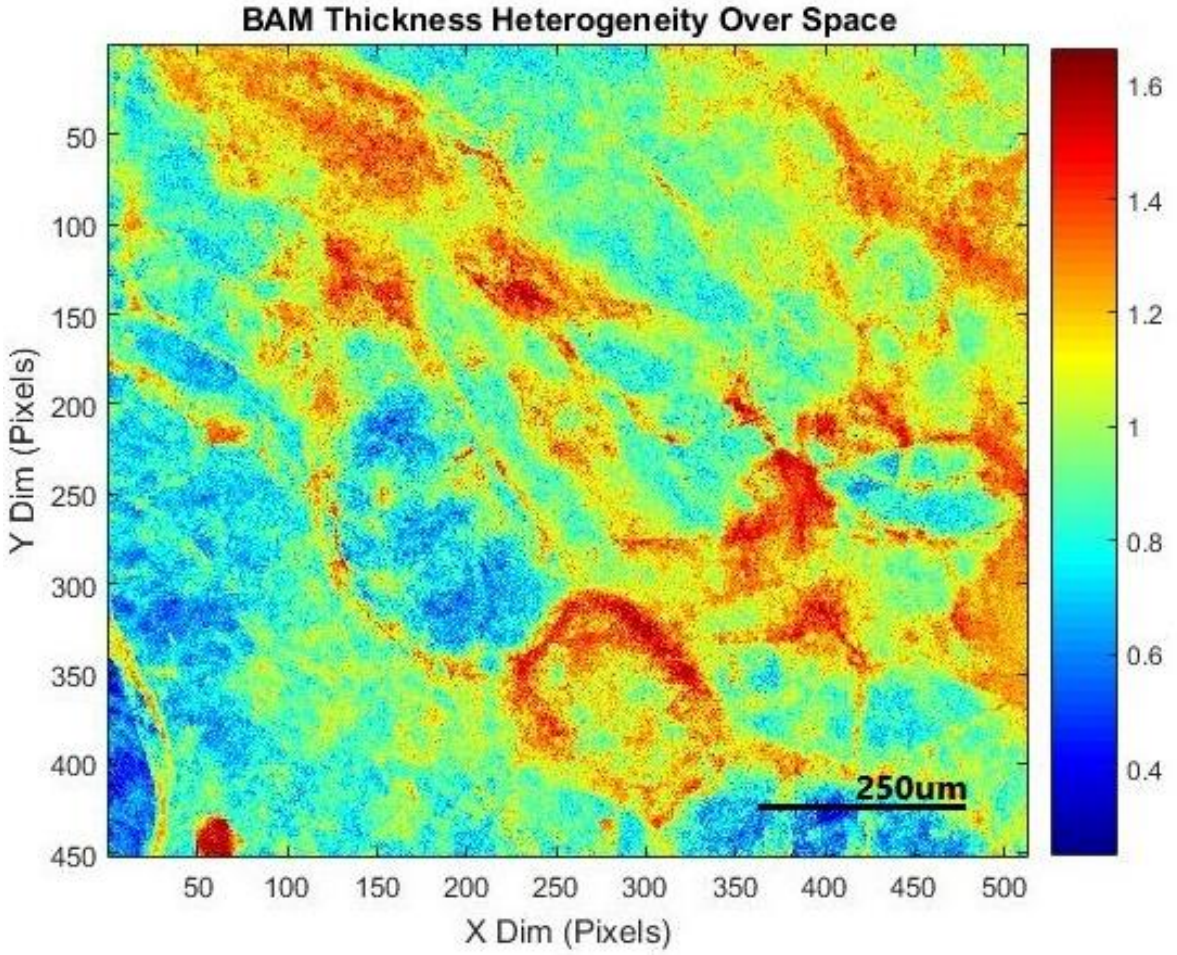

Figure 3.12, BAM Thickness Heterogeneity via Confocal Analysis

thickness variability exists on a macroscopic level. It is reasonable to assume that such variability may be represented on a microscopic level as well. To identify such variability, a MATLAB script was composed to take the z-stack data from confocal imaging of the BAM scaffold and sum the number of times each pixel exceeded a threshold value throughout the z-plane. The result is a colormap image (Figure 3.12) showing the variability in scaffold thickness across the physical surface of the scaffold. The brightness threshold used in determining a pixel's inclusion in each z-stack image was calculated based on the minimum average pixel brightness in the upper and lower surface boundaries of the confocal imaging measurement. Of note, this sample had a thickness of 60μm as calculated by previous confocal analysis. A thickness of "1" on the colorbar correlates to 60μm.

3.4 Effect of Bioreactor Preconditioning on BAM Scaffolds

In normal cellular microenvironments, cells constantly remodel their extracellular matrix surroundings (Lu, Takai, Weaver, & Werb, 2011). In the context of myogenic progenitor cells (MPCs) seeded onto a BAM scaffold and preconditioned in a bioreactor, little to no literature information nor intuition exists. While muscle cells tend to perform less remodeling than other cells such as fibroblasts, initial data from thickness measurements and stress-strain testing indicate that the MPCs were in fact remodeling the scaffold during bioreactor preconditioning. This led us to pursue definitive evidence of such a process. In this process, we employed mechanical thickness testing, scanning electron microscopy (SEM), atomic force microscopy (AFM), and stress-strain testing.

3.4.1 Thinning of scaffold

To begin the experiment, TEMR scaffolds were produced as previously described (Ma, Sahoo, Baker, & Derwin, 2015). One set was preconditioned in our proprietary cyclic-stretch bioreactor for 5 days at 10% strain while the other was left stationary on its silicone mold with cell media in a culture dish for the 5 days. A control sample was also prepared which did not come into contact with cells. The cells on all scaffolds were then detached from the scaffolds by trypsinization and rinsing in PBS. The

cleared scaffolds were then allowed to air dry for 24 hours and taken for imaging. The captured SEM and AFM images are attached in supplementary figure S3.2. While the images show collagen fibers and fibrils, they poorly capture the remodeling experienced by the BAM scaffolds after bioreactor preconditioning and do not clearly indicate any change in scaffold isotropy. However, a more revealing measure of the scaffold phenotype was thickness measurement. The Digimatic method was again used to measure the thickness of two of each of the digested, preconditioned, TEMRs, and the digested, non-preconditioned, TEMRs. Due to wrinkling of the scaffolds during measurement, three measures were made on each, except on one of the preconditioned scaffolds, where only one measure was taken. The results from these measurements are shown in Figure 3.13.

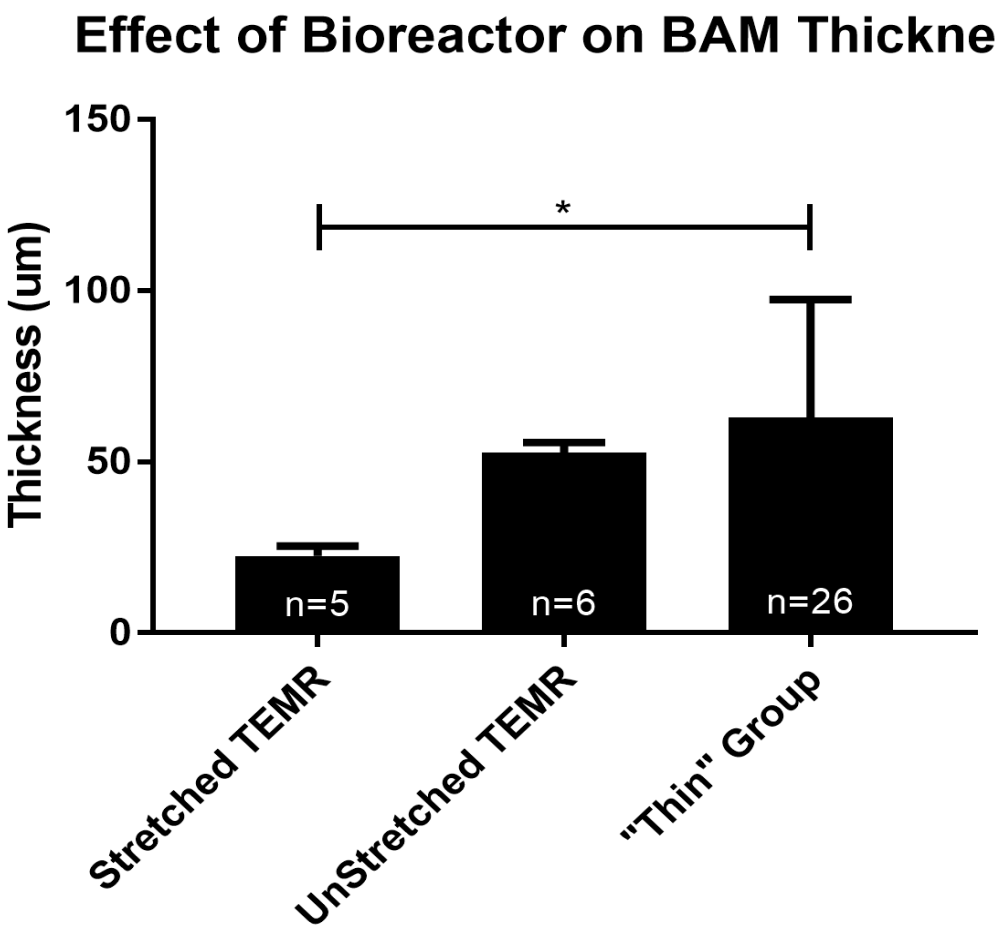

Figure 3.13, Effect of Bioreactor Preconditioning on BAM Thickness

It is apparent that when myogenic progenitor cells (MPCs) are seeded onto lamina propria, the scaffold is remodeled in such a manner to cause it to thin, especially when mechanical loading from bioreactor preconditioning is applied. This agrees with our experience in TEMR treatments where the lamina propria is dissolved before a period of two months post-implantation. However, further study on this issue is warranted so that the specific mechanisms at play can be understood.

3.5 Finite Element Models

Computer modeling is a highly valuable tool within the biomedical community as it facilitates experiments which could otherwise be too expensive, unethical, or even physiologically impossible. In addition, models provide valuable insight by affording the opportunity to significantly vary numerous parameters and observe these effects.

To this end, two members of the M3 lab are working on creating finite-element (FE) models of the rat LD injury. Xiao Hu is working to create a model which largely encompasses the ex vivo DMT active force analysis and puts a strong focus on the interface of the injured and normal muscle areas. Amanda Meppelink is also developing a model which is intended to emulate in situ testing conditions.

When complete, we hope for these models to provide accurate information as to the complex intra-muscular dynamics of repair and hypertrophy, thus adding a new depth of meaning and understanding to our measurements of active force production across a range of assessment modalities. Key to the proper functionality of the models is accurate thickness information – both of the muscle itself and the scaffold. This is yet another reason why the development of a measurement protocol employing the Absolute Digimatic indicator is so crucial to the advancement of our research.

3.6 Discussion/Future Directions

Accurate characterization of bladder acellular matrix scaffolds is crucial, especially given the current and future biomedical applications of such scaffolds. While the efforts so far are important and valuable, significant work remains. Initial evidence indicates that cellular remodeling of myogenic cells in

our TEMR treatment results in a scaffold that is ultimately thinner than when the cells were seeded. The cause of this remodeling is unknown, but inference suggests that the cells are simply following their natural programming of constant environmental remodeling. An important future study would be to examine the impact that initial scaffold thickness has on cellular attachment, ultimate scaffold thickness, and efficacy as a treatment protocol. Such a study would aid in determining a proper release criteria for raw BAM scaffolds. Until this point, we can only estimate how the BAM thickness affects these factors and attempt to hold this variable within a specified boundary.

However, we suggest that one immediate change should be made to normal BAM experimental protocol. After scaffold lyophilization but before sterilization, each BAM should be subject to thickness measurement by the Digimatic indicator. Multiple measures should be taken, and all thicknesses recorded on each scaffold's individual container. In addition, after the experimental implantation duration has expired and the muscle is removed for force testing, the thickness of the implant should be measured according to the same protocol. This updated standardized protocol would involve removing the scaffold area from an experimentally-treated muscle and digesting cellular material via trypsinization. AFM and SEM could then be used to analyze the composition and orientation of the remaining or newly-formed scaffold material from the treatment area. SEM would provide indication of general ECM arrangement, while AFM could provide more information regarding material composition and intra-scaffold orientations. Recording all of this information along with all other normal experimental information adds another dimension to the standard analysis of active force production, and may yield valuable insight into the effect of implant thickness on efficacy of muscle recovery.

4. Advances in Assessment of Repaired Skeletal Muscle TIssue

4.1 Introduction

In the Regenerative Therapeutics Laboratory, the bioreactor is a critical step in the production of effective and consistent skeletal muscle tissue engineered implants. While sufficient evidence on the advantageous effect of bioreactors has been collected to warrant their use (Brown, 2000) (Martin, Wendt, & Heberer, 2004) (An & Li, 2014), further development of bioreactor-related issues is needed, especially given new and future developments in bioreactor protocol – such as that accomplished by the capstone team. This section largely "steps back" from a direct look at the bioreactor, and instead examines factors succedent to bioreactor operation. These pertain to active force recording from bioreactor-conditioned muscles.

Myogenic active force production is held as the gold standard in the lab; as such, our TEMR treatments are analyzed via histology, but the main quantification is via active force recording. The current primary active force analysis is via a method which requires entirely explanting the analyzed muscle. In an attempt to record more physiologically-relevant active force production features, I have developed an in-situ analysis method. We will compare the background, protocol, and results from both our current ex vivo method and the in situ method.

4.2 Ex Vivo vs In Situ Active Force Measurement

4.2.1 DMT Analysis Protocol

Currently, active force production from TEMR-treated rat latissimus dorsi (LD) injuries is measured via an ex vivo procedure. To begin this process, the rat is anesthetized and an incision the length of the LD muscle created on the back. The skin and fascia is gradually separated to expose the entire muscle. The tendon connecting the LD to the humerus is isolated, and a suture bundle is tightly tied around it. The tendon is then cut at the humerus, and gradual posterior dissection begins along the spine and bottom of the rib cage. Near the completion of the muscle dissection, the end of the muscle

proximal to the spine is left attached to the rat via a roughly 1cm-wide strip. Another suture bundle is tied here as a second attachment point, and the muscle is cut free. The actual active force measurement is performed in a DMT Tissue Organ Bath System (Danish MyoTechnology, Denmark). The muscle is mounted vertically and attached at each suture point to metal hooks (Figure 4.1) in a bath of Krebs Ringer solution. The bottom hook is fixed in space, while the other is attached to a force transducer. Parallel to the muscle run two platinum electrodes. When an electrical stimulus is sent through the electrodes, the resultant field stimulation initiates muscle contraction which is recorded via the force transducer. While this method provides repeatable muscle force recording, it is quite physiologically irrelevant for several reasons. First, all vasculature is obviously severed in the explant process. Second, the latissimus dorsi is a highly pennate muscle, thus active force measurement between two linearly separated points likely does not convey accurate muscle characteristics, especially in the context of a severe muscle injury and complex repair, as is the case in our TEMR treatment protocol. Finally, muscle stimulation is accomplished via field stimulation, which tends to recruit roughly 10% less active force than neural stimulation (Ward, Corona, Yoo, Harrison, & Christ, 2013). With these issues in mind, I have attempted to develop a more physiologically-relevant protocol and equipment suite for active force production recording of rat LD muscle.

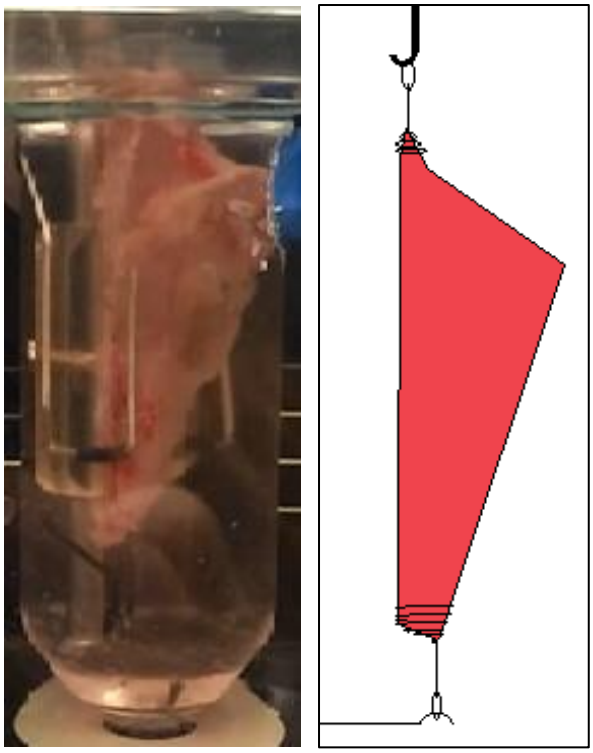

Figure 4.1, DMT Active Force Measurement
A) LD Muscle in DMT
B) Schematic of muscle attachment

4.2.2 In Situ Analysis

Device Development

Dr. Thomas Walters provided an outline for such a system in a 2013 paper (Chen & Walters, 2013) However, this paper provided only an image of the process. In translation of this image to a functional device, I wanted to fulfill several criteria. First, I hoped to use as much existing equipment as possible. Second, I intended to design the device to be convertible, so that the existing equipment used in the new device construction could continue in its present use and also perform in the new role. To this end, I selected the Aurora Scientific 305C (Aurora, Ontario) system currently employed as an in vivo tibialis anterior (TA) transducer in our lab. With some common hardware sourced from McMaster Carr and machining performed by the UVA Physics Dept. machine shop, I was able to create a device that met these specifications. An image of the completed device can be observed in Figure 4.2. In addition, nerve cuffs suitable for motor nerve stimulation based on Dr. Walters' design were created as well.

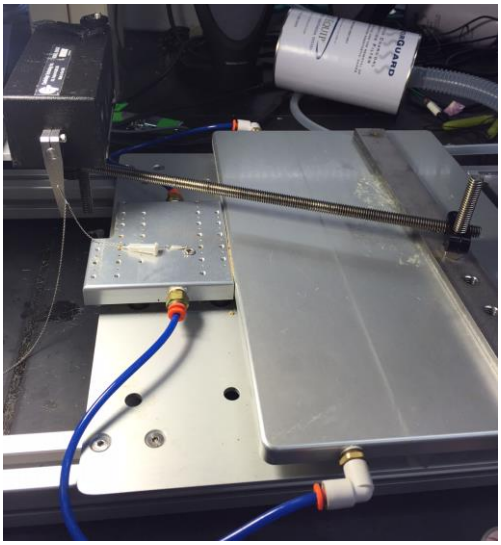

Figure 4.2, In Situ LD Device

The nerve cuff is a relatively simple device, although significant care and precision must be exercised in its manufacture. It consists of a short (~2mm) length of small silastic tubing. Extremely small-gauge insulated wire is fed into the tip of a 20g needle, and the wire-carrying needle is used to pierce across the diameter of the tubing, forming bipolar electrodes. This piercing occurs in two places, separated down the length of the tubing by roughly 1mm. Next, the portions of the wire transiting the tubing are stripped of their insulation, and the wire ends on each side of the tube are tied into place with silk suture. Medical grade adhesive is then used to cover and bulk the outside of the silastic tubing and the wires directly leading to the tubing. The adhesive is allowed to

dry, then the silastic is sliced down its length, allowing the cuff assembly to be placed directly over the nerve. An example cuff is shown in Figure 4.3. To secure the cuff to the nerve during an experiment, a suture is tied around the body of the cuff. The next step in development of this new active muscle force measurement required creating a device protocol.

Figure 4.3, Nerve Cuff Electrode

In Situ Protocol

The procedure for performing an in situ LD muscle test begins similarly to the ex vivo DMT method. At a surgery station, a large incision is created down the back and the humoral tendon is carefully isolated. A silk suture bundle (3-0) is placed around the tendon, although experience has shown that this attachment must be heavily reinforced to avoid the tendon fibers splitting from the tensile force. Next, the nerve cuff is sutured into place on the primary LD motor nerve. After the cuff is placed over the nerve, three sutures are threaded underneath the spine; these are spaced roughly equally from the base of the neck to the posterior attachment of the LD. The rat is then transferred to the testing rig, where the spine sutures are tied around the spine support threaded rod. A suture is tied around the end of the nerve proximal to the rib cage, which prevents it from slipping through the cuff. The nerve is then severed and the cuff electrodes connected to the Grass stimulator leads. The suture tied into the humoral tendon junction is then attached to the transducer arm with a jewelers chain (Figure 4.4).

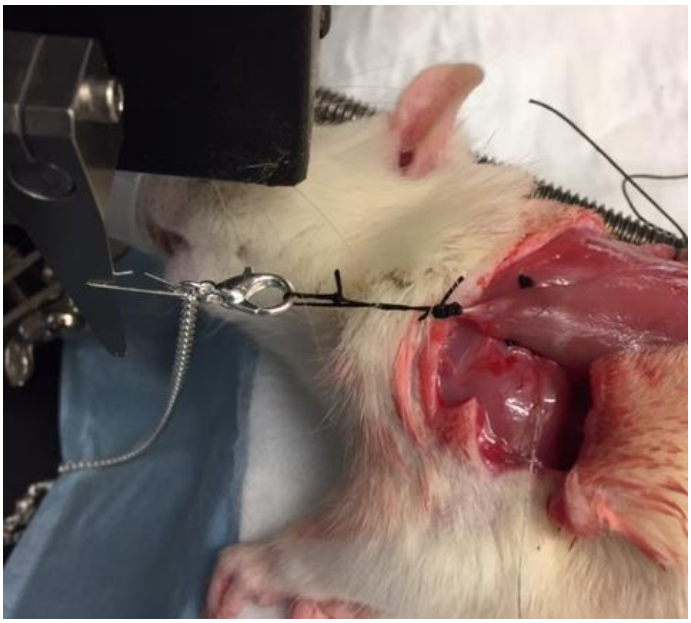

Figure 4.4, Muscle to transducer attachment

4.3 In Situ Experimental Results

4.3.1 DMT vs In Situ

The in situ measurement method is significantly more physiologically relevant than the DMT. Given this fact, it is not surprising that in situ measurements record, on average, greater than 2x higher raw force than that recorded by the DMT. Undoubtedly, this is due to factors such as intact vasculature, neural stimulation (via the nerve cuff), and intact muscle attachment; none of which are present in the DMT analysis. However, it has been interesting to note that with the in situ, smaller differences have thus far seen between non-treated, BAM-treated, and TEMR-treated muscles. Logically, this may proceed from the fact that the applied treatment lies directly in the linear path between the two attachment points in DMT analysis, while the in situ method maintains physiological muscle attachments and the active force features of a highly pennate muscle. The comparison between DMT measurement and in situ testing is shown in Figure 4.5.

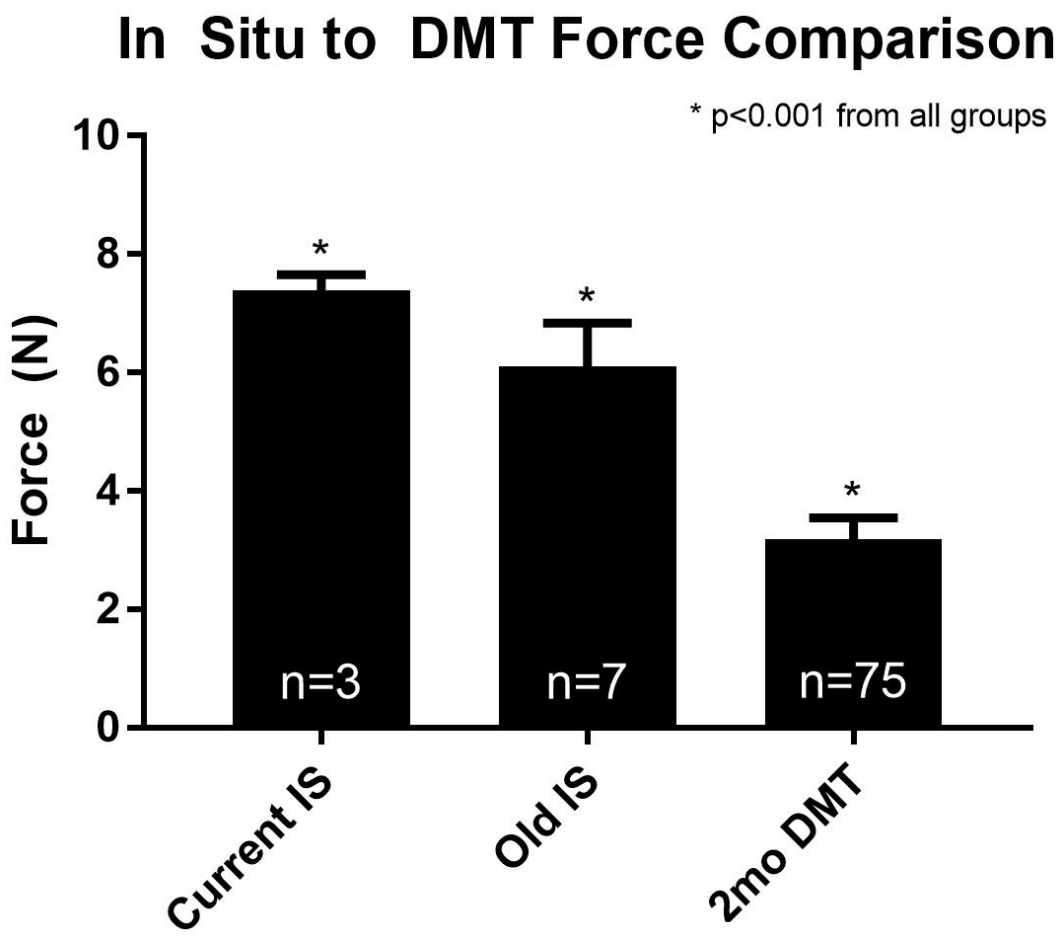

Figure 4.5, In Situ to DMT Comparison

4.3.2 Optimized In Situ Testing Results

In the beginning stages of in situ testing, results were consistently lower than that recorded by Walters (Chen & Walters, 2013). Although a direct comparison cannot be made due to the differing strain of rat, the deficit was roughly 30%. To address this, Amanda and I have applied improvement to the cuff manufacturing, spine suturing, and muscle attachment and pretensioning. For all experiments, we have ensured that the attachment from the spine to the threaded rod is extremely secure, as well as attachment of the tendon to the transducer (via a chain) without penetrating the muscle body with suture. The most current round of in situ baseline testing is also shown against the previous set of non-optimized in situ testing in Figure 4.5.

4.3.3 Trial Combination of In Situ + DMT Testing

In an effort to maximize the utility of each harvested muscle, we attempted to measure the active force by means of in situ first, then explant the muscle and perform DMT analysis. The protocol for the in situ was modified to reduce the number of stimuli to 4, and the DMT protocol was normal. As shown in Figure 4.6, performing the in situ testing first causes some type of performance degradation which does not permit this double-measurement protocol to produce useful data. Although the p-value between the trials was slightly >0.05 due to the low n-value, the trend is very clear and all further attempts have been halted.

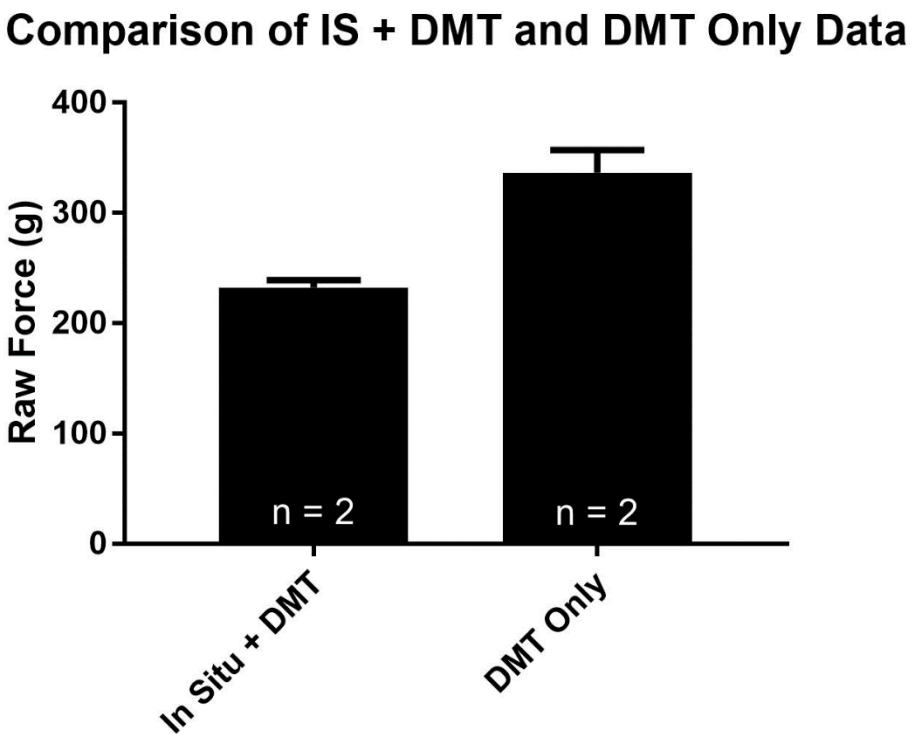

Figure 4.6, IS+DMT to DMT-only Comparison

4.4 In Situ Challenges and Future Directions

Several issues have repeatedly plagued development of the in situ testing method. One of these is slippage of the nerve through the cuff. When the muscle contracts during the test protocol, the nerve is pulled along with the muscle while the cuff is restricted between the muscle and rib cage. This puts significant stress on the cuff, and often resulted in the nerve slipping out. However, this problem has been countered by several methods. First, a suture is tied over the distal end of the nerve; the resultant knot greatly reduces the chance of the nerve slipping through. Second, the new generation of nerve cuffs we have produced employs a smaller, 0.03in inner dia Silastic tubing for the basis of the cuff.

In situ testing of the active force produced by the latissimus dorsi muscle may well develop into a valuable experimental modality. While this method has some increased challenges due to the greater forces involved as well as manipulation of the animal, the concurrently increased physiological relevance may reveal some as of yet unknown factors in the methodology of our attempts to create implantable muscle tissue repairs.

Conclusion

Development of the TEMR technology platform is a highly complex multi-step manufacturing process that requires further optimization for more widespread clinical applications. Improved precision, automation and scalability is still required, but as described in this document, significant progress and improved understanding has already been achieved with respect to many critical aspects of the manufacturing process. While significant work remains to be done, the advances described in this thesis are encouraging and provide both initial guidance, as well as an important first step in this direction.

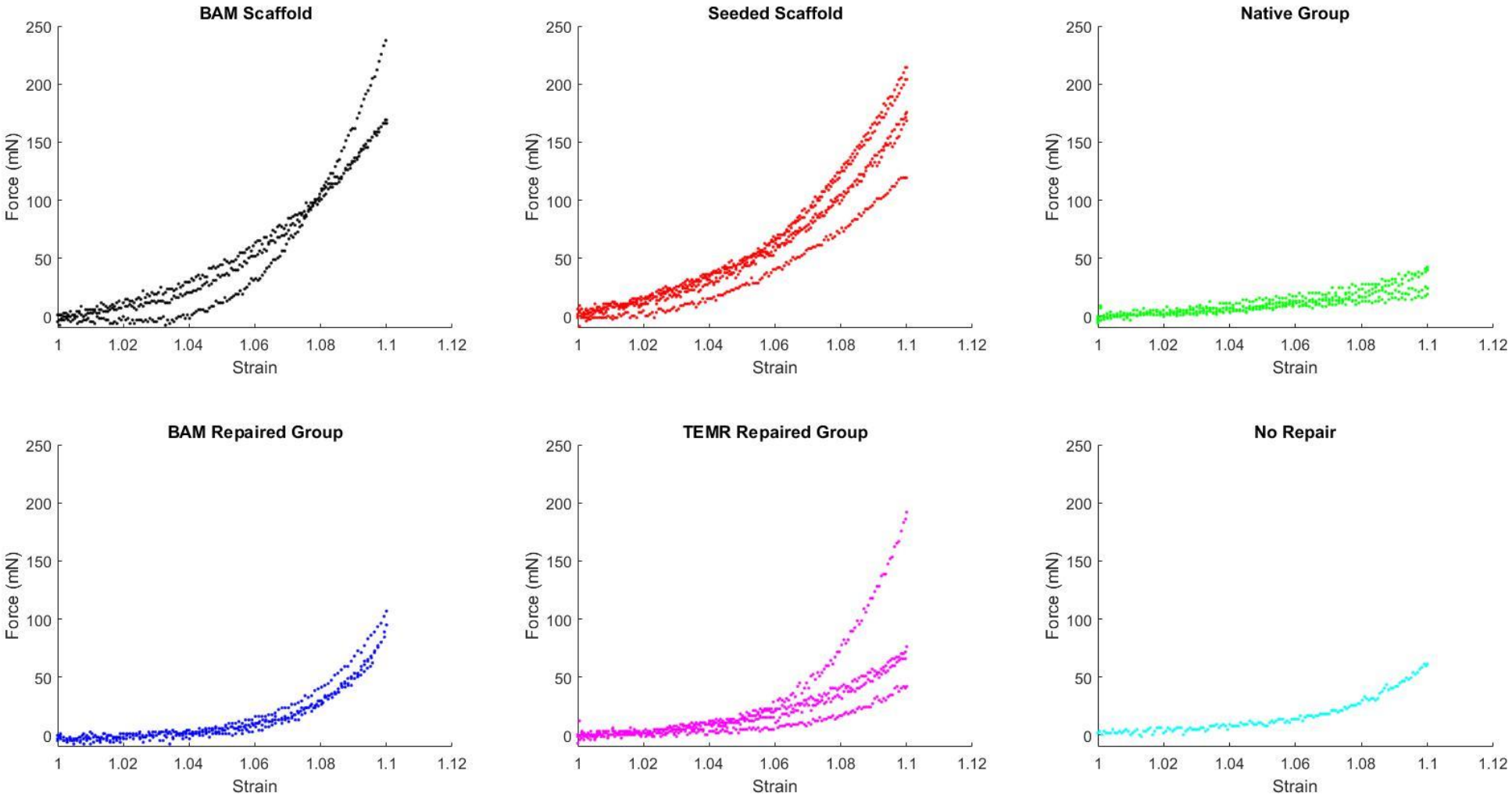

Figure S3.1, Stress-Strain Analysis of Varied Tissue-Engineering Constructs

N1

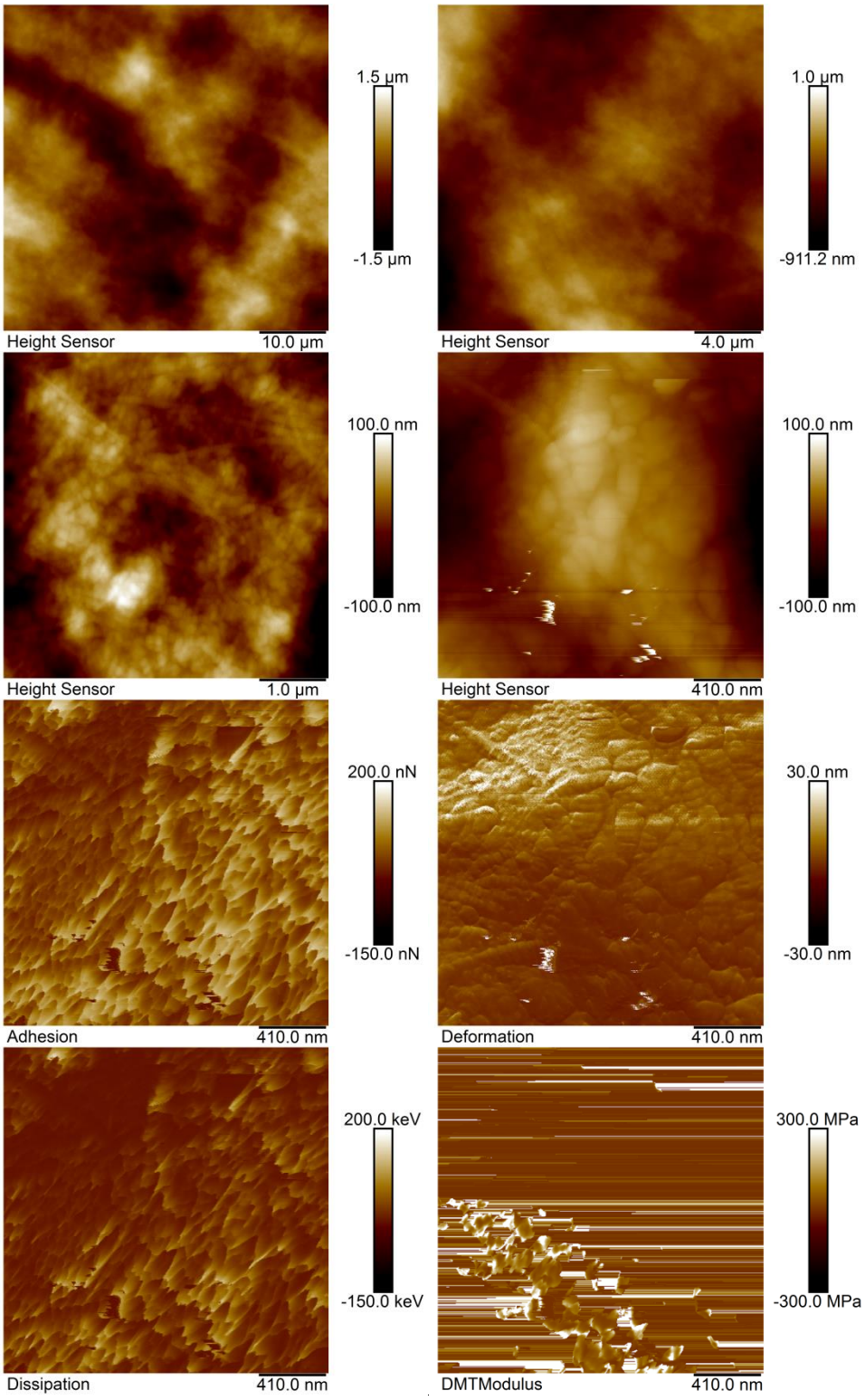

Figure S3.2a, AFM Images of Digested TEMR Scaffolds. N1 and N2 not preconditioned, T1 and T2 preconditioned.

N2

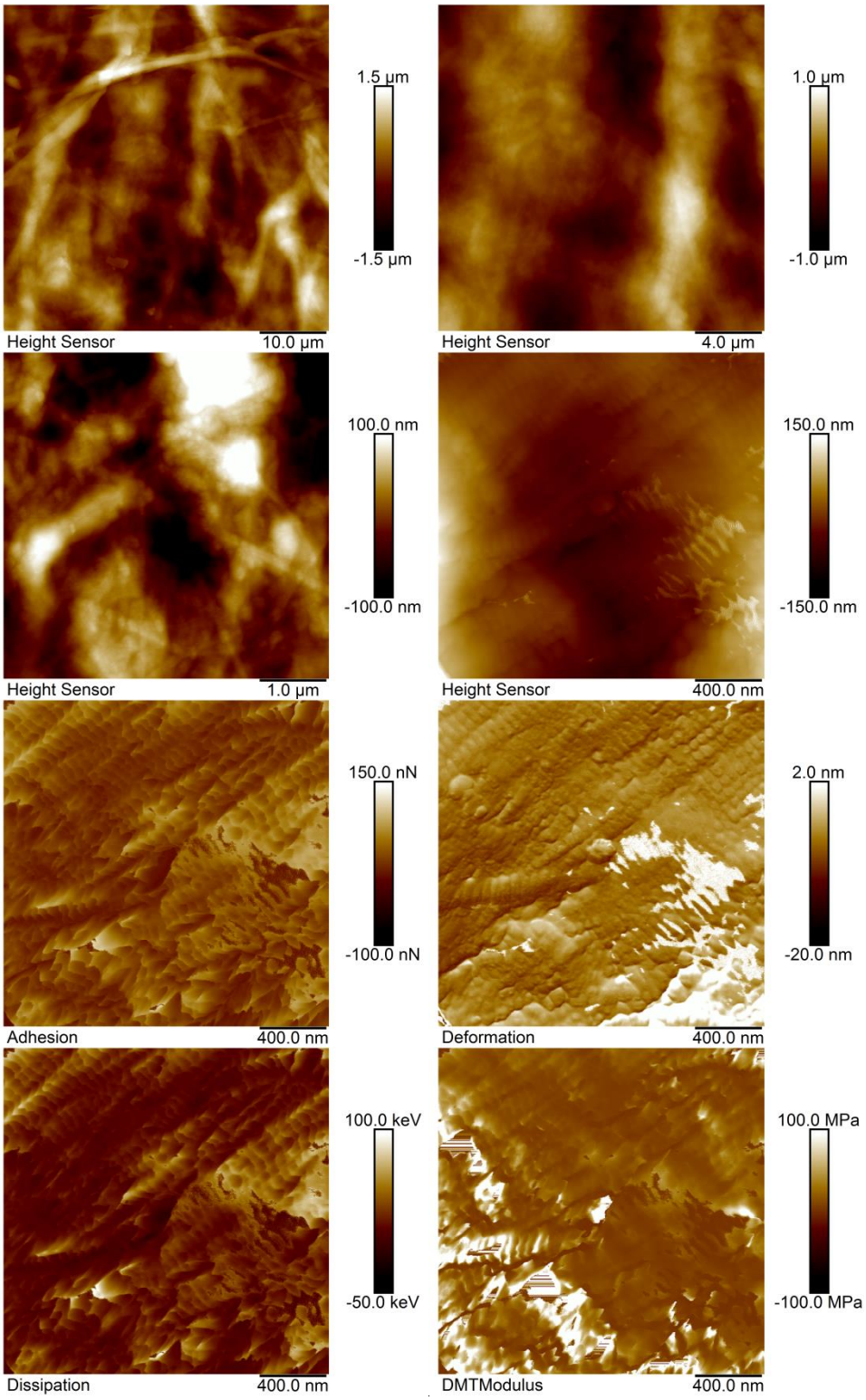

Figure S3.2a (cont.), AFM Images of Digested TEMR Scaffolds. N1 and N2 not preconditioned, T1 and T2 preconditioned.

T1

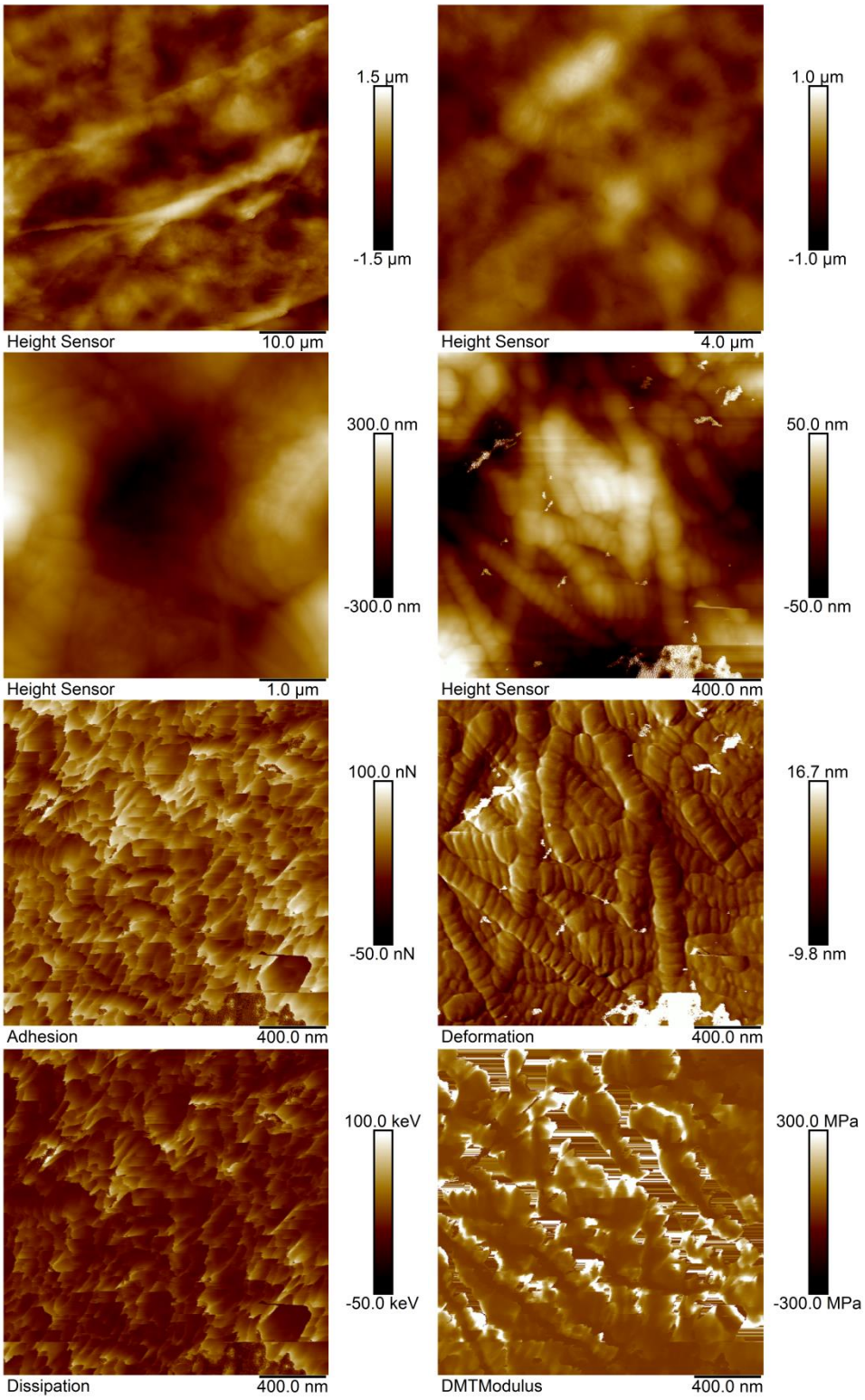

Figure S3.2a (cont.), AFM Images of Digested TEMR Scaffolds. N1 and N2 not preconditioned, T1 and T2 preconditioned.

T2

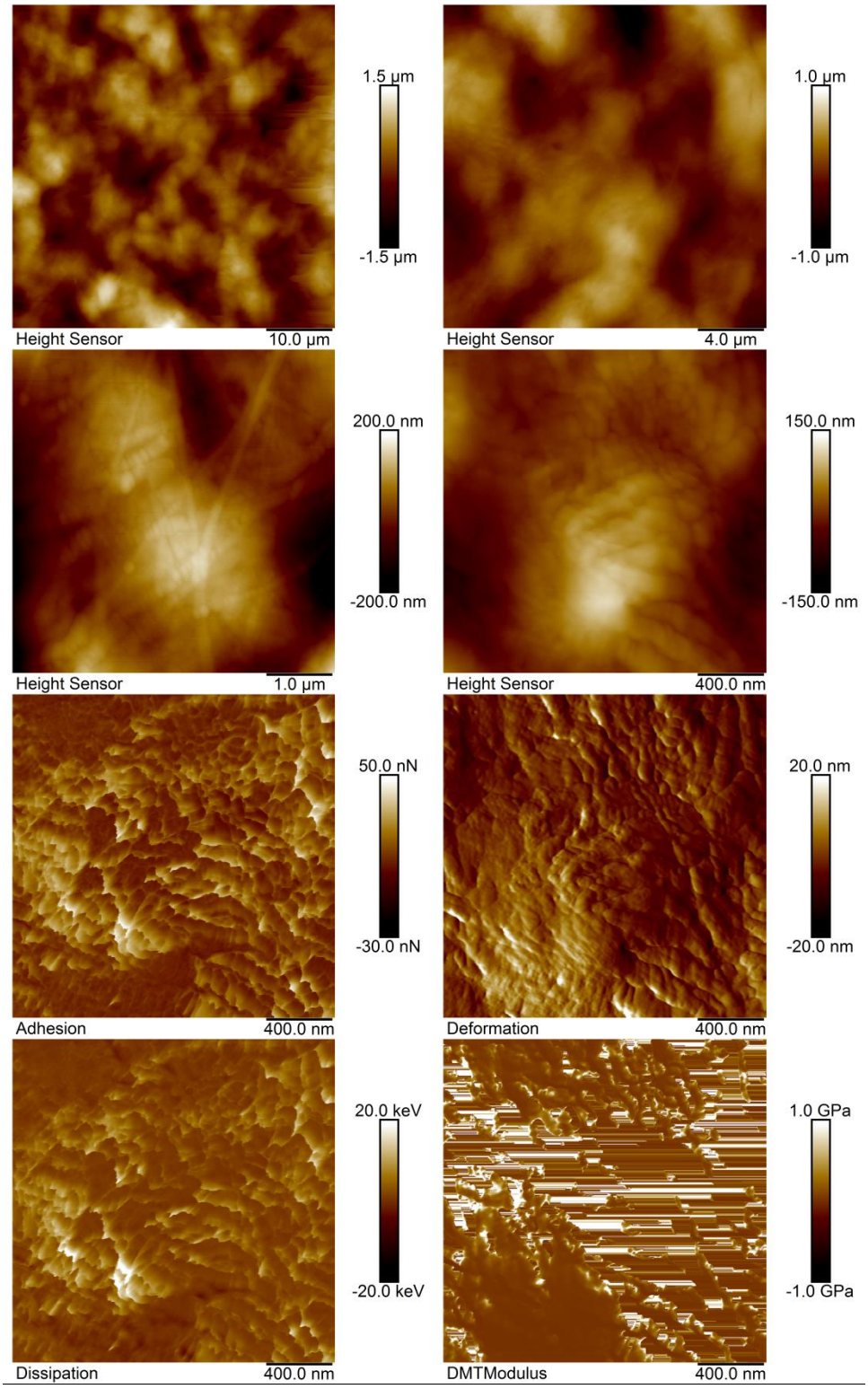

Figure S3.2a (cont.), AFM Images of Digested TEMR Scaffolds. N1 and N2 not preconditioned, T1 and T2 preconditioned.

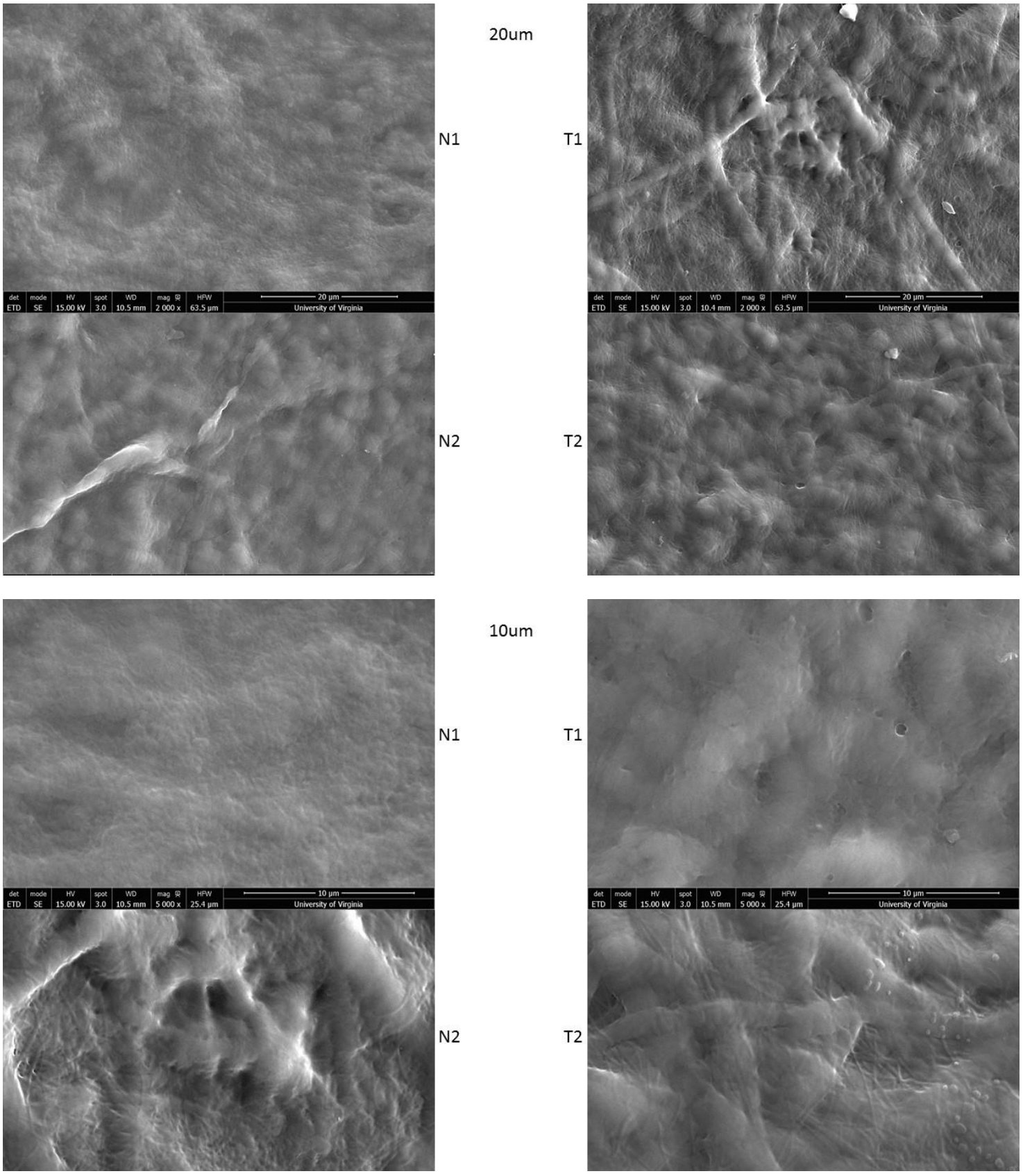

Figure S3.2b, SEM Images of Digested TEMR Scaffolds. N1 and N2 not preconditioned, T1 and T2 preconditioned.

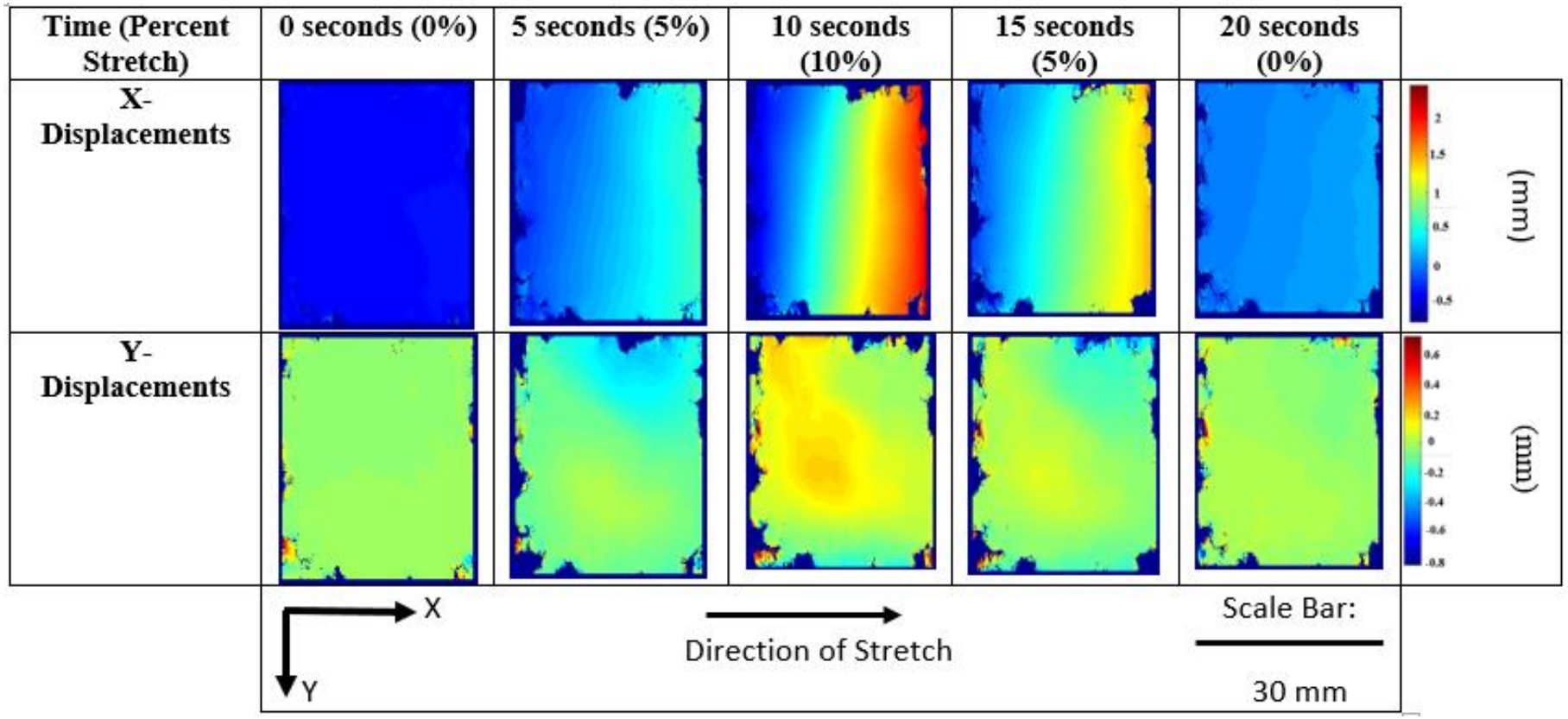

Figure S3.3,
BAM Digital Image Correlation

References

Abousleiman, Rita I., and Vassilios I. Sikavitsas. 2006. “Bioreactors for Tissues of the Musculoskeletal System.” *Advances in Experimental Medicine and Biology* 585: 243–59.

An, Yang, and Dong Li. 2014a. “Engineering Skeletal Muscle Tissue in Bioreactor Systems.” *Chinese Medical Journal* 127 (23): 4130–39.

———. 2014b. “Engineering Skeletal Muscle Tissue in Bioreactor Systems.” *Chinese Medical Journal* 127 (23): 4130–39.

Andersson, Karl-Erik, and Karen D. McCloskey. 2014. “Lamina Propria: The Functional Center of the Bladder?” *Neurourology and Urodynamics* 33 (1): 9–16. doi:10.1002/nau.22465.

Askanas, Valerie, Helen Kwan, Renate B. Alvarez, W. King Engel, Takayoshi Kobayashi, Andrea Martinuzzi, and Edward F. Hawkins. 1987. “De Novo Neuromuscular Junction Formation on Human Muscle Fibres Cultured in Monolayer and Innervated by Foetal Rat Spinal Cord: Ultrastructural and Ultrastructural-Cytochemical Studies.” *Journal of Neurocytology* 16 (4): 523–37. doi:10.1007/BF01668506.

Badylak, Stephen F., Donald O. Freytes, and Thomas W. Gilbert. 2009. “Extracellular Matrix as a Biological Scaffold Material: Structure and Function.” *Acta Biomaterialia* 5 (1): 1–13. doi:10.1016/j.actbio.2008.09.013.

Balice-Gordon, R. J., and J. W. Lichtman. 1994. “Long-Term Synapse Loss Induced by Focal Blockade of Postsynaptic Receptors.” *Nature* 372 (6506): 519–24. doi:10.1038/372519a0.

Bannister, Roger A. 2016. “Bridging the Myoplasmic Gap II: More Recent Advances in Skeletal Muscle Excitation-Contraction Coupling.” *The Journal of Experimental Biology* 219 (Pt 2): 175–82. doi:10.1242/jeb.124123.

Bardouille, C., J. Lehmann, P. Heimann, and H. Jockusch. 2001. “Growth and Differentiation of Permanent and Secondary Mouse Myogenic Cell Lines on Microcarriers.” *Applied Microbiology and Biotechnology* 55 (5): 556–62.

Baugh, Reginald F., Gregory J. Basura, Lisa E. Ishii, Seth R. Schwartz, Caitlin Murray Drumheller, Rebecca Burkholder, Nathan A. Deckard, et al. 2013. “Clinical Practice Guideline: Bell’s Palsy.” *Otolaryngology--Head and Neck Surgery: Official Journal of American Academy of Otolaryngology-Head and Neck Surgery* 149 (3 Suppl): S1-27. doi:10.1177/0194599813505967.

Bian, Weining, and Nenad Bursac. 2009. “Engineered Skeletal Muscle Tissue Networks with Controllable Architecture.” *Biomaterials* 30 (7): 1401–12. doi:10.1016/j.biomaterials.2008.11.015.

Bodine, Sue C., Esther Latres, Susanne Baumhueter, Venus K.-M. Lai, Lorna Nunez, Brian A. Clarke, William T. Poueymirou, et al. 2001. “Identification of Ubiquitin Ligases Required for Skeletal Muscle Atrophy.” *Science* 294 (5547): 1704–8. doi:10.1126/science.1065874.

Brown, Thomas D. 2000. “Techniques for Mechanical Stimulation of Cells in Vitro: A Review.” *Journal of Biomechanics* 33 (1): 3–14. doi:10.1016/S0021-9290(99)00177-3.

Bursac, N., M. Papadaki, R. J. Cohen, F. J. Schoen, S. R. Eisenberg, R. Carrier, G. Vunjak-Novakovic, and L. E. Freed. 1999. “Cardiac Muscle Tissue Engineering: Toward an in Vitro Model for Electrophysiological Studies.” *The American Journal of Physiology* 277 (2 Pt 2): H433-444.

Bursac, Nenad, Maria Papadaki, John A. White, Solomon R. Eisenberg, Gordana Vunjak-Novakovic, and Lisa E. Freed. 2003. “Cultivation in Rotating Bioreactors Promotes Maintenance of Cardiac Myocyte Electrophysiology and Molecular Properties.” *Tissue Engineering* 9 (6): 1243–53. doi:10.1089/10763270360728152.

Cairns, Simeon P., Eva R. Chin, and Jean-Marc Renaud. 2007. “Stimulation Pulse Characteristics and Electrode Configuration Determine Site of Excitation in Isolated Mammalian Skeletal Muscle:

Implications for Fatigue." *Journal of Applied Physiology* 103 (1): 359–68. doi:10.1152/japplphysiol.01267.2006.

Carrier, R. L., M. Papadaki, M. Rupnick, F. J. Schoen, N. Bursac, R. Langer, L. E. Freed, and G. Vunjak-Novakovic. 1999. "Cardiac Tissue Engineering: Cell Seeding, Cultivation Parameters, and Tissue Construct Characterization." *Biotechnology and Bioengineering* 64 (5): 580–89.

Cerino, Giulia, Emanuele Gaudiello, Thomas Grussenmeyer, Ludovic Melly, Diana Massai, Andrea Banfi, Ivan Martin, Friedrich Eckstein, Martin Grapow, and Anna Marsano. 2016. "Three Dimensional Multi-Cellular Muscle-like Tissue Engineering in Perfusion-Based Bioreactors." *Biotechnology and Bioengineering* 113 (1): 226–36. doi:10.1002/bit.25688.

Chan, Yau-Chi, Sherwin Ting, Yee-Ki Lee, Kwong-Man Ng, Jiao Zhang, Zi Chen, Chung-Wah Siu, Steve K. W. Oh, and Hung-Fat Tse. 2013. "Electrical Stimulation Promotes Maturation of Cardiomyocytes Derived from Human Embryonic Stem Cells." *Journal of Cardiovascular Translational Research* 6 (6): 989–99. doi:10.1007/s12265-013-9510-z.

Chen, Xiaoyu K., and Thomas J. Walters. 2013. "Muscle-Derived Decellularised Extracellular Matrix Improves Functional Recovery in a Rat Latissimus Dorsi Muscle Defect Model." *Journal of Plastic, Reconstructive & Aesthetic Surgery: JPRAS* 66 (12): 1750–58. doi:10.1016/j.bjps.2013.07.037.

Chromiak, Joseph A., Janet Shansky, Carmen Perrone, and Herman H. Vandenburgh. 1998. "Bioreactor Perfusion System for the Long-Term Maintenance of Tissue-Engineered Skeletal Muscle Organoids." *In Vitro Cellular & Developmental Biology - Animal* 34 (9): 694–703. doi:10.1007/s11626-998-0065-2.

Chua, Su-Kiat, Bao-Wei Wang, Li-Ming Lien, Huey-Ming Lo, Chiung-Zuan Chiu, and Kou-Gi Shyu. 2016. "Mechanical Stretch Inhibits MicroRNA499 via p53 to Regulate Calcineurin-A Expression in Rat Cardiomyocytes." *PloS One* 11 (2): e0148683. doi:10.1371/journal.pone.0148683.

Chun, So Young, Grace Jeong Lim, Tae Gyun Kwon, Eun Kyoung Kwak, Bup Wan Kim, Anthony Atala, and James J. Yoo. 2007. "Identification and Characterization of Bioactive Factors in Bladder Submucosa Matrix." *Biomaterials* 28 (29): 4251–56. doi:10.1016/j.biomaterials.2007.05.020.

Cimetta, E., M. Flaibani, M. Mella, E. Serena, L. Boldrin, P. De Coppi, and N. Elvassore. 2007. "Enhancement of Viability of Muscle Precursor Cells on 3D Scaffold in a Perfusion Bioreactor." *The International Journal of Artificial Organs* 30 (5): 415–28.

Colman, H., J. Nabekura, and J. W. Lichtman. 1997. "Alterations in Synaptic Strength Preceding Axon Withdrawal." *Science (New York, N.Y.)* 275 (5298): 356–61.

Cook, Colin A., Pinar Y. Huri, Brian P. Ginn, Jordana Gilbert-Honick, Sarah M. Somers, Joshua P. Temple, Hai-Quan Mao, and Warren L. Grayson. 2016. "Characterization of a Novel Bioreactor System for 3D Cellular Mechanobiology Studies." *Biotechnology and Bioengineering* 113 (8): 1825–37. doi:10.1002/bit.25946.

Corona, Benjamin T., Masood A. Machingal, Tracy Criswell, Manasi Vadhavkar, Ashley C. Dannahower, Christopher Bergman, Weixin Zhao, and George J. Christ. 2012. "Further Development of a Tissue Engineered Muscle Repair Construct In Vitro for Enhanced Functional Recovery Following Implantation In Vivo in a Murine Model of Volumetric Muscle Loss Injury." *Tissue Engineering. Part A* 18 (11–12): 1213–28. doi:10.1089/ten.tea.2011.0614.

Corona, Benjamin T., Catherine L. Ward, Hannah B. Baker, Thomas J. Walters, and George J. Christ. 2014. "Implantation of In Vitro Tissue Engineered Muscle Repair Constructs and Bladder Acellular Matrices Partially Restore In Vivo Skeletal Muscle Function in a Rat Model of Volumetric Muscle Loss Injury." *Tissue Engineering. Part A* 20 (3–4): 705–15. doi:10.1089/ten.tea.2012.0761.

De Filippo, Roger E., James J. Yoo, and Anthony Atala. 2002. "Urethral Replacement Using Cell Seeded Tubularized Collagen Matrices." *The Journal of Urology*, Part 2 of 2, 168 (4, Supplement): 1789–93. doi:10.1016/S0022-5347(05)64414-X.

Dennis, R. G., B. Smith, A. Philp, K. Donnelly, and K. Baar. 2009. “Bioreactors for Guiding Muscle Tissue Growth and Development.” *Advances in Biochemical Engineering/Biotechnology* 112: 39–79. doi:10.1007/978-3-540-69357-4_3.

Dhawan, Vikas, Ian F. Lytle, Douglas E. Dow, Yen-Chih Huang, and David L. Brown. 2007. “Neurotization Improves Contractile Forces of Tissue-Engineered Skeletal Muscle.” *Tissue Engineering* 13 (11): 2813–21. doi:10.1089/ten.2007.0003.

Donnelly, Kenneth, Alastair Khodabukus, Andrew Philp, Louise Deldicque, Robert G. Dennis, and Keith Baar. 2010. “A Novel Bioreactor for Stimulating Skeletal Muscle in Vitro.” *Tissue Engineering. Part C, Methods* 16 (4): 711–18. doi:10.1089/ten.TEC.2009.0125.

Dow, Douglas E., Paul S. Cederna, Cheryl A. Hassett, Tatiana Y. Kostrominova, John A. Faulkner, and Robert G. Dennis. 2004. “Number of Contractions to Maintain Mass and Force of a Denervated Rat Muscle.” *Muscle & Nerve* 30 (1): 77–86. doi:10.1002/mus.20054.

Duffy, Rebecca M., and Adam W. Feinberg. 2014. “Engineered Skeletal Muscle Tissue for Soft Robotics: Fabrication Strategies, Current Applications, and Future Challenges.” *Wiley Interdisciplinary Reviews. Nanomedicine and Nanobiotechnology* 6 (2): 178–95. doi:10.1002/wnan.1254.

Dugan, James M, Sarah H Cartmell, and Julie E Gough. 2014. “Uniaxial Cyclic Strain of Human Adipose–derived Mesenchymal Stem Cells and C2C12 Myoblasts in Coculture.” *Journal of Tissue Engineering* 5 (March). doi:10.1177/2041731414530138.

Edman, K A, G Elzinga, and M I Noble. 1978. “Enhancement of Mechanical Performance by Stretch during Tetanic Contractions of Vertebrate Skeletal Muscle Fibres.” *The Journal of Physiology* 281 (August): 139–55.

Feng, Zhonggang, T. Matsumoto, Y. Nomura, and T. Nakamura. 2005. “An Electro-Tensile Bioreactor for 3-D Culturing of Cardiomyocytes.” *IEEE Engineering in Medicine and Biology Magazine* 24 (4): 73–79. doi:10.1109/MEMB.2005.1463399.

Flaibani, Marina, Luisa Boldrin, Elisa Cimetta, Martina Piccoli, Paolo De Coppi, and Nicola Elvassore. 2009. “Muscle Differentiation and Myotubes Alignment Is Influenced by Micropatterned Surfaces and Exogenous Electrical Stimulation.” *Tissue Engineering. Part A* 15 (9): 2447–57. doi:10.1089/ten.tea.2008.0301.

Fujita, Hideaki, Taku Nedachi, and Makoto Kanzaki. 2007. “Accelerated de Novo Sarcomere Assembly by Electric Pulse Stimulation in C2C12 Myotubes.” *Experimental Cell Research* 313 (9): 1853–65. doi:10.1016/j.yexcr.2007.03.002.

Fujita, Hideaki, Kazunori Shimizu, and Eiji Nagamori. 2010. “Novel Method for Measuring Active Tension Generation by C2C12 Myotube Using UV-Crosslinked Collagen Film.” *Biotechnology and Bioengineering* 106 (3): 482–89. doi:10.1002/bit.22705.

Gilbert, Scott F. 2000. “Myogenesis: The Development of Muscle.” https://www.ncbi.nlm.nih.gov/books/NBK10006/.

Goodman, Craig A., Troy A. Hornberger, and Alexander G. Robling. 2015. “Bone and Skeletal Muscle: Key Players in Mechanotransduction and Potential Overlapping Mechanisms.” *Bone* 80 (November): 24–36. doi:10.1016/j.bone.2015.04.014.

Govoni, Marco, Fabrizio Lotti, Luigi Biagiotti, Maurizio Lannocca, Gianandrea Pasquinelli, Sabrina Valente, Claudio Muscari, et al. 2014. “An Innovative Stand-Alone Bioreactor for the Highly Reproducible Transfer of Cyclic Mechanical Stretch to Stem Cells Cultured in a 3D Scaffold.” *Journal of Tissue Engineering and Regenerative Medicine* 8 (10): 787–93. doi:10.1002/term.1578.

Grayson, Warren L., Timothy P. Martens, George M. Eng, Milica Radisic, and Gordana Vunjak-Novakovic. 2009. “Biomimetic Approach to Tissue Engineering.” *Seminars in Cell & Developmental Biology*, Regenerative Biology and Medicine: II and Patterning and Evolving the Vertebrate Forebrain, 20 (6): 665–73. doi:10.1016/j.semcdb.2008.12.008.

Grogan, Brian F., Joseph R. Hsu, and Skeletal Trauma Research Consortium. 2011. "Volumetric Muscle Loss." *The Journal of the American Academy of Orthopaedic Surgeons* 19 Suppl 1: S35-37.

Gundersen, Kristian. 2011. "Excitation-Transcription Coupling in Skeletal Muscle: The Molecular Pathways of Exercise." *Biological Reviews of the Cambridge Philosophical Society* 86 (3): 564–600. doi:10.1111/j.1469-185X.2010.00161.x.

Hall, Judith G. 2010. "Importance of Muscle Movement for Normal Craniofacial Development." *The Journal of Craniofacial Surgery* 21 (5): 1336–38. doi:10.1097/SCS.0b013e3181ebcd4f.

Hall, John E. 2010. *Guyton and Hall Textbook of Medical Physiology, 12e*. 12th ed. Saunders/Elsevier.

Heher, Philipp, Babette Maleiner, Johanna Prüller, Andreas Herbert Teuschl, Josef Kollmitzer, Xavier Monforte, Susanne Wolbank, Heinz Redl, Dominik Rünzler, and Christiane Fuchs. 2015. "A Novel Bioreactor for the Generation of Highly Aligned 3D Skeletal Muscle-like Constructs through Orientation of Fibrin via Application of Static Strain." *Acta Biomaterialia* 24 (September): 251–65. doi:10.1016/j.actbio.2015.06.033.

Hinds, Sara, Weining Bian, Robert G Dennis, and Nenad Bursac. 2011. "The Role of Extracellular Matrix Composition in Structure and Function of Bioengineered Skeletal Muscle." *Biomaterials* 32 (14): 3575–83. doi:10.1016/j.biomaterials.2011.01.062.

Holcomb, John B., Lynn G. Stansbury, Howard R. Champion, Charles Wade, and Ronald F. Bellamy. 2006. "Understanding Combat Casualty Care Statistics." *The Journal of Trauma* 60 (2): 397–401. doi:10.1097/01.ta.0000203581.75241.f1.

Huxley, Andrew, Sir. 1980. *Reflections on Muscle*. Liverpool University Press. http://trove.nla.gov.au/version/11823164.

Jansen, J. K., and T. Fladby. 1990. "The Perinatal Reorganization of the Innervation of Skeletal Muscle in Mammals." *Progress in Neurobiology* 34 (1): 39–90.

Järvinen, Tero A. H., Teppo L. N. Järvinen, Minna Kääriäinen, Ville Äärimaa, Samuli Vaittinen, Hannu Kalimo, and Markku Järvinen. 2007. "Muscle Injuries: Optimising Recovery." *Best Practice & Research. Clinical Rheumatology* 21 (2): 317–31. doi:10.1016/j.berh.2006.12.004.

Jiang, Yunan, Yu Wang, and Guohua Tang. 2016. "Cyclic Tensile Strain Promotes the Osteogenic Differentiation of a Bone Marrow Stromal Cell and Vascular Endothelial Cell Co-Culture System." *Archives of Biochemistry and Biophysics* 607 (October): 37–43. doi:10.1016/j.abb.2016.08.015.

Jolesz, F, and Streter, F A. 1981. "Development, Innervation, and Activity-Pattern Induced Changes in Skeletal Muscle." *Annual Review of Physiology* 43 (1): 531–52. doi:10.1146/annurev.ph.43.030181.002531.

Juhas, Mark, George C. Engelmayr, Andrew N. Fontanella, Gregory M. Palmer, and Nenad Bursac. 2014. "Biomimetic Engineered Muscle with Capacity for Vascular Integration and Functional Maturation in Vivo." *Proceedings of the National Academy of Sciences* 111 (15): 5508–13. doi:10.1073/pnas.1402723111.

Juhas, Mark, Jean Ye, and Nenad Bursac. 2016. "Design, Evaluation, and Application of Engineered Skeletal Muscle." *Methods (San Diego, Calif.)* 99 (April): 81–90. doi:10.1016/j.ymeth.2015.10.002.

Khodabukus, Alastair, and Keith Baar. 2011. "Defined Electrical Stimulation Emphasizing Excitability for the Development and Testing of Engineered Skeletal Muscle." *Tissue Engineering Part C: Methods* 18 (5): 349–57. doi:10.1089/ten.tec.2011.0364.

Langelaan, Marloes L. P., Kristel J. M. Boonen, Kang Yuen Rosaria-Chak, Daisy W. J. van der Schaft, Mark J. Post, and Frank P. T. Baaijens. 2011. "Advanced Maturation by Electrical Stimulation: Differences in Response between C2C12 and Primary Muscle Progenitor Cells." *Journal of Tissue Engineering and Regenerative Medicine* 5 (7): 529–39. doi:10.1002/term.345.

Lieber, Richard L. 2002. *Skeletal Muscle Structure, Function, and Plasticity*. Lippincott Williams & Wilkins.

Lu, Pengfei, Ken Takai, Valerie M. Weaver, and Zena Werb. 2011. “Extracellular Matrix Degradation and Remodeling in Development and Disease.” *Cold Spring Harbor Perspectives in Biology* 3 (12). doi:10.1101/cshperspect.a005058.

Ma, Jinjin, Sambit Sahoo, Andrew R. Baker, and Kathleen A. Derwin. 2015. “Investigating Muscle Regeneration with a Dermis/small Intestinal Submucosa Scaffold in a Rat Full-Thickness Abdominal Wall Defect Model.” *Journal of Biomedical Materials Research. Part B, Applied Biomaterials* 103 (2): 355–64. doi:10.1002/jbm.b.33166.

Maas, Huub, and Thomas G. Sandercock. 2010. “Force Transmission between Synergistic Skeletal Muscles through Connective Tissue Linkages.” *BioMed Research International* 2010 (April): e575672. doi:10.1155/2010/575672.

Machingal, Masood A., Benjamin T. Corona, Thomas J. Walters, Venu Kesireddy, Christine N. Koval, Ashley Dannahower, Weixin Zhao, James J. Yoo, and George J. Christ. 2011. “A Tissue-Engineered Muscle Repair Construct for Functional Restoration of an Irrecoverable Muscle Injury in a Murine Model.” *Tissue Engineering. Part A* 17 (17–18): 2291–2303. doi:10.1089/ten.TEA.2010.0682.

MacIntosh, Brian R, Phillip F. Gardiner, and Alan J McComas. 2006. *Skeletal Muscle : Form and Function*. 2nd ed. Champaign, IL : Human Kinetics. http://trove.nla.gov.au/version/44898559.

Madden, Lauran, Mark Juhas, William E. Kraus, George A. Truskey, and Nenad Bursac. 2015. “Bioengineered Human Myobundles Mimic Clinical Responses of Skeletal Muscle to Drugs.” *eLife* 4 (January): e04885. doi:10.7554/eLife.04885.

Martin, Ivan, David Wendt, and Michael Heberer. 2004. “The Role of Bioreactors in Tissue Engineering.” *Trends in Biotechnology* 22 (2): 80–86. doi:10.1016/j.tibtech.2003.12.001.

Martin, Neil R. W., Samantha L. Passey, Darren J. Player, Vivek Mudera, Keith Baar, Linda Greensmith, and Mark P. Lewis. 2015. “Neuromuscular Junction Formation in Tissue-Engineered Skeletal Muscle Augments Contractile Function and Improves Cytoskeletal Organization.” *Tissue Engineering. Part A* 21 (19–20): 2595–2604. doi:10.1089/ten.TEA.2015.0146.

Molnar, G., N. A. Schroedl, S. R. Gonda, and C. R. Hartzell. 1997. “Skeletal Muscle Satellite Cells Cultured in Simulated Microgravity.” *In Vitro Cellular & Developmental Biology. Animal* 33 (5): 386–91. doi:10.1007/s11626-997-0010-9.

Moon, Du Geon, George Christ, Joel D. Stitzel, Anthony Atala, and James J. Yoo. 2008. “Cyclic Mechanical Preconditioning Improves Engineered Muscle Contraction.” *Tissue Engineering Part A* 14 (4): 473–82. doi:10.1089/tea.2007.0104.

Morimoto, Yuya, Midori Kato-Negishi, Hiroaki Onoe, and Shoji Takeuchi. 2013. “Three-Dimensional Neuron-Muscle Constructs with Neuromuscular Junctions.” *Biomaterials* 34 (37): 9413–19. doi:10.1016/j.biomaterials.2013.08.062.

Nishi, Masanori, Rena Matsumoto, Jian Dong, and Toshimasa Uemura. 2013. “Engineered Bone Tissue Associated with Vascularization Utilizing a Rotating Wall Vessel Bioreactor.” *Journal of Biomedical Materials Research Part A* 101A (2): 421–27. doi:10.1002/jbm.a.34340.

Papadaki, M., N. Bursac, R. Langer, J. Merok, G. Vunjak-Novakovic, and L. E. Freed. 2001. “Tissue Engineering of Functional Cardiac Muscle: Molecular, Structural, and Electrophysiological Studies.” *American Journal of Physiology. Heart and Circulatory Physiology* 280 (1): H168-178.

Passipieri, J. A., and G. J. Christ. 2016. “The Potential of Combination Therapeutics for More Complete Repair of Volumetric Muscle Loss Injuries: The Role of Exogenous Growth Factors And/or Progenitor Cells in Implantable Skeletal Muscle Tissue Engineering Technologies.” *Cells Tissues Organs* 202 (3–4): 202–13. doi:10.1159/000447323.

Pellegrino, Claudio, and Clara Franzini. 1963. “AN ELECTRON MICROSCOPE STUDY OF DENERVATION ATROPHY IN RED AND WHITE SKELETAL MUSCLE FIBERS.” *The Journal of Cell Biology* 17 (2): 327–49.

Perrone, C. E., D. Fenwick-Smith, and H. H. Vandenburgh. 1995. “Collagen and Stretch Modulate Autocrine Secretion of Insulin-like Growth Factor-1 and Insulin-like Growth Factor Binding Proteins from Differentiated Skeletal Muscle Cells.” *The Journal of Biological Chemistry* 270 (5): 2099–2106.

Pollard, A S, I M McGonnell, and A A Pitsillides. 2014. “Mechanoadaptation of Developing Limbs: Shaking a Leg.” *Journal of Anatomy* 224 (6): 615–23. doi:10.1111/joa.12171.

Powell, Courtney A., Beth L. Smiley, John Mills, and Herman H. Vandenburgh. 2002. “Mechanical Stimulation Improves Tissue-Engineered Human Skeletal Muscle.” *American Journal of Physiology - Cell Physiology* 283 (5): C1557–65. doi:10.1152/ajpcell.00595.2001.

Radtke, Andrea L., and Melissa M. Herbst-Kralovetz. 2012. “Culturing and Applications of Rotating Wall Vessel Bioreactor Derived 3D Epithelial Cell Models.” *JoVE (Journal of Visualized Experiments)*, no. 62(April): e3868–e3868. doi:10.3791/3868.

Ramaswamy, Krishnan S, Mark L Palmer, Jack H van der Meulen, Abigail Renoux, Tatiana Y Kostrominova, Daniel E Michele, and John A Faulkner. 2011. “Lateral Transmission of Force Is Impaired in Skeletal Muscles of Dystrophic Mice and Very Old Rats.” *The Journal of Physiology* 589 (Pt 5): 1195–1208. doi:10.1113/jphysiol.2010.201921.

Rangarajan, Swathi, Lauran Madden, and Nenad Bursac. 2014. “Use of Flow, Electrical, and Mechanical Stimulation to Promote Engineering of Striated Muscles.” *Annals of Biomedical Engineering* 42 (7): 1391–1405. doi:10.1007/s10439-013-0966-4.

Rebbeck, Robyn T., Yamuna Karunasekara, Philip G. Board, Nicole A. Beard, Marco G. Casarotto, and Angela F. Dulhunty. 2014. “Skeletal Muscle Excitation-Contraction Coupling: Who Are the Dancing Partners?” *The International Journal of Biochemistry & Cell Biology* 48 (March): 28–38. doi:10.1016/j.biocel.2013.12.001.

REDDY, PRAMOD P., DIEGO J. BARRIERAS, GREGORY WILSON, DARIUS J. BÄGLI, GORDON A. McLORIE, ANTOINE E. KHOURY, and PAUL A. MERGUERIAN. 2000. “REGENERATION OF FUNCTIONAL BLADDER SUBSTITUTES USING LARGE SEGMENT ACELLULAR MATRIX ALLOGRAFTS IN A PORCINE MODEL.” *The Journal of Urology*, Part 2 of 2, 164 (3, Part 2): 936–41. doi:10.1016/S0022-5347(05)67221-7.

Riso, Eva-Maria, Priit Kaasik, and Teet Seene. 2016. “Remodelling of Skeletal Muscle Extracellular Matrix: Effect of Unloading and Reloading.” doi:10.5772/62295.

Rosario, Derek J., Gwendolen C. Reilly, Emadaldeen Ali Salah, Maggie Glover, Anthony J. Bullock, and Sheila Macneil. 2008. “Decellularization and Sterilization of Porcine Urinary Bladder Matrix for Tissue Engineering in the Lower Urinary Tract.” *Regenerative Medicine* 3 (2): 145–56. doi:10.2217/17460751.3.2.145.

Ross, J. J., M. J. Duxson, and A. J. Harris. 1987. “Neural Determination of Muscle Fibre Numbers in Embryonic Rat Lumbrical Muscles.” *Development (Cambridge, England)* 100 (3): 395–409.

Saha, Somen, Lin Ji, Juan J. de Pablo, and Sean P. Palecek. 2006. “Inhibition of Human Embryonic Stem Cell Differentiation by Mechanical Strain.” *Journal of Cellular Physiology* 206 (1): 126–37. doi:10.1002/jcp.20441.

Salmons, S., and G. Vrbová. 1967. “Changes in the Speed of Mammalian Fast Muscle Following Longterm Stimulation.” *The Journal of Physiology* 192 (2): 39P–40P.

Schiaffino, Stefano, Kenneth A. Dyar, Stefano Ciciliot, Bert Blaauw, and Marco Sandri. 2013. “Mechanisms Regulating Skeletal Muscle Growth and Atrophy.” *The FEBS Journal* 280 (17): 4294–4314. doi:10.1111/febs.12253.

Scott, John B., Catherine L. Ward, Benjamin T. Corona, Michael R. Deschenes, Benjamin S. Harrison, Justin M. Saul, and George J. Christ. 2017. “Achieving Acetylcholine Receptor Clustering in Tissue-Engineered Skeletal Muscle Constructs In Vitro through a Materials-Directed Agrin Delivery Approach.” *Frontiers in Pharmacology* 7 (January). doi:10.3389/fphar.2016.00508.

Serena, Elena, Marina Flaibani, Silvia Carnio, Luisa Boldrin, Libero Vitiello, Paolo De Coppi, and Nicola Elvassore. 2008. “Electrophysiologic Stimulation Improves Myogenic Potential of Muscle Precursor Cells Grown in a 3D Collagen Scaffold.” *Neurological Research* 30 (2): 207–14. doi:10.1179/174313208X281109.

Shadrin, I. Y., A. Khodabukus, and N. Bursac. 2016. “Striated Muscle Function, Regeneration, and Repair.” *Cellular and Molecular Life Sciences*, June, 1–28. doi:10.1007/s00018-016-2285-z.

Sicari, Brian M., J. Peter Rubin, Christopher L. Dearth, Matthew T. Wolf, Fabrisia Ambrosio, Michael Boninger, Neill J. Turner, et al. 2014. “An Acellular Biologic Scaffold Promotes Skeletal Muscle Formation in Mice and Humans with Volumetric Muscle Loss.” *Science Translational Medicine* 6 (234): 234ra58. doi:10.1126/scitranslmed.3008085.

Skardal, Aleksander, Shameema F. Sarker, Aurélie Crabbé, Cheryl A. Nickerson, and Glenn D. Prestwich. 2010. “The Generation of 3-D Tissue Models Based on Hyaluronan Hydrogel-Coated Microcarriers within a Rotating Wall Vessel Bioreactor.” *Biomaterials* 31 (32): 8426–35. doi:10.1016/j.biomaterials.2010.07.047.

Slentz, D. H., G. A. Truskey, and W. E. Kraus. 2001. “Effects of Chronic Exposure to Simulated Microgravity on Skeletal Muscle Cell Proliferation and Differentiation.” *In Vitro Cellular & Developmental Biology. Animal* 37 (3): 148–56. doi:10.1290/1071-2690(2001)037<0148:EOCETS>2.0.CO;2.

Stern-Straeter, J., A.d. Bach, L. Stangenberg, V.t. Foerster, R.e. Horch, G.b. Stark, and J.p. Beier. 2005. “Impact of Electrical Stimulation on Three-Dimensional Myoblast Cultures - a Real-Time RT-PCR Study.” *Journal of Cellular and Molecular Medicine* 9 (4): 883–92. doi:10.1111/j.1582-4934.2005.tb00386.x.

Street, S. F. 1983. “Lateral Transmission of Tension in Frog Myofibers: A Myofibrillar Network and Transverse Cytoskeletal Connections Are Possible Transmitters.” *Journal of Cellular Physiology* 114 (3): 346–64. doi:10.1002/jcp.1041140314.

Syverud, Brian C., Keith W. VanDusen, and Lisa M. Larkin. 2016. “Growth Factors for Skeletal Muscle Tissue Engineering.” *Cells, Tissues, Organs* 202 (3–4): 169–79. doi:10.1159/000444671.

Tchao, Jason, Jong Jin Kim, Bo Lin, Guy Salama, Cecilia W. Lo, Lei Yang, and Kimimasa Tobita. 2013. “Engineered Human Muscle Tissue from Skeletal Muscle Derived Stem Cells and Induced Pluripotent Stem Cell Derived Cardiac Cells.” *International Journal of Tissue Engineering* 2013 (December). doi:10.1155/2013/198762.

Thiele, Oliver C., Robin Seeberger, Michael Engel, Kolja Freier, and Jürgen Hoffmann. 2014. “Development of the Clinical Use of Distant Flaps for Head and Neck Reconstruction.” *Journal of Cranio-Maxillo-Facial Surgery: Official Publication of the European Association for Cranio-Maxillo-Facial Surgery* 42 (1): 79–83. doi:10.1016/j.jcms.2013.02.006.

Tidball, James G. 2005. “Mechanical Signal Transduction in Skeletal Muscle Growth and Adaptation.” *Journal of Applied Physiology (Bethesda, Md.: 1985)* 98 (5): 1900–1908. doi:10.1152/japplphysiol.01178.2004.

Umbach, Joy A., Katrina L. Adams, Cameron B. Gundersen, and Bennett G. Novitch. 2012. “Functional Neuromuscular Junctions Formed by Embryonic Stem Cell-Derived Motor Neurons.” *PLOS ONE* 7 (5): e36049. doi:10.1371/journal.pone.0036049.

Vandenburgh, H. H. 1987. “Motion into Mass: How Does Tension Stimulate Muscle Growth?” *Medicine and Science in Sports and Exercise* 19 (5 Suppl): S142-149.

Vandenburgh, H. H., S. Hatfaludy, P. Karlisch, and J. Shansky. 1989. “Skeletal Muscle Growth Is Stimulated by Intermittent Stretch-Relaxation in Tissue Culture.” *The American Journal of Physiology* 256 (3 Pt 1): C674-682.

———. 1991. “Mechanically Induced Alterations in Cultured Skeletal Muscle Growth.” *Journal of Biomechanics* 24 Suppl 1: 91–99.

VanDusen, Keith W., Brian C. Syverud, Michael L. Williams, Jonah D. Lee, and Lisa M. Larkin. 2014. "Engineered Skeletal Muscle Units for Repair of Volumetric Muscle Loss in the Tibialis Anterior Muscle of a Rat." *Tissue Engineering Part A* 20 (21–22): 2920–30. doi:10.1089/ten.tea.2014.0060.

Vunjak-Novakovic, Gordana, Lisa E. Freed, Robert J. Biron, and Robert Langer. 1996. "Effects of Mixing on the Composition and Morphology of Tissue-Engineered Cartilage." *AIChE Journal* 42 (3): 850–60. doi:10.1002/aic.690420323.

Wagner, Stéphanie, Olivier M. Dorchies, Herrade Stoeckel, Jean-Marie Warter, Philippe Poindron, and Kenneth Takeda. 2003. "Functional Maturation of Nicotinic Acetylcholine Receptors as an Indicator of Murine Muscular Differentiation in a New Nerve-Muscle Co-Culture System." *Pflügers Archiv* 447 (1): 14–22. doi:10.1007/s00424-003-1135-7.

Walsh, Mark K., and Jeff W. Lichtman. 2003. "In Vivo Time-Lapse Imaging of Synaptic Takeover Associated with Naturally Occurring Synapse Elimination." *Neuron* 37 (1): 67–73. doi:10.1016/S0896-6273(02)01142-X.

Walters, Thomas J., Koyal Garg, and Benjamin T. Corona. 2015. "Activity Attenuates Skeletal Muscle Fiber Damage after Ischemia and Reperfusion." *Muscle & Nerve* 52 (4): 640–48. doi:10.1002/mus.24581.

Ward, Catherine L., Benjamin T. Corona, James J. Yoo, Benjamin S. Harrison, and George J. Christ. 2013. "Oxygen Generating Biomaterials Preserve Skeletal Muscle Homeostasis under Hypoxic and Ischemic Conditions." *PLOS ONE* 8 (8): e72485. doi:10.1371/journal.pone.0072485.

Williams, Michael L., Tatiana Y. Kostrominova, Ellen M. Arruda, and Lisa M. Larkin. 2013. "Effect of Implantation on Engineered Skeletal Muscle Constructs." *Journal of Tissue Engineering and Regenerative Medicine* 7 (6): 434–42. doi:10.1002/term.537.

Wilson, S. J., and A. J. Harris. 1993. "Formation of Myotubes in Aneural Rat Muscles." *Developmental Biology* 156 (2): 509–18. doi:10.1006/dbio.1993.1097.

Yoo, J. J., J. Meng, F. Oberpenning, and A. Atala. 1998. "Bladder Augmentation Using Allogenic Bladder Submucosa Seeded with Cells." *Urology* 51 (2): 221–25.